Florida State University Libraries

Electronic Theses, Treatises and Dissertations The Graduate School

2017

Mathematical Modeling and Analysis of Gene Knockout Compensation in Pancreatic B-Cells

Vehpi Yildirim

Follow this and additional works at the DigiNole: FSU's Digital Repository. For more information, please contact lib-ir@fsu.edu

FLORIDA STATE UNIVERSITY

COLLEGE OF ARTS AND SCIENCES

MATHEMATICAL MODELING AND ANALYSIS OF GENE KNOCKOUT COMPENSATION IN PANCREATIC β-CELLS

By

VEHPI YILDIRIM

A Dissertation submitted to the
Department of Mathematics
in partial fulfillment of the
requirements for the degree of
Doctor of Philosophy

2017

Vehpi Yildirim defended this dissertation on February 28, 2017.
The members of the supervisory committee were:

Richard Bertram
Professor Directing Dissertation

Debra A. Fadool
University Representative

Washington Mio
Committee Member

Giray Okten
Committee Member

Michael Roper
Committee Member

The Graduate School has verified and approved the above-named committee members, and certifies that the dissertation has been approved in accordance with university requirements.

Bismillahirrahmanirrahim
Dedicated to my family

ACKNOWLEDGMENTS

First and foremost, I would like to thank to my advisor Dr. Richard Bertram for accepting me as a Ph.D. student and for his extraordinary guidance throughout my training. I can't tell how many times I walked into his office with fears and doubts and, on every occasion, I left his office with peace of mind. I did not only learn how to do research from him, I also learned how to deal with people, how to collaborate with others and how to proceed strategically in the research. I have always been and I will always be grateful for being your student. Thank you very much for being such an excellent role model and mentor.

I would like to give special thanks to our collaborators, Dr. Leslie S. Satin and his lab members at the University of Michigan. Without the experimental data and the valuable ideas that they generously provided, this dissertation would not be complete. I would like to also thank to Dr. Arthur Sherman from NIH, for the valuable feedback he gave throughout the research.

Members of my committee, thank you very much. I appreciate very much for the time and effort you devoted for serving on my committee.

I would like to also thank to all the faculty members of the department of mathematics for being so kind and generous. I have learned a lot from you and, after five years I am proud to say that, thanks to you, we have an excellent graduate program.

People behind the scene, mathematics department's staff, they are amazing. They have always been very supportive and helpful. They always figured a way out for solving my problems and made things a lot easier. Thank you very much guys.

All my friends at FSU, thank you very much for being there when I needed you. In a country far, far away, you made me feel like at home. May the force be with you.

Finally, my family, there are no words to describe my feelings for you. Even dedication of this dissertation to you does not show how grateful I am. Thank you…

TABLE OF CONTENTS

LIST OF TABLES

LIST OF FIGURES

ABSTRACT

Living systems consist of several complex interacting components. Depending on the complexity of the organism, these components can span from molecules to tissues and organs. Systems biology is the interdisciplinary field of study that uses mathematical and computational tools to describe and investigate the roles these components play in biological systems and the way their interactions result in functionality. The collaborative work between biological and mathematical sciences brings deeper insights into understanding living systems because, even with the recent advancements in technology, it is impossible to acquire all types of empirical data on many living systems. Technical restrictions together with the complexity of the system components usually give rise to this limitation. Hence, this interdisciplinary field of study makes great contributions to both clinical and basic research by solving these complexities and helping to better interpret the acquired data. Besides, biological experiments can be expansive and time consuming. Therefore, testing biological hypotheses with mathematical models can be significantly beneficial. In this regard, mathematical models can be thought as microscopes developed for specific living systems and inexpensive and fast ways of simulating experiments.

Insulin secreting pancreatic β-cells are very good examples of such complex systems. Activity of these cells is controlled by extremely complex metabolic and electrophysiological pathways. Therefore, mathematical modeling approaches are proven to be very effective in the study of pancreatic β-cells. Impairments in the activity of these cells lead to impaired insulin secretion, which can have life threatening complications in the body. Thus, understanding the mechanisms underlying β-cell activity and insulin secretion is crucial.

Pancreatic β-cells are excitable cells and they produce electrical activity with the ion channels they express in their plasma membranes. In pancreatic β-cells, insulin secretion is regulated through pathways that link cellular metabolism to the membrane potential through ion channels they express in their plasma membranes. In the initiation and modulation of the insulin secretion ATP-sensitive K^+ channels (K(ATP) channels) play a significant role by coupling cell metabolism to the membrane potential. Defects in the expression of K(ATP) channels lead to hypoglycemia associated with excessive insulin secretion in humans. However, mice seem to be

able to overcome these defects by employing alternative mechanisms. In this dissertation, we investigate the pathological conditions associated with ATP-sensitive K^+ channel deficiency in β-cells and, with a systems biology approach, we propose mechanisms through which mice can compensate for these defects. Using mathematical modeling we explain the dynamics of these compensatory mechanisms and make predictions to test their plausibility. We also demonstrate the results of the *in vitro* experiments performed in accordance with our model predictions.

One of the long-term goals of this study is helping to identify possible therapeutic targets for the treatment of the congenital hypoglycemia that results from K(ATP) channel deficiency. The overall aim of this dissertation is using mathematical modeling and analysis techniques to better understand the experimental data on pancreatic β-cells and guide future research by making testable predictions.

CHAPTER 1

INTRODUCTION

Insulin is the body's unique hormone that can reduce plasma glucose levels by activating glucose uptake in the liver, muscle and adipose tissues (Alberts et al. 2008). Insulin is secreted from pancreatic β-cells when blood glucose concentration is increased. Impairment in the insulin secretion leads to abnormal blood glucose concentrations, which causes several severe complications in the body. Therefore, it is a matter of life and death that pancreatic β-cells secrete the right amount of insulin at the right time. Understanding the mechanisms that regulate insulin secretion is crucial for identifying causes of the defects and possible targets for the therapies.

Insulin secretion is a highly dynamic process and regulated through a complex network that involves electrical and metabolic components. At stimulatory levels of glucose pancreatic β-cells secrete insulin in an oscillatory fashion, which has physiological importance in blood glucose regulation (Matthews et al. 1983b; Paolisso et al. 1991; Hellman 2009) because the body uses insulin more effectively when it is delivered with oscillations (Matveyenko et al. 2012). Furthermore, in type 2 diabetic patients and their near relatives, insulin oscillations are impaired (Matthews et al. 1983a; O'Rahilly et al. 1988; Polonsky et al. 1988). Insulin oscillations result from oscillations in the cytosolic Ca^{2+} concentration, which themselves result from the bursting electrical activity of β-cells (Gilon et al. 1993; Bergsten et al. 1994; Hellman 2009). Electrical activity of pancreatic β-cells, like all other excitable cells, is regulated by the ion channels expressed in their plasma membranes. In the initiation and modulation of the oscillatory insulin secretion, ATP-sensitive K^+ channels play a key role. These channels couple cell metabolism to the membrane potential and ensure that β-cells respond blood glucose levels properly.

Defects in the expression of K(ATP) channels have serious consequences because, without these channels, the insulin signaling apparatus can not sense the blood glucose level and fails to secrete the appropriate amount of insulin. In humans, K(ATP) channel deficiency leads to congenital hypoglycemia associated with excessive insulin secretion (Kane et al. 1996). β-cells

of these patients exhibit a high level of electrical activity and continuously secret insulin even when blood glucose is low. However, in mice, when K(ATP) channels are genetically knocked out, bursting electrical activity persists and the mice exhibit normal blood glucose levels unless metabolically stressed (Seghers et al. 2000; Düfer et al. 2004). This is paradoxical because when K(ATP) channels are blocked with pharmacological agents in wild-type mice β-cells, bursting electrical activity converts to continuous spiking and the cells exhibit a phenotype similar to human (Larsson et al. 1996; Gomis and Valdeolmillos 1998; Ren et al. 2013). That means the mechanism preserving oscillations in the K(ATP) channel deficient mice β-cells is not present or not effective in the wild-type cells. This indicates that mice can compensate for the genetic defects of K(ATP) channels by engaging alternative mechanisms. In this dissertation, we explore the consequences of genetic defects in the expression of the K(ATP) channels in β-cell membranes and investigate the compensatory mechanisms that are employed in mouse islets to overcome these defects.

In Chapter 2 we provide biological background for the following chapters. We begin with a brief historical sketch of the discovery of the insulin hormone and major pathological conditions associated with the impairments in the insulin-glucose network. We then give the biological motivation behind this study and explain the significance of the work. We illustrate the structure of the pancreatic islets with a deeper focus on β-cells and briefly explain mechanisms that have been proposed to explain the bursting electrical activity and resulting Ca^{2+} oscillations in these cells over the past decades. We discuss the structure of K(ATP) channels and explain the pathological consequences of their deficiency in humans. We introduce the biophysical concept of the activity-dependent homeostatic compensation through upregulation of other ion channel types in mice. We discuss the necessity of an accurate control mechanism for setting ion channel conductance levels and explain the crucial role that cytosolic Ca^{2+} plays as a control element in the homeostatic compensation.

Chapter 3 consists of a collaborative experimental and mathematical study that demonstrates upregulation of an inward rectifier K^+ current (Kir2.1 current) in mice in which islet K(ATP) channels are genetically knocked out (KO islets) and the mechanisms through which this upregulated current can drive Ca^{2+} oscillations in these cells. We start with

experimental data that show paradoxical Ca^{2+} oscillations in the KO cells and our novel finding that Kir2.1 current is upregulated in these cells. We introduce the mathematical model and illustrate the pathways through which upregulated Kir2.1 channels can take over the role of the K(ATP) channels in the knockout β-cells. We show that Kir2.1 channels can couple cell metabolism to the membrane potential through a cAMP dependent pathway and drive slow cytosolic Ca^{2+} oscillations in the KO cells. We then mathematically explore whether upregulation of other ion channel types can also compensate for the loss of K(ATP) channels. We propose an alternate mechanism that can also restore slow oscillations in the absence of K(ATP) channels and illustrate the differences between two models. We analyze the dynamics of both models in detail and perform *in silico* experiments to distinguish between them. We then describe *in vitro* experiments that were performed by a collaborating lab to test our model predictions, the results of which lend support to the Kir2.1 compensation model

In Chapter 4 we address the question of how the β-cell determines the correct level of compensating current upregulation so that oscillations are restored. We discuss the necessity of an accurate control mechanism and demonstrate that gene regulation via cytosolic Ca^{2+} can be employed as a control element for determining the appropriate level of upregulation. We introduce a mathematical model for a Ca^{2+}-oscillation-frequency sensitive gene transcription network and analyze this network with respect to its frequency decoding properties. We show that the proposed gene regulation network is sensitive to the pattern of the Ca^{2+} signal and hence it can naturally define a target pattern of activity for compensation. Finally, incorporating the Ca^{2+} frequency decoding gene transcription network into a well-studied β-cell model, we show that this mechanism can dynamically set the compensating current conductance to the right level and restore homeostasis when K(ATP) channels are knocked out. We illustrate the evolution of the dynamics of the model cell throughout the compensation process and make testable predictions for future work.

Chapter 5 concludes the dissertation by giving a summary of the work and future perspectives.

CHAPTER 2

BIOPHYSICAL BACKGROUND AND SIGNIFICANCE

2.1 The History of Diabetes and the Discovery of Insulin

Insulin is the body's only hormone capable of reducing blood glucose and it is secreted from pancreatic β-cells at elevated blood glucose levels. Insulin reduces blood glucose by activating insulin receptors on the liver, muscle and adipose cells and initiating glucose uptake in these tissues. There are several pathological conditions identified to be directly related to the impairments in the insulin-glucose regulation network. The most intensively studied conditions are insulin resistance, persistent hyperinsulinemic hypoglycemia of infancy and diabetes mellitus.

Insulin resistance is associated with the body's inability to efficiently utilize insulin. Under normal conditions, increased blood glucose leads to increased insulin secretion, which activates glucose uptake in the target tissue cells. However, in patients with insulin resistance, cells become insensitive to the insulin and hence insulin does not activate proper glucose uptake into these cells. Consequently, sustained high blood glucose forces pancreatic β-cells to increase insulin release, which may ultimately result with β-cell failure. Insulin resistance is a precursor of diabetes mellitus and appears years before the diagnosis of the disease (Leibiger et al. 2008; Olokoba et al. 2012).

Persistent hyperinsulinemic hypoglycemia of infancy (PHHI) is the pathological condition where excessive amounts of insulin is secreted by β-cells even when blood glucose is low (Kane et al. 1996). The disease is caused by impairments in the glucose sensing mechanisms in pancreatic β-cells due to genetic defects. Pancreatic β-cells of these patients lack the key mechanisms that sense the blood glucose levels and stop insulin secretion when blood glucose is low. Therefore, β-cells of these patients continuously secret insulin, which leads to hypoglycemia. In patients with PHHI, excessive activity may eventually lead to β-cell failure, which results in diabetes that requires insulin treatment (Huopio et al. 2003).

Among the metabolic diseases, diabetes mellitus is by far the most common one. There are two types of diabetes mellitus, called type 1 diabetes mellitus (T1DM) and type 2 diabetes mellitus (T2DM). Patients with T1DM constitute approximately 5% of the total diabetic population. T1DM results from complete loss of insulin secreting β-cells due to malfunctioning autoimmune responses and patients with the disease depend on insulin injections (Van Belle et al. 2011). T2DM is the more common form of the disease, which is associated with impairments in insulin secretion from β-cells and the body's inability to use insulin properly. T2DM also leads to β-cell death and insulin dependency in later life (Olokoba et al. 2012). In the development of the both forms of the disease, genetic and environmental factors such as diet and life style play a role. At early stages, T2DM can be treated with drugs that target hormonal, metabolic or electrophysiological pathways that either amplify insulin secretion from the pancreas or reduce glucose production in the liver (Olokoba et al. 2012). However, severe T2DM as well as T1DM can only be treated with insulin injections, or islet transplants, or pancreas transplants (Eisenbarth et al. 2011). According to the Center for Disease Control and Prevention: *National Diabetes Statistics Report 2014*, 29.1 million Americans were diagnosed with diabetes in 2012, which was over 9% of the entire population. In 2010, diabetes was reported as the cause of 69,071 deaths, and was a contributing factor to an additional 234,041 deaths. According to the report the total cost of diabetes to the United States was 245 billion dollars in 2012.

The first records of pathological conditions that are associated with impaired blood glucose regulation goes back more than two millennia. The term diabetes first appears in ancient texts as "diabaino", which means "to go or run through" (Laios et al. 2012). In his work from the 1st century AD, Areateus of Cappadocia gives the description and the symptoms of the disease as follows: "Diabetes is a remarkable affliction, not very frequent among men… The course is the common one, namely, the kidneys and the bladder; for the patients never stop making water, but the flow is incessant, as if from the opening of aqueducts… The nature of the disease, then, is chronic, and it takes a long period to form; but the patient is short-lived, if the constitution of the disease be completely established; for the melting is rapid, the death speedy. Moreover, life is disgusting and painful… Hence, the disease appears to me to have got the name diabetes as if from the Greek word διαβήτης (which signifies a siphon), because the fluid does not remain in the body, but uses the man's body as a ladder, whereby to leave it." (Adams 1856). The

characterization and the symptoms given by Areateus are significantly accurate. In his work, he also suggests remedies for the disease but, unfortunately, they are not effective measures in the treatment of the disease. Eighteen centuries after the name diabetes was established, the 17th century English anatomist and physician Thomas Willis coined the name "mellitus", Latin for honey, and used the name 'diabetes mellitus' for the first time (Ahmed 2002).

In 1869 in Berlin, a medical PhD student, Paul Langerhans, made the discovery of distinct cell clusters located within the rabbit pancreas. Even though he could not suggest a functional role for these cell clusters, in his doctoral thesis he referred to these richly innervated structures as "clear cell clusters" ("Zellhaufen") (Morrison 1937). These were, as we know now, clusters of endocrine cells, including pancreatic β-cells. These micro-organs are named after him as 'islets of Langerhans'. Luck and being at the right place at the right time have always been key contributors in the scientific discoveries in many fields. The first conclusive evidence for the role that the pancreas plays in blood glucose regulation came in 1889 as a coincidence when Oscar Minkowski and Joseph von Mering performed a pancreatectomy on dogs to study the role that the pancreas plays in digestion. After the operation, they discovered glucose in the dogs' urine when they noticed that flies were feeding off the urine (Von Engelhardt 1989). These experiments showed that the pancreas played an important role in blood glucose regulation. The discovery of the role that islets of Langerhans play in diabetes was made in the John Hopkins University by Eugene Lindsay Opie in 1900. He examined the pancreas of a patient recently deceased from diabetes and discovered that the islets were significantly degenerated. This discovery directed closer attention to the islets in the search for therapies to diabetes (Kidd 1971).

Finally, in 1921 a group of Canadian researchers at the University of Toronto performed a series of groundbreaking experiments. Physician Frederick Banting and medical student Charles H. Best discovered insulin in pancreatic extracts of dogs. Injecting the hormone into a dog, they found it lowered blood glucose levels. With the help of Canadian chemist James B. Collip and Scottish physiologist J. J. R. Macleod they developed insulin for human subjects and successfully treated the first patient in 1922. In 1923 Banting and Macleod, who developed a procedure for purifying insulin from pancreatic extracts, were awarded with the Nobel Price for

their discovery (Rosenfeld 2002). It is noteworthy to mention that, even though Macleod immediately offered half of his prize money to Best, the selection of Macleod but not Best by the Nobel Committee was considered to be unfair by the scientific community, especially by Banting, at the time (Rosenfeld 2002). In this short historical sketch, only a handful of researchers who contributed to this great discovery were mentioned. There are several other contributors who must also be given credit.

2.2 Pancreatic Islets and β-cells

Islets of Langerhans are endocrine cell clusters located in the pancreas (Fig. 2.1), and are separated from the surrounding tissue by a thin layer of fibroblasts (Stendahl et al. 2009). Islets are richly vascularized structures such that, even though they only constitute 1-2% of the total pancreatic volume, they receive 10-15% of the blood that flows through the pancreas (Stendahl et al. 2009). There are between 250,000-1,000,000 islets in a healthy adult human pancreas and each islet contains approximately 1000 endocrine cells (Tomita 2002). The three major endocrine cell types expressed in pancreatic islets are somatostatin secreting δ-cells, glucagon secreting α-cells and insulin secreting β-cells. Somatostatin is also known as the growth hormone inhibiting hormone, which regulates neurotransmission and cell proliferation through its action on G-protein coupled receptors. Somatostatin is involved in the regulation of several key hormones in the body, including the inhibition of glucagon and insulin secretion from pancreatic islets (Weckbecker et al. 2003). Glucagon is another key player in blood glucose regulation. The hormone is secreted from α-cells in response to low blood glucose concentrations and results in the breakdown of stored glycogen in the liver to glucose, which is then secreted into the blood stream through a process called glycogenolysis (Quesada et al. 2008). It also inhibits liver glucose consumption, which helps to increase the blood glucose level. The action of glucagon is balanced by the counter action of insulin in the body.

2.2.1 Insulin Secretion and Action

Insulin controls the blood glucose level by activating insulin receptors on the liver, muscle and adipose cells, which require insulin for glucose uptake (Alberts et al. 2008). Glucose

taken up by these cells is either stored or metabolized for the energy needs of the cell. Cells in the brain, nervous system, heart, vessels and kidney do not need insulin for glucose uptake. Therefore, when there is impairment in insulin secretion, exposure to prolonged high blood glucose increases glucose levels excessively in these cells. Consequently, increased cellular glucose causes damage in these tissues by preventing normal cell functioning. Hence, the hyperglycemia that is associated with deficient insulin secretion causes several complications in the body, including kidney and vascular diseases, and neural damage. Impaired insulin-glucose regulation also affects lipoprotein metabolism and increases plasma triglyceride levels, which can lead to heart diseases and increased risk of stroke (Taskinen and Borén 2015).

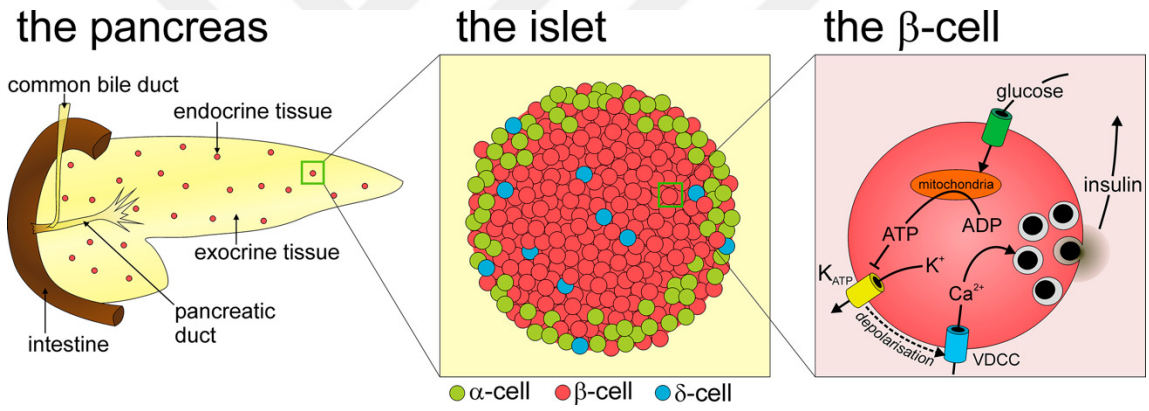

Figure 2.1. Endocrine tissue of the pancreas and islet structure. Structure of the pancreas and endocrine cell distribution within a mouse islet are pictured on the left and middle panels, respectively. The mechanism for glucose-induced insulin secretion in a single β-cell is depicted in the right panel. Adapted from (MacDonald and Rorsman 2006).

Insulin is produced in the pancreatic β-cells' endoplasmic reticulum in its inactive form as proinsulin, which is composed of a polypeptide chain-A and a polypeptide chain-B linked by a connecting terminal-C. Proinsulin molecules are then folded and two disulfide bonds are established between polypeptide chains A and B. After that, the insulin molecule is activated by the removal of the C-terminal from the complex. The mature form of the insulin molecule is then packed into granules and stored inside the cytosol (Weiss et al. 2000). Increased blood glucose initiates a chain of events and leads to exocytosis of granules and insulin secretion (Rorsman and Braun 2013). Pancreatic islets are well vascularized structures and hence β-cells can quickly respond to increased blood glucose levels. When the blood glucose concentration is increased,

glucose transport into β-cells also increases, which is mediated by the GLUT-2 glucose transporter protein located in the β-cell plasma membrane (Rorsman and Braun 2013). Inside the β-cells, glucose is metabolized and adenosine triphosphate (ATP) is produced. Increased ATP blocks K(ATP) channels in the plasma membrane, which carry hyperpolarizing outward current when they are open. Therefore, blockade of these channels by ATP leads to membrane depolarization, which activates voltage-dependent Ca^{2+} ion channels and increases Ca^{2+} influx. The subsequent increase in cytosolic Ca^{2+} evokes the exocytosis of insulin filled granules and secretion (Fig. 2.1, right panel). The dependency of exocytosis of insulin granules on the rise of the cytosolic Ca^{2+} concentration is well established, but the exact mechanism is unknown (Henquin 2009). It is also known that glucose metabolism has an additional, amplifying effect on insulin secretion. Despite the significant experimental evidence showing this amplifying effect, the exact pathways have not yet been identified (Nenquin et al. 2004).

2.2.2 Glucose Metabolism in β-cells

Pancreatic β-cells are unique endocrine cell types in their ability to respond directly to changes in the blood glucose concentration. They do that by coupling cell metabolism to the membrane potential through an ATP-dependent pathway. ATP is the molecular energy currency of the cell and it transfers energy through its high energy phosphate groups (Alberts et al. 2008). Stored chemical energy in the bound phosphate groups of ATP molecules are released and used for regulating cellular processes that require energy. When one phosphate group of an ATP molecule is released, a lower energy containing molecule, adenosine diphosphate (ADP), is produced. However, in the regulation of the K(ATP) channel activity, ATP does not transfer energy but instead acts as a second messenger.

ATP is produced from ADP through cellular metabolism. β-cells metabolize glucose through the same well-known processes that is used by all other eukaryotic cells (Fig. 2.2). The initial process of glucose metabolism is glycolysis, in which glucose is broken down to pyruvate (Alberts et al. 2008) (Fig. 2.2, left), which is the substrate of mitochondrial respiration (Fig. 2.2, right). Glycolysis starts with the phosphorylation of the glucose molecules to glucose 6-phosphate (G6P) by attachment of a phosphate group from an ATP molecule to the 6^{th} carbon

atom of glucose. The next step of glycolysis is the isomerization of G6P to fructose 6-phosphate (F6P). This step is catalyzed by the enzyme phophoglucose isomerase (PGI). Isomerization is a reaction in which the product has the same atoms as the substrate, but with a different arrangement. The next step in glycolysis is phosphorylation of F6P to fructose 1-6-bisphosphate (FBP). As the name of the product indicates, in this reaction another phosphate group from an ATP molecule is linked to the carbon molecule of the F6P, at the 1st position. This step is catalyzed by the enzyme phosphofructokinase (PFK), which plays the key role in the generation of glycolytic oscillations that can sometimes occur (Tornheim 1997). In the next reaction, the enzyme aldolase cleaves FBP and produces two molecules that each contain three carbon atoms: glyceraldehyde 3-phosphate (GADP) and dihydroxyacetone phosphate (DHAP).

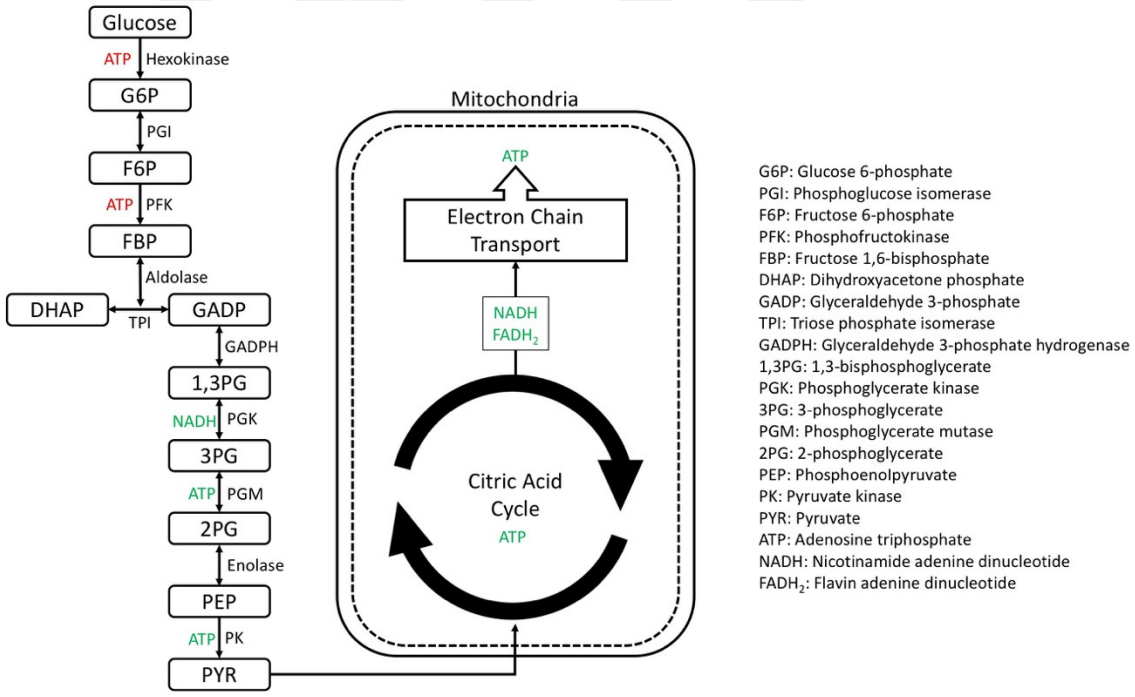

Figure 2.2. Glucose metabolism. In eukaryotic cells, glucose is metabolized through glycolysis (left) and mitochondrial respiration (right), which take place in the cytosol and mitochondria, respectively.

The glycolytic steps explained above are considered as preparation steps, where energy is actually consumed. These steps are followed by payoff steps, where energy is produced. GADP that is produced at the end of the preparation steps is converted to 1,3 bisphosphoglycerate (1,3BPG) through oxidation, which is the first step of energy production in glycolysis since a

molecule of NADH is produced and a high-energy phosphate linkage is established in this step. The DHAP produced in the previous step can also be converted to GADP by triose phosphate isomerase (TPI) and can be added to the glycolytic chain. Therefore, payoff steps usually occur twice for each glucose molecule. The high-energy phosphate group linkage established in the previous step is transferred to an ADP molecule by phosphoglycerate kinase (PGK) and one molecule of ATP and one molecule of 3-phosphoglycerate (3PG) are produced. Then 3PG is converted to 2-phosphoglycerate (2PG) by moving the phosphate group on the 3rd carbon to the 2nd carbon. One molecule of water is removed from 2PG by the enzyme enolase and a molecule of phosphoenolpyruvate (PEP) is produced. Finally, PEP is converted to pyruvate by transferring the remaining phosphate group to an ADP molecule, producing another ATP molecule. Thus, from each glucose molecule there is a net production of two molecules of ATP and two molecules of NADH.

The chain of reactions comprising glycolysis is followed by mitochondrial respiration (Alberts et al. 2008). In this step, the pyruvate produced through glycolysis is transported into the mitochondria, where it is further metabolized through the citric acid cycle and electron chain transport. From the citric acid cycle, each pyruvate molecule results in the production of 2 molecules of ATP, 3 molecules of NADH and 1 molecule of $FADH_2$. The NADH and $FADH_2$ are used to establish electron chain transport and a proton gradient across the mitochondrial inner membrane, which underlies oxidative phosphorylation, where the majority of the ATP is produced. From the breakdown of one glucose molecule approximately 30 ATP molecules are produced on average (Alberts et al. 2008).

2.2.3 Insulin Oscillations

Overall insulin secretion from the pancreas into the hepatic portal vein is oscillatory, with a period ranging from tens of seconds to several minutes (Pørksen 2002; Nunemaker et al. 2005; Song et al. 2007; Matveyenko et al. 2008). Insulin oscillations are known to have physiological importance for normal blood glucose regulation (Matthews et al. 1983b; Paolisso et al. 1991; Hellman 2009). In a recent study, using a hepatic portal vein insulin infusion protocol, it was shown that the liver uptakes glucose more effectively when insulin is delivered in an oscillatory

fashion rather than when it is infused at a constant rate (Matveyenko et al. 2012). In addition, insulin oscillations are impaired in type 2 diabetic patients and their near relatives (Matthews et al. 1983a; O'Rahilly et al. 1988; Polonsky et al. 1988). It is not clear whether disrupted insulin oscillations are among the causes or the consequences of the type 2 diabetes. However, experimental evidence demonstrates the importance of the oscillations, which makes understanding the mechanisms underlying them vital.

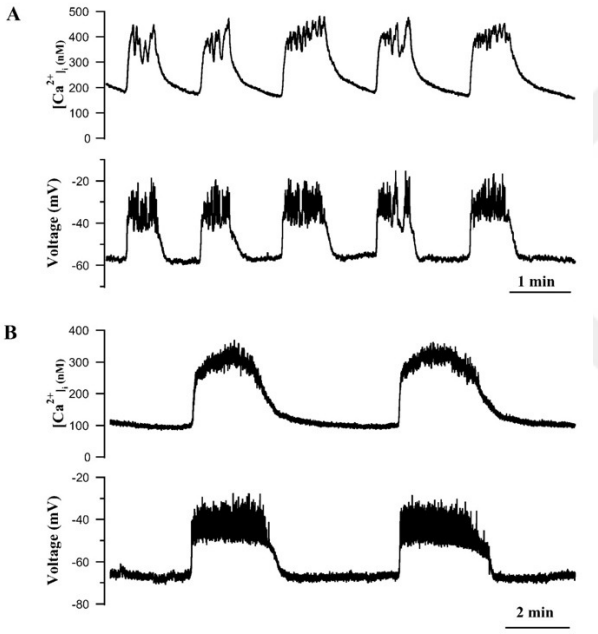

Figure 2.3. Simultaneous cytosolic Ca^{2+} and voltage recordings in pancreatic islets. Synchronous Ca^{2+} (top) and voltage (bottom) oscillations in two different islets. Adapted from (Zhang et al. 2003) with permission.

Plasma insulin oscillations result from the bursting electrical activity of the single β-cells and their intra- and inter-islet synchronization. The biophysical mechanism underlying the inter-islet synchronization is unknown, but the intra-islet synchronization is a result of the gap-junctional coupling between β-cells within islets (Gilon et al. 2002). Gap-junctions are protein structures that are located on the β-cell plasma membranes and which ion flux between connected cells. This electrical coupling allows β-cells to function in synchrony with the neighboring cells within the islet.

At stimulatory levels of glucose, pancreatic β-cells exhibit bursting electrical activity and cytosolic Ca^{2+} oscillations. A burst is a depolarized phase of action potentials followed by a hyperpolarized long silent phase. *In vitro* electric recordings and simultaneous Ca^{2+} imaging show that Ca^{2+} oscillations are well coupled with bursting electrical activity in pancreatic β-cells (Fig. 2.3) (Zhang et al. 2003). Ca^{2+} oscillations result from the activation of voltage-gated Ca^{2+} channels during each burst and result in oscillatory insulin secretion (Gilon et al. 1993; Bergsten et al. 1994; Hellman 2009). Several mechanisms have been proposed to explain the dynamics of busting in pancreatic β-cells (Chay and Keizer 1983; Keizer and Magnus 1989; Fridlyand et al. 2003; Cha et al. 2011). One theory is based on the negative feedback provided by cytosolic Ca^{2+}, which acts on the membrane potential in two ways: (1) directly by activating a hyperpolarizing Ca^{2+}-sensitive K^+ current (Atwater et al. 1980) and (2) indirectly by increasing ATP consumption by Ca^{2+}-ATPase pumps (Detimary et al. 1998) and regulating ATP production (Keizer and Magnus 1989). The latter indirect pathways act on the membrane potential by regulating cytosolic ATP concentration and the activity of the K(ATP) channels. An alternative mechanism suggests that in β-cells bursting electrical activity results from glycolytic oscillations due to the allosteric activity of the enzyme phosphofructokinase (PFK) (Tornheim 1997). According to this theory, oscillations in glycolysis eventually lead to oscillations in ATP production, which drives bursting electrical activity by turning K(ATP) current on and off. This theory is supported by data showing that the PFK isoform that is dominantly expressed in pancreatic β-cells drives glycolytic oscillations in muscle extracts (Tornheim 1988).

A recent mathematical model, which is a combination of two of these mechanisms, can reproduce bursting with a wide range of periods, as has been observed in experiments (Bertram et al. 2007). In this model, one mechanism is responsible for producing fast oscillations, while the other produces slow oscillations. Both mechanisms can oscillate independently, which gives the model the name the Dual Oscillator Model (DOM) (Fig. 2.4). In the DOM, the fast bursting results from the negative feedback provided by Ca^{2+} on the membrane potential through Ca^{2+}-activated K^+ current. The oscillations that have longer periods result from the oscillations in the glycolytic chain (Fig. 2.4, blue). Glycolytic oscillations are driven by the action of the allosteric enzyme phosphofructokinase (PFK) (Smolen 1995; Tornheim 1997), which phosphorylates F6P to FBP in glycolysis. The activity of PFK is increased by its product FBP, which increases the

conversion rate of F6P to FBP. This positive feedback loop eventually causes F6P depletion, which causes FBP concentration to crash due to lack of substrate. Decreased FBP turns PFK off, which allows F6P to accumulate and restart the cycle. FBP oscillations produced this way drive oscillations in the downstream metabolites. Subsequent oscillations in the ATP production act on the K(ATP) channels and produce oscillations in K(ATP) current and lead to bursting (Bertram et al. 2004; Watts et al. 2014). With a recent modification, the stimulatory effect of Ca^{2+} on the mitochondrial ATP production through its action on the mitochondrial pyruvate dehydrogenase (PDH) (Denton 2009) is incorporated into the DOM (McKenna et al. 2016).

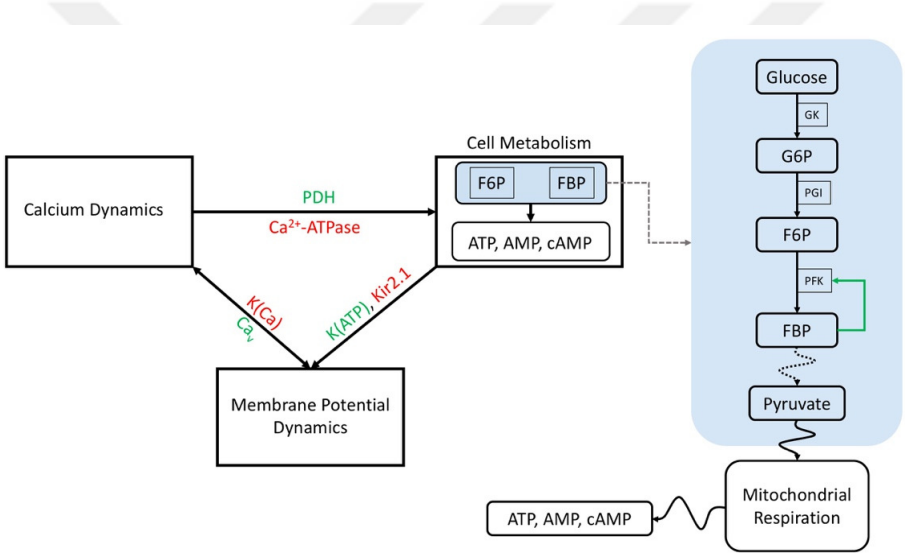

Figure 2.4. The Dual Oscillator Model (DOM). Multi-compartmental structure of the DOM, which has calcium, electrical, and metabolic compartments. Red indicates inhibitory and green indicates stimulatory pathways.

2.3 Electrophysiology of Pancreatic β-cells

2.3.1 Conductance-based Membrane Potential Models

Before introducing the details of the electrical properties of the pancreatic β-cells, in this section we briefly discuss the biophysical motivation behind the conductance-based membrane potential models, which are employed to describe the electrical properties of the β-cells in several computational models. In the conductance-based models, ion channels are the key elements, which are proteins that are located in the cell membranes. When they are in their open

state, ion channels conduct ionic current by allowing the flux of specific ion species down the concentration gradient. The concentration gradient of the ions is maintained by the ion pumps located in the cell membranes (Gadsby 2009), which pump ions against their concentration gradient by hydrolyzing ATP. Since ions are charged particles, their separation by the phospholipid bilayer of the cell membrane generates both concentration and electric gradients across the cell membrane. Thus, ion flow through channels is determined by the balance between these two forces. The equation that defines this balance for each ion species is derived from the Nernst-Planck equation and formulated by the Nernst equation as follows:

$$V_i = \frac{RT}{z_i F} ln\left(\frac{i_{out}}{i_{in}}\right) \quad , \tag{2.1}$$

where V_i is the equilibrium or reversal potential of the ion species i, T is the temperature, R is the gas constant, F is Faraday's constant, z_i is the ion valance and i_{out} and i_{in} are the extracellular and intracellular concentration of the ion species, respectively. This formulation is used for calculation of the reversal potentials or the Nernst potential of the ionic current in the conductance-based models.

The first conductance-based membrane potential model was developed on the basis of a series of groundbreaking experiments performed by Alan Hodgkin and Andrew Huxley in the early 1950s. The aim of these experiments was understanding the kinetics of the ion movements and action potential generation in neurons (Hodgkin and Huxley 1952a; Hodgkin and Huxley 1952b; Hodgkin and Huxley 1990; Grayson 2011). They were later awarded the Nobel prize in Physiology or Medicine for their work. In their experiments, they used a squid giant axon, which was large enough in diameter to pass a wire through it and thereby establish a spatially uniform system. The axon is also relatively simple, containing only one type of K^+ ion channel and one type of Na^+ ion channel. By making a series of electrical recordings via a sharp electrode, they were able to determine the roles of the two types of ion channels in the production of an action potential. After removal of the wire from the axon, they were also able to predict, with their mathematical model, the propagation characteristics of the action potential down the axon.

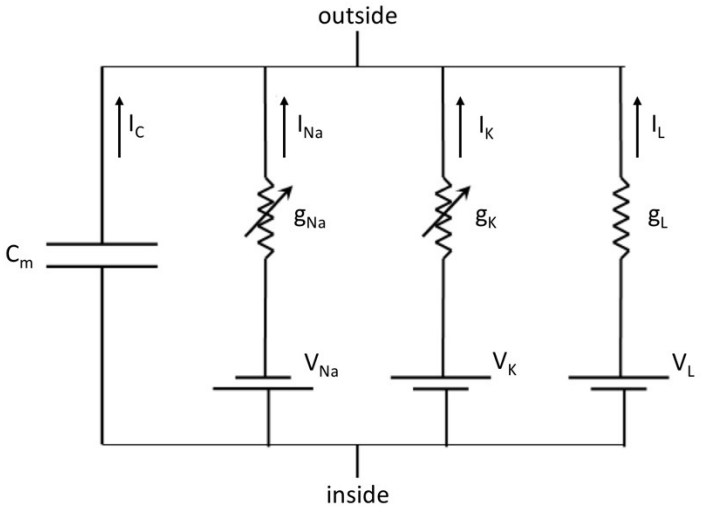

Figure 2.5. The circuit diagram for a patch of neural membrane. A representation of the simple circuit diagram that was introduced by K.S. Cole, which describes the electrical properties of a patch of a neural membrane.

In accordance with the groundbreaking work of Hodgkin and Huxley, K. S. Cole later suggested that the electrophysiological properties of a patch of a neural membrane can be described by an electric circuit diagram (Fig. 2.5) (Cole 1972). In the model he proposed, the phospholipid bilayer of the cell membrane is a capacitor that separates charge and ion channels act as variable resisters that conduct current. The batteries that drive charges in the circuit are the Nernst potential of the ion species. From this circuit model, one can use laws of physics to derive a differential equation for the potential difference across the circuit, or the membrane potential (V) of the cell. The circuit has three ionic currents, which were identified by Hodgkin and Huxley: a Na^+ current, a K^+ current and a leak current due primarily to the flux of chloride ions. In the model, Na^+ and K^+ currents are voltage activated and the leak current is passive. According to Kirchoff's current law, the sum of the currents across the branches of a parallel circuit must be zero. Therefore, the total current across the circuit diagram given in Fig. 2.5 is given by:

$$I_C + \sum I_i = 0 \quad , \tag{2.2}$$

where I_C is the capacitive current and I_i is the ionic current that is induced by the ion species i. The capacitive current is equal to the rate of change of the total charge that the capacitor holds, where the total charge, q, is given by:

$$q = C_m V \tag{2.3}$$

and

$$\frac{dq}{dt} = C_m \frac{dV}{dt} \quad , \tag{2.4}$$

where C_m is the capacitance of phospholipid bilayer. Substituting the rate of change of q by I_C, Eq. 2.2 becomes:

$$C_m \frac{dV}{dt} = -\sum I_i \quad . \tag{2.5}$$

This equation gives the rate of change of the membrane potential across a patch of cell membrane.

Ionic current that flows through an ion channel depends on the difference between the membrane potential and the reversal potential of the ion species, and the conductance provided by the ion channel. Each ionic current I_i given in Eq. 2.5 is then formulated by an equation of the following form that is derived from Ohm's law:

$$I_i = g_i m_i (V - V_i) \quad , \tag{2.6}$$

where g_i is the maximal conductance of the ion channel, m_i is the activation variable of the channel and V_i is the reversal potential of the corresponding ion species. The maximal conductance is the total conductance provided by all channels of a single type when they are all in their open states. The activation variable, $m_i \in [0,1]$, represents the probability of that channel type's being in an open state. The open probability of a channel can depend on the concentration

of a chemical, membrane potential, temperature or the mechanical tension applied to the channel (Hille 2001; Marks et al. 2009). The activation variable is then given by an algebraic or a differential equation that depends on either one of these components or a combination of several of them. For example, in the β-cell model that we use, the delayed rectifier K^+ current is described with the following equation:

$$I_K = g_K n(V - V_K) \quad , \tag{2.7}$$

where g_K is the maximal conductance provided by the voltage-gated K^+ channels and n is the voltage dependent activation variable and its rate of change is given with the following differential equation:

$$\frac{dn}{dt} = (n_\infty(V) - n)/\tau_n \quad , \tag{2.8}$$

where τ_n is the time constant that determines how fast the activation variable approaches to its steady-state value, $n_\infty(V)$, that is given with the following Boltzmann relation:

$$n_\infty(V) = \frac{1}{1+e^{(V_{sk}-V)/S_K}} \tag{2.9}$$

where V_{sk} is the half-activation potential and S_K is the slope factor that determines the sensitivity to the voltage. For the currents whose activations are assumed to be instantaneous, activation variables are usually set to the steady state activation functions. For the leak or passive currents, activation variables are assumed to be constant and equal to 1.

2.3.2 Electrical Properties of Pancreatic β-cells

Pancreatic β-cells produce bursting electrical activity due to the actions of ion channels they express in their plasma membranes, similar to that of neurons (Rorsman et al. 2011). Depolarization of the β-cell membrane is induced by Ca^{2+} ion channels. β-cells express three types of Ca^{2+} channels in their plasma membranes: L-type, R-type and P/Q-type Ca^{2+} channels

(Satin and Cook 1985). These are voltage-dependent ion channels and their activation requires depolarization of the cell membrane. When K(ATP) channels are blocked by increased ATP, the resulting depolarization of the cell membrane causes conformational changes in the voltage-dependent channels and activates them. In β-cells, under normal conditions, extracellular Ca^{2+} concentration is higher than the intracellular Ca^{2+} concentration. Therefore, activation of Ca^{2+} channels (Ca_v channels) allows Ca^{2+} ions to flow into the cell down the concentration gradient, which further depolarizes the cell membrane.

Other important ion channels expressed in the β-cell membranes are K^+ ion channels. There are three major types of K^+ channels expressed in β-cell membranes, which are Ca^{2+} activated K^+ channels (K(Ca) channels), ATP sensitive K^+ channels (K(ATP) channels) and delayed rectifier K^+ channels (K_v channels). Unlike Ca^{2+}, the intracellular concentration of K^+ is higher than its extracellular concentration. Therefore, K^+ channels conduct hyperpolarizing outward currents when they are activated. Activation of K(Ca) and K(ATP) channels depend on the cytosolic Ca^{2+} and ATP concentrations, respectively. Since concentrations of these molecules change on relatively slower time scales, K(Ca) and K(ATP) currents do not play a direct role in the production of action potentials. Instead, K(Ca) and K(ATP) currents are responsible for packaging action potentials into bursts (Fig. 2.6). In contrast, activity of the delayed rectifier K^+ channels is regulated by voltage. Therefore, they respond directly to the depolarization induced by Ca^{2+} current and repolarize the cell membrane during the downstroke of an action potential. When β-cell membrane is depolarized over the action potential threshold, first voltage-dependent Ca^{2+} channels get activated, which further depolarizes the cell membrane and generates the upstroke of an action potential. This activates delayed rectifier K^+ channels, which causes the action potential downstroke (Fig. 2.6, inset).

Pancreatic β-cells also express voltage gated Na^+ channels (Na_v channels) in their plasma membranes, which have both voltage-dependent activation and inactivation properties. However, the isoforms of the Na_v channels that are expressed in the mouse β-cells are inactivated at very low voltages (Plant 1988). Therefore, Na_v current does not have a substantial effect on the membrane potential and hence it is not included in the β-cell models.

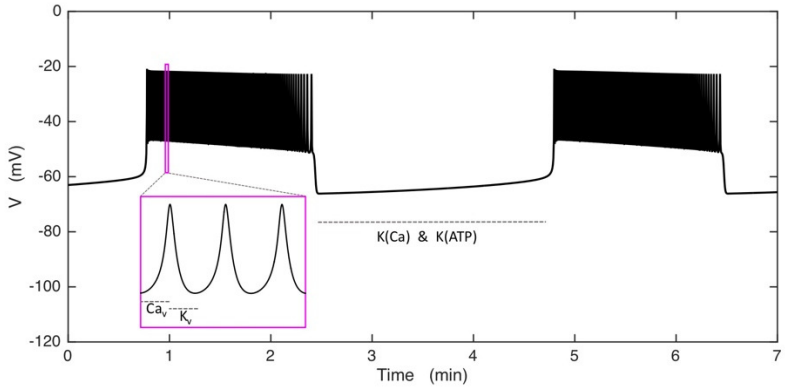

Figure 2.6. Bursting in the model β-cells. In Dual Oscillator Model, voltage-activated Ca^{2+} and K^{+} currents (Ca_v and K_v, respectively) generate action potentials, while K(Ca) and K(ATP) currents package action potentials into bursts.

Producing bursting electrical activity at stimulatory levels of glucose is a distinctive feature of pancreatic β-cells. A burst is a multiscale oscillation where trains of fast oscillations (action potentials) are separated by long hyperpolarized silent phases (Fig. 2.6). In the proposed β-cell model (the DOM) the slow negative feedback provided by K(Ca) and K(ATP) currents is responsible for the long hyperpolarized silent phases that separate trains of action potentials (Fig. 2.6). K(Ca) current is Ca^{2+} sensitive and activated by increased cytosolic Ca^{2+} concentration, where K(ATP) current is sensitive to the ratio of the cytosolic concentration of ATP to ADP. Increased blood glucose concentration increases the conversion rate of ADP to ATP through cell metabolism, which increases the ATP/ADP ratio. The increased ATP/ADP ratio leads to inactivation of the K(ATP) current and depolarizes the cell membrane. The glycolytic oscillations explained above lead to oscillations in the ATP/ADP ratio and drives membrane potential oscillations by turning K(ATP) current on and off. In the DOM, during the active phase of a burst, the ATP/ADP ratio declines, which eventually leads to reactivation of the K(ATP) current. Also during the active phase of a burst the cytosolic Ca^{2+} concentration is increased, which hyperpolarizes the cell membrane by activating K(Ca) current. These two currents provide enough negative feedback for termination of the active phase of a burst by hyperpolarizing the cell membrane. During the following silent phase, cytosolic Ca^{2+} concentration declines and the ATP/ADP ratio concentration increases, which eventually restarts an active phase of electrical activity. Together these two currents time bursts and drive membrane potential oscillations.

2.3.3 K(ATP) Channels and Their Deficiency

Electrical activity of pancreatic β-cells is regulated by the plasma glucose level, which exerts its regulatory effect by inducing blockade of K(ATP) channels in a concentration dependent manner. In fasting mice, a low blood glucose concentration of 5 mM can block approximately 90% of the K(ATP) channels (Smith et al. 1990). However, the remaining 10% of the K(ATP) channels are enough for keeping the membrane potential below the spike threshold. In a postprandial state plasma glucose concentration increases to 8-10 mM, which can induce enough depolarization to increase the membrane potential above the spike threshold by blocking many of the remaining K(ATP) channels.

In the bursting mechanism explained above, K(ATP) channels play a significant role in both initiation and modulation of the bursting electrical activity by coupling oscillatory cell metabolism to the membrane potential. K(ATP) channels comprise two protein subunits: an inward rectifying K^+ channel subunit (Kir6.2) and a sulfonylurea receptor subunit (SUR1). Four Kir6.2 subunits constitute the K^+ ion selective pore and each one is associated with a SUR1 subunit (Nichols 2006). ATP inhibits K(ATP) channels by interacting with the Kir6.2 subunits, while SUR1 subunits are the targets of the family of channel blocking drugs called sulfonylureas. Sulfonylureas are a family of organic compounds, which are used in the treatment of type 2 diabetes mellitus (Seino 2012). These drugs increase insulin secretion by blocking K(ATP) channels at SUR1 subunits and depolarizing the cell membrane.

A disruption or mutation in the genes that regulate either Kir6.2 or SUR1 subunits prevents K(ATP) channel trafficking to the plasma membrane (Nichols 2006). Deficiency in the expression of functional K(ATP) channels causes persistent hyperinsulineamic hypoglycemia of infancy (PHHI) in human (Kane et al. 1996), a condition characterized by high insulin secretion even when the blood glucose level is low. Excessive insulin secretion in patients with PHHI results from the continuously high Ca^{2+} influx that is due to the membrane depolarization caused by the lack of the large hyperpolarizing K(ATP) current. These patients exhibit severe hypoglycemia due to the high electrical activity of their β-cells, which may lead to β-cell failure

and the development of type 2 diabetes that requires insulin treatment in later life (Huopio et al. 2003).

In order to study the role that K(ATP) channels play in β-cell activity and the amplifying role that glucose metabolism play in insulin secretion, researchers have developed genetically engineered K(ATP) channel deficient mice by suppressing the gene that regulates expression of SUR1 subunits ($SUR1^{-/-}$ mice) (Seghers et al. 2000; Nenquin et al. 2004; Szollosi et al. 2007). Just like PHHI patients, these mice β-cells do not express K(ATP) channels in their plasma membranes. However, in $SUR1^{-/-}$ mice β-cells (KO cells) bursting electrical activity and Ca^{2+} oscillations persist. Furthermore, these mice have almost normal blood glucose levels unless metabolically stressed (Seghers et al. 2000; Düfer et al. 2004). These knockout mice models have been studied extensively but no underlying mechanism has yet been identified for their β-cell oscillations or normal blood glucose levels (Seghers et al. 2000; Düfer et al. 2004; Nenquin et al. 2004). Even though the underlying mechanism for this unexpected behavior is not understood, it is evident that there is some form of compensation mechanism because in wild-type mice β-cells, when K(ATP) channels are blocked with sulfonylureas such as tolbutamide, the cell membrane is immediately depolarized and bursting oscillations are replaced by tonic spiking (Fig. 2.7) (Larsson et al. 1996; Gomis and Valdeolmillos 1998; Ren et al. 2013). That means the mechanism that underlies the oscillations in the KO cells is not present or not effective in the wild-type mouse β-cells. In other words, the mechanism that drives oscillations in the KO cells only becomes effective after a long-term loss of K(ATP) channels, which indicates compensation. Such a compensation can be achieved through upregulation of other types of K^+ channels. Studies show that in pancreatic β-cells long term exposure to K(ATP) channel blocking agents leads to cell apoptosis associated with excitotoxicity that is induced by elevated cytosolic Ca^{2+} as a result of the high electrical activity (Efanova et al. 1998; Iwakura et al. 2000; Maedler et al. 2005). Thus, exposure to long-term high electrical activity that follows K(ATP) channel knockout could cause β-cell death if not compensated. Therefore, homeostatic compensation that can be achieved through upregulation of another hyperpolarizing K^+ channel would both protect β-cells against excitotoxicity and restore their normal functional roles in the insulin-glucose regulation network.

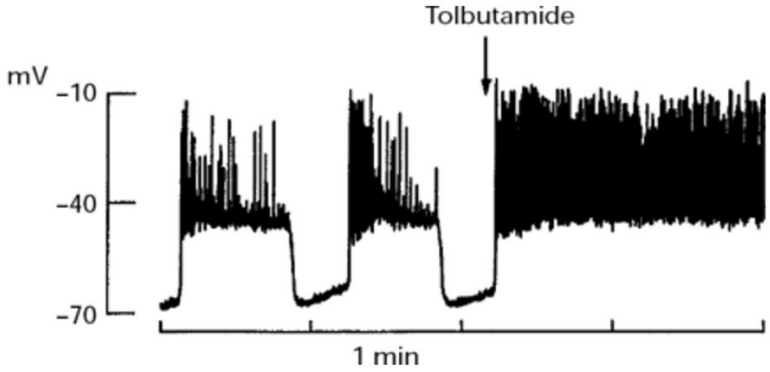

Figure 2.7. The effect of pharmacologically blocking K(ATP) channels in intact mouse islet β-cells *in vivo*. In electrical recordings from β-cells in intact mice a 50 μl injection of a 10 mM sulfonylurea (tolbutamide) solution immediately converts oscillations to tonic spiking. Adapted from (Gomis and Valdeolmillos 1998) with permission.

2.3.4 Kir2.1 Channels and Their Upregulation

Another K^+ ion channel type that is expressed in the β-cell membrane is the Kir2.1 inward rectifying K^+ channel (Riz et al. 2015). These channels conduct outward currents at voltages above the K^+ reversal potential, but they are blocked by membrane depolarization. This diode-like property is called inward rectification and results from the blockade of the channel pore by intracellular ions and polyamines as the membrane potential is increased (Matsuda et al. 1987; Lopatin et al. 1994; Bradley et al. 1999). In addition to the voltage dependency, Kir2.1 channels have phosphorylation sites for protein kinase-A (PKA) (Fakler et al. 1994; Brugada et al. 2013; Zhang L et al. 2013). One study shows that a phosphatase inhibitor can prevent rundown of the Kir2.1 current that is activated by PKA, which indicates activation of the channels is regulated by protein phosphorylation (Ruppersberg and Fakler 1996). PKA is also known as the cyclic adenosine monophosphate (cAMP) dependent protein kinase since it is activated by this nucleotide. In the absence of cAMP, PKA resides in the cytosol in its inactive form as a tetramer of two catalytic and two regulatory subunits (Alberts et al. 2008). In order to be activated, the catalytic subunits must be detached from the regulatory subunits and this is facilitated by cAMP, which binds to the regulatory subunits of PKA and causes a conformational change that detaches them from the catalytic subunits. Each catalytic subunit then independently phosphorylates target proteins on the specific phosphorylation sites.

cAMP takes place in several cellular processes as a second messenger and it is derived from ATP by the enzyme adenylyl cyclase (AC) and degraded by the enzyme phosphodiesterase (PDE) (Alberts et al. 2008). In pancreatic β-cells, Ca^{2+} dependent isoforms of both AC and PDE are expressed (Cooper et al. 1995; Pyne and Furman 2003). In addition to the Ca^{2+} dependency, adenosine monophosphate (AMP) is known to be a potent inhibitor of AC (Blume and Foster 1975; Londos and Preston 1977). Therefore, cAMP production is closely related with cytosolic Ca^{2+} and AMP concentrations. Recent fluorescent resonance energy transfer (FRET) based studies show glucose induced cAMP oscillations in pancreatic β-cells (Dyachok et al. 2006; Dyachok et al. 2008). One theory suggests that cAMP oscillations result from the AMP oscillations that themselves are driven by the glycolytic oscillations (Peercy et al. 2015).

In a recent study our collaborators (Satin lab at the Brehm Center for Diabetes Research at the University of Michigan) demonstrated an upregulation in Kir2.1 inward rectifying K^+ ion channel protein in mice in which the $SUR1^{-/-}$ subunit was knocked out in β-cells, stopping K(ATP) channel trafficking to the plasma membrane (manuscript in preparation). Since the activity of the Kir2.1 channels is regulated by cell metabolism through the cAMP dependent pathway explained above, it is arguable that in the KO cells these channels could be taking over the role that K(ATP) channels play in the modulation of slow Ca^{2+} oscillations in wildtype cells. This will, of course, depend on whether upregulated Kir2.1 protein actually has an electrophysiological function in regulating the membrane potential in these cells. In Chapter 3 we demonstrate that an inward rectifying K^+ current that is not present in the wild type β-cells is upregulated in the KO-cells. This upregulated current is most likely conducted by the upregulated Kir2.1 channels. Using mathematical modeling we demonstrate that Kir2.1 channels can indeed drive slow Ca^{2+} oscillations in the KO cells through a cAMP dependent pathway.

2.4 Homeostatic Compensation

If the upregulation of the Kir2.1 channels is the mechanism through which KO cells compensate for the loss of K(ATP) channels, then the question is how does the cell determine the right level of Kir2.1 channel expression? If the expression of the Kir2.1 channels is not high enough then they will not provide enough hyperpolarization and KO cells will remain in a

depolarized state. On the other hand, an excessive Kir2.1 channel expression will produce too much hyperpolarization, which will completely terminate the electrical activity. Yet, in KO islets there are bursting oscillations, just as in wild type islets. Therefore, there must be a control mechanism that continuously monitors the electrical activity of the cell and regulates the Kir2.1 channel expression accordingly to recover the wild type like behavior. This control mechanism is called activity-dependent homeostatic compensation, which can be achieved through regulated gene expression.

2.4.1 Activity-dependent Regulation of Gene Expression

Proteins are the building blocks of all living organisms. There are 20 different types of amino acids and each protein is composed of a different sequential combination of these amino acids bound through peptide bonds (Alberts et al. 2008). Information regarding the type of the amino acids that proteins contain and their sequential combinations are stored in the genetic material of the organism. The expression of proteins is regulated by a process called gene expression. Some genes are expressed on an almost constant rate throughout the life span of the organism while others are expressed when the protein that they code is needed. Cellular activity is one of the key determinants of this demand. Activity-dependent gene expression is most widely studied in the nervous system, where several transcription factors and enzymes that are associated with activity-dependent gene expression have been identified (Lyford et al. 1995; Jia et al. 2008). The development of motor and cognitive skills, like memory formation and learning, are closely related with the long-term plasticity that results from activity-dependent gene expression in the nervous system (Bruel-Jungerman et al. 2007; Maffei et al. 2012; Ganguly and Poo 2013). In addition, expression of several proteins including ion channels are regulated through activity-dependent gene expression in excitable cells (Turrigiano et al. 1994; Rosati and McKinnon 2004; Moody and Bosma 2005).

A gene is a piece of DNA that has a certain length and nucleotide sequence, which keeps the genetic code of a specific protein. Gene expression is the process where the information encoded in the nucleotide sequence of a gene is used for producing functional proteins. The initial step of gene expression is gene transcription, which takes place inside the nucleus in all

eukaryotic cells. Through gene transcription, messenger RNA (mRNA) molecules are produced by the enzyme RNA polymerase. The mRNA molecules leave the nucleus and enter the cytosol for translation, where mRNA molecules are used as templates by ribosomes for producing proteins from amino acids. Translation is followed by post-translational modifications, such as phosphorylation. The mature proteins are then trafficked to the cellular locations where they are needed (Alberts et al. 2008).

Even though, every step of gene expression is a regulated process, among these, the most intensively studied and probably the most important one is the transcriptional regulation since it is the initial step of the gene expression and affects all the subsequent steps. Gene transcription is primarily regulated by proteins called transcription factors, which either directly act on the RNA polymerase or bind to the specific nucleotide sequences on the promoter regions of the genes and assist or impede RNA polymerase binding (Alberts et al. 2008). The promoter region of a gene is a specific DNA sequence located upstream of the gene. The promotor sequences are not transcribed into the mRNA molecules but they play an essential role in gene transcription. Transcription is initiated when RNA polymerase binds to the promoter region of a gene. Once RNA polymerase binds to a gene, it moves downstream and reads the nucleotide sequence and copies this sequence into a strand of mRNA.

A transcription factor can either be an activator or an inhibitor, which promotes and suppresses gene expression, respectively (Alberts et al. 2008). Activity of several transcription factors are regulated through phosphorylation (Hunter and Karin 1992; Whitmarsh and Davis 2000). Some transcription factors are activated when they are phosphorylated (Segil et al. 1991; Oeckinghaus and Ghosh 2009), while others are activated when dephosphorylated (Rao et al. 1997). Phosphorylation is the process where a phosphate group is added to a molecule where dephosphorylation is the opposite. In living systems protein phosphorylation and its counterpart dephosphorylation are the most important regulators of cellular processes, which are catalyzed by enzymes called kinases and phosphatases, respectively. The activity of several isoforms of these enzymes is regulated by signals that depend on the cellular activity. Consequently, kinases and phosphatases transmit the information regarding cellular activity to the gene transcription machinery by regulating downstream transcription factors. Together with transcription factors,

activity-dependent regulation of these enzymes makes them key players in activity-dependent gene expression (Deisseroth and Tsien 2002).

2.4.2 Regulation of Ion Channel Expression and Compensation

The electrical activity produced by excitable cells is primarily determined by the type and density of ion channels distributed in their plasma membrane. There are three major processes that determine the regulation of ion channel expression in excitable cells: developmental regulation, homeostatic regulation, and mutation (Rosati and McKinnon 2004). Developmental regulation employs gene transcription at early developmental stages and results with a fixed outcome of a large number of ion channel distributions. Developmental regulation can lead to expression of different phenotypical cell types that have distinct ion channel distributions. Homeostatic regulation operates in response to the cellular demand during development and maturity. Through homeostatic regulation, expression of ion channels is determined by the current cellular demand and the activity of the cell, which ensures homeostatic functionality (Turrigiano et al. 1994; Temporal et al. 2014; O'Leary et al. 2014).

Most excitable cells express different channel types of the same ion species. Through this diversity they can maintain their electrophysiological properties throughout their life span even after perturbations, like defects in the expression of ion channels. Studies show that there is a bi-directional relation between cellular activity and ion channel expression, which provides activity-dependent homeostasis in case of a perturbation like genetic mutations or knockouts of ion channels (Turrigiano et al. 1994; Rosati and McKinnon 2004; Davis 2006; Temporal et al. 2014). In excitable cells, one way of maintaining homeostatic function when there is a defect in the expression of an ion channel is compensating the loss of this channel by regulating the expression of other ion channel types (Zhou et al. 2003; Xu 2003; Rosati and McKinnon 2004). This adaptation mechanism is referred to as activity-dependent homeostatic compensation, where the cell keeps track of the cellular activity by monitoring some signaling element and regulates expression of ion channels until a homeostatic target is achieved. In this process, the activity of the cell is transmitted to the gene transcription machinery through a signaling cascade that

involves activity-dependent enzymes and downstream transcription factors (Vigmond et al. 2001; Deisseroth and Tsien 2002).

Through activity-dependent regulation of ion channel expression the cell can maintain its functional role both at the single cell and the network level. In many cases the activity of excitable cells is regulated by the extracellular signals they receive. These signals can be transmitted as electrical or chemical signals, such as hormones or other molecules like glucose. For proper network functionality, it is crucial for these cells to respond to the signals they receive appropriately. Insulin secretion from pancreatic β-cells is regulated by blood glucose and it is crucial that these cells secrete the right amount of insulin at the right time. Insufficient insulin secretion at high blood glucose levels would lead to hyperglycemia while excessive insulin secretion when blood glucose is low would lead to hypoglycemia. Both conditions can be life threatening, particularly the latter, if not treated. Since insulin secretion results from the electrical activity of β-cells, maintaining their electrical properties is pivotal for the normal functioning of these cells and thus for normal glucose homeostasis. Activity-dependent gene regulation can ensure the right response by regulating the expression of ion channels in these cells by monitoring the activity of the cell. In addition to ensuring functionality, activity-dependent regulation of ion channel expression can also protect β-cells against apoptosis that can be induced by excitotoxicity (Efanova et al. 1998; Iwakura et al. 2000; Maedler et al. 2005).

2.4.3 Ca^{2+}-dependent Ion Channel Expression

Activity-dependent compensation mechanisms need a feedback element that can reflect the activity of the cell. Without a well-tuned feedback element, activity-dependent gene expression will operate like a truck without breaks and instead of restoring homeostasis it can produce pathological conditions (O'Leary et al. 2014). Due to the voltage-dependent Ca^{2+} channels expressed in their plasma membranes, electrical activity of pancreatic β-cells is well coupled with cytosolic Ca^{2+} (Zhang et al. 2003). Therefore, Ca^{2+} can be a very accurate readout for monitoring the activity of these cells. Furthermore, as a second messenger, Ca^{2+} is known to regulate the expression of several proteins, including ion channels in excitable cells (Sheng et al. 1991; Barish 1998; Vigmond et al. 2001; West et al. 2001). Computational studies show that

Ca^{2+} can indeed be a very accurate tuning signal for activity-dependent regulation of ion channel expression (LeMasson et al. 1993; Liu et al. 1998; Olypher and Prinz 2010; O'Leary et al. 2014).

One study on clonal rat insulinoma RINm5F cells shows that DNA synthesis is increased in these cell lines when K(ATP) channels are blocked with pharmacological agents for a long term (Sjöholm 1995). This study also shows that inhibiting Ca^{2+} influx or Ca^{2+} dependent enzymes reduces DNA synthesis in these cells. Together these results indicate that increased electrical activity due to the blockade of K(ATP) channels can regulate gene expression in insulin secreting cell lines through a mechanism that depends on cytosolic Ca^{2+}. Therefore, the Kir2.1 channel upregulation observed in K(ATP) channel deficient mouse pancreatic β-cells can be a result of increased cytosolic Ca^{2+} that is secondary to the increased electrical activity. In that case, Ca^{2+} could be the feedback element used by the KO cells to keep track of and regulate the expression of compensating channels. According to this hypothesis, when K(ATP) channels are knocked out, the cell membrane will be depolarized and the cytosolic Ca^{2+} concentration will be increased. High cytosolic Ca^{2+} will result in increased expression of compensating K^+ channels, which will provide negative feedback on the electrical activity by hyperpolarizing the cell membrane. The upregulation will continue until a homeostatic target is achieved. The question then is, what is this target and how is it imposed?

In gene transcription networks Ca^{2+} exerts its regulator effect by binding and activating Ca^{2+}-dependent enzymes, like Ca^{2+}-calmodulin dependent kinases, protein kinase-C, and calcineurin (Rosen et al. 1995; Vigmond et al. 2001). These enzymes then regulate the activity of transcription factors and gene expression. Theoretical and computational studies show that the information regarding cellular activity can be encoded in the frequency and amplitude of the Ca^{2+} signal (Dupont and Goldbeter 1998; Li et al. 2012; Smedler and Uhlén 2014). It has been shown that several cellular processes, such as activation of several transcription factors (Dolmetsch et al. 1998; Tsien et al. 1998; Zhu et al. 2008) and enzymes (Li et al. 2012), and mitochondrial responses (Hajnóczky et al. 1995; Robb-Gaspers et al. 1998; Collins et al. 2001) are sensitive to the frequency of the Ca^{2+} oscillations. In gene transcription networks, it has been shown that oscillatory Ca^{2+} is more effective than constant Ca^{2+} at regulating gene expression (Dolmetsch et al. 1998; Tsien et al. 1998). Furthermore, for some genes there is an optimum Ca^{2+}

oscillation frequency range for which their expression is maximized (Tsien et al. 1998; Zhu et al. 2008). Theoretical and computational studies show that, in gene regulation networks, increased efficiency and specificity due to the Ca^{2+} oscillations are results of the nonlinear interactions between network components (Dupont et al. 2003; Schuster et al. 2005; Salazar et al. 2008), which may result from cooperative Ca^{2+} binding, zero-order ultra-sensitivity, homo-dimerization or -trimerization and cooperative activation through multiple pathways (Zhang et al. 2013).

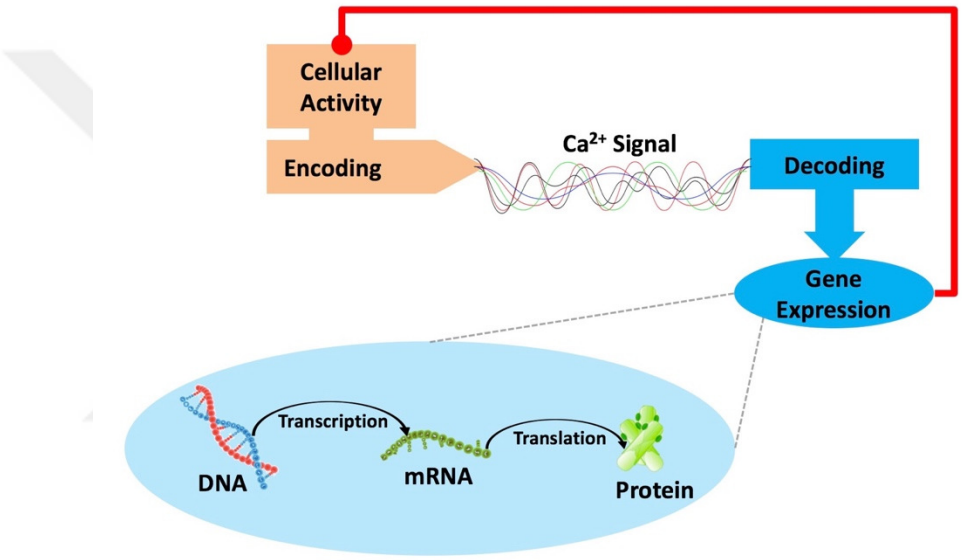

Figure 2.8. Activity-dependent homeostatic compensation. In the proposed model, activity of the cell is encoded in the Ca^{2+} signal, which is decoded by the gene transcription network. The expression of the compensating ion channel is then regulated according to that signal. The compensating channel completes the feedback loop by regulating cellular activity.

Together these findings indicate that Ca^{2+} oscillations can increase both efficiency and specificity of gene expression. Thus, in Ca^{2+} frequency sensitive gene transcription networks, when the same average concentration of Ca^{2+} is delivered with different patterns, each pattern will result in a different level of gene expression. Therefore, a Ca^{2+} frequency sensitive gene transcription network can decode the pattern of the Ca^{2+} signal and regulate ion channel expression according to that pattern (Fig. 2.8). Regulated ion channel expression will provide feedback on the membrane potential and regulate the cellular activity. In that case, the homeostatic target to be achieved will be determined by the pattern of activity of the cell that is encoded in the Ca^{2+} signal. Pancreatic β-cells produce bursting electrical activity, which is the

basis of oscillatory insulin secretion, and plasma insulin oscillations have physiological importance in blood glucose regulation. Therefore, a target that is defined by the oscillatory pattern of activity of these cells can be extremely beneficial for the insulin-glucose network. In Chapter 4 we introduce and analyze a Ca^{2+} frequency sensitive gene transcription network and show that this network can dynamically set the compensating channel conductance to the right level and restore homeostatic oscillations in model β-cells when K(ATP) channels are knocked out. We also demonstrate that gene regulation through two opposing Ca^{2+} dependent enzymes can lead to qualitatively distinct frequency responses, such that the gene transcription network can be adjusted to account for both monotonic and bell shaped frequency response regimes, which have been previously observed in experimental studies (Tsien et al. 1998; Zhu et al. 2008).

CHAPTER 3

DYNAMICAL ANALYSIS OF BURSTING IN SUR1$^{-/-}$ MOUSE β-CELLS

The results presented in this chapter are submitted to PLoS Computational Biology for publication (Yildirim V, Vadrevu S, Thompson B, Satin LS, Bertram R).

3.1 Introduction

In this chapter, we demonstrate that after gene-targeted deletion of K(ATP) channels, mice pancreatic islets exhibit sustained Ca^{2+} oscillations at stimulatory levels of glucose and that the level of an inward rectifying K^+ current is increased in the β-cells of these mice. We use mathematical modeling to explore the functional role that this current can have on the electrical activity of islet β-cells when K(ATP) channels are absent. In particular, we investigate whether this inward-rectifying K^+ current has the ability to rescue the normal electrical bursting pattern that characterizes the β-cells of SUR$^{-/-}$ mouse islets (KO cells). We also investigate whether upregulation of other K^+ channel types can also save slow Ca^{2+} oscillations. We introduce an alternative mechanism and analyze the dynamics of both models in detail. The models are used to design an experimental study that can distinguish between the two mechanisms. At the end of the chapter, we present the results of this experimental study, which shows that the model in which Kir2.1 channels drive bursting in KO β-cells is the more likely mechanism.

3.2 Incorporating cAMP and Kir2.1 Current Dynamics into the Dual Oscillator Model

An illustration of the β-cell model used in this chapter is shown in Figure 3.1. We used the Dual Oscillator Model (DOM), which has electrical, Ca^{2+} and metabolic components (Watts et al. 2014; McKenna et al. 2016). In the DOM, the fast oscillatory component is based on negative Ca^{2+} feedback onto the membrane potential through Ca^{2+}-sensitive K^+ current ($I_{K(Ca)}$). This mechanism can drive fast bursting. The second oscillatory component is due to metabolic oscillations, which result from the activity of the allosteric enzyme phosphofructokinase (PFK). In the process of glycolysis, PFK catalyzes the phosphorylation of fructose 6-phosphate (F6P) to fructose 1,6-bisphosphate (FBP). The activity of PFK is increased by its product FBP, so that

increased FBP increases the reaction rate and causes a sharp rise in FBP. This eventually depletes the substrate of the reaction, F6P and turns off flux through PFK, resulting in a reduction in FBP. This allows the substrate, F6P, to recover and the cycle to restart. Oscillatory FBP levels in turn cause oscillations in pyruvate, the end product of glycolysis and the substrate for mitochondrial respiration. The oscillatory glycolytic input results in oscillatory levels of the nucleotide concentrations (ATP, ADP and AMP). The membrane potential is then affected through the action of ATP and ADP on K(ATP) channels, which can drive slow bursting in the model.

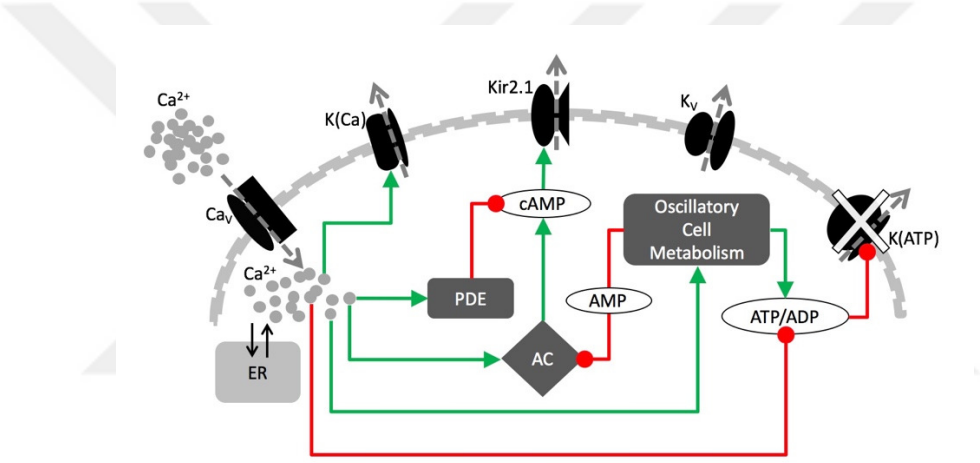

Figure 3.1. Key components of the model. Green arrows are for stimulatory and red circles are for inhibitory pathways. In the wild-type cells, bursting is paced by metabolic oscillations acting on K(ATP) channels. In the KO cells, genetic disruption of K(ATP) channels leads to increased Kir2.1 current, which now drives bursting.

Equations for the dynamics of cAMP were recently added to an earlier version of the DOM (Peercy et al. 2015) and it was shown that this version was capable of producing cAMP oscillations in model β-cells. We incorporate these equations into the current version of the DOM, where the cAMP concentration is determined by the difference between its production by adenylyl cyclase (V_{AC}) and degradation by phosphodiesterases (V_{PDE}):

$$\frac{dcAMP}{dt} = V_{AC} - V_{PDE} \tag{3.1}$$

where,

$$V_{AC} = \bar{v}_{AC}\left(\alpha_{AC} + \beta_{AC}\frac{c^3}{c^3+K_{ACca}^3}\right)\left(\beta_{amp}\frac{K_{amp}^2}{AMP_c^2+K_{amp}^2}\right) \tag{3.2}$$

$$V_{PDE} = \bar{v}_{PDE}\left(\alpha_{PDE} + \beta_{PDE}\frac{c^3}{c^3+K_{PDEca}^3}\right)\frac{cAMP}{cAMP+K_{PDEcamp}} \tag{3.3}$$

where c is the cytosolic free Ca^{2+} concentration, which stimulates both AC and PDE. Cytosolic AMP (AMP_c) inhibits AC and thus the production of cAMP (Blume and Foster 1975; Londos and Preston 1977; Johnson et al. 1989). We modified the V_{AC} equation from the original model to incorporate a higher-order dependence on AMP. In the model, slow cAMP oscillations are the result of AMP oscillations and the accompanying Ca^{2+} oscillations, which are both the product of glycolytic oscillations.

In the DOM, the rate of change of the membrane potential of a wildtype β-cell is given by a conductance-based Hodgkin-Huxley type equation:

$$\frac{dV}{dt} = -\left(I_K + I_{Ca} + I_{K(Ca)} + I_{K(ATP)}\right)/C_m \tag{3.4}$$

where, C_m is the membrane capacitance, I_K is the delayed rectifier K^+ current, I_{Ca} is a voltage-sensitive Ca^{2+} current, $I_{K(Ca)}$ is a Ca^{2+}-sensitive K^+ current and $I_{K(ATP)}$ is an ATP-sensitive K^+ current. The rate of change of the free cytosolic Ca^{2+} concentration is:

$$\frac{dc}{dt} = f_{cyt}\left(\overbrace{-\alpha I_{Ca} - k_{pmca}c}^{J_{mem}} + \overbrace{k_{leak}(c_{er} - c) - k_{SERCA}c}^{J_{ER}}\right) \tag{3.5}$$

where terms labeled by J_{mem} and J_{ER} represent the Ca^{2+} flux across the plasma membrane and net flux out of the endoplasmic reticulum (ER), respectively. Here, f_{cyt} is the fraction of free to total cytosolic Ca^{2+}, α converts current to flux, k_{pmca} is the Ca^{2+} pumping rate across the plasma membrane, k_{leak} is the rate of the Ca^{2+} leak from the ER and k_{SERCA} is the Ca^{2+} pumping rate into the ER. The ER Ca^{2+} concentration (c_{er}) is also dynamic and given by:

$$\frac{dc_{er}}{dt} = -f_{er}V_{cte}(k_{leak}(c_{er} - c) - k_{SERCA}c) \quad (3.6)$$

where f_{er} is the ratio of the free Ca^{2+} in the ER and V_{cte} is the ratio of the volume of the cytosol to the volume of the ER compartment. The equation for the Ca^{2+}-sensitive K^+ current ($I_{K(Ca)}$) is,

$$I_{K(Ca)} = g_{K(Ca)}\omega(V - V_K) \quad (3.7)$$

where, $g_{K(Ca)}$ is the maximal conductance of the current, and ω is the following Ca^{2+}-dependent activation function,

$$\omega = \frac{c^2}{c^2 + K_c^2} \quad (3.8)$$

where K_c is the affinity constant.

In the KO-cells lacking K(ATP) channels there is no $I_{K(ATP)}$ present. In the model KO-cells, K(ATP) current is replaced by the following Kir2.1-mediated inward-rectifying K^+ current:

$$I_{Kir} = g_{Kir}k_{\infty}c_{\infty}(V - V_K) \quad . \quad (3.9)$$

Here g_{Kir} is the maximal Kir2.1 channel conductance, k_{∞} is the voltage-dependent block of the channel by polyamines and c_{∞} is the cAMP-dependent activation of the channels. We use a Boltzmann function to describe k_{∞}:

$$k_{\infty} = \frac{1}{1 + exp\left(\frac{V - V_{kir}}{s_{kir}}\right)} \quad , \quad (3.10)$$

where v_{Kir} is the half activation potential and s_{Kir} is the slope factor that determines the sensitivity to the voltage. The resulting voltage-dependent k_{∞} curve is shown in Fig. 3.2A.

Kir2.1 current has both cAMP dependent and independent components (Fakler et al. 1994), which are incorporated into the activation function c_∞ as follows:

$$c_\infty = \alpha_{camp} + \beta_{camp} \frac{cAMP^4}{cAMP^4 + K_{camp}^4} \tag{3.11}$$

where α_{camp} is the cAMP independent component, and the cAMP dependency of the current is described by the second term. The c_∞ function is illustrated in Fig. 3.2B. See the Appendix A and Table A.1 for the complete set of equations and parameter values.

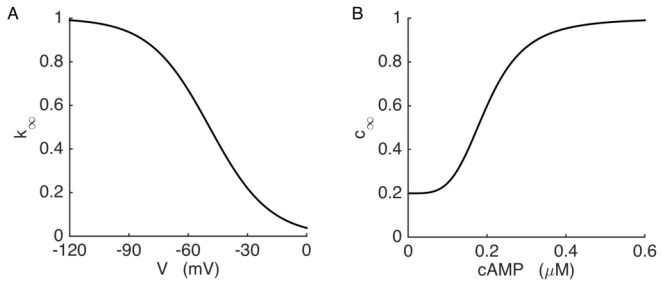

Figure 3.2. Kir2.1 channel conductance depends on the voltage and cAMP concentration. (A) Voltage-dependent blockade of the Kir2.1 current. (B) cAMP-dependent activation of the Kir2.1 current.

3.3 Slow Ca^{2+} Oscillations and Kir2.1 Current Upregulation in $SUR1^{-/-}$ Mouse β-Cells

Ca^{2+} and membrane potential oscillations in $SUR1^{-/-}$ islets, lacking functional K(ATP) channels, have been reported previously (Düfer et al. 2004; Nenquin et al. 2004). We used the Fura-2 Ca^{2+} imaging technique to measure the free cytosolic Ca^{2+} concentrations in wildtype and KO islets. Fura-2 is a ratiometric fluorescent indicator dye for free cytosolic Ca^{2+}, which is excited at 340 and 380 nm wavelengths of light at low concentrations. When Ca^{2+} binds to fura-2, its emission levels for each wavelength of light changes. Therefore, the ratio of emissions at these wavelengths is proportional to the cytosolic free Ca^{2+} concentration. Our fura-2 Ca^{2+} measurements verified slow cytosolic Ca^{2+} oscillations in both wild-type (Fig. 3.3A) and KO-islets (Fig. 3.3B) perfused with 11 mM glucose. These data show that our $SUR1^{-/-}$ islets recapitulate the Ca^{2+} oscillations observed in (Düfer et al. 2004; Nenquin et al. 2004).

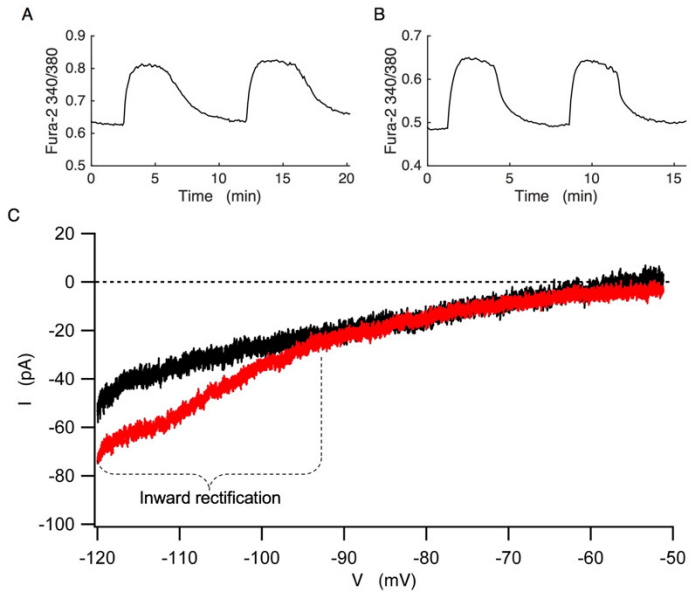

Figure 3.3. Ca^{2+} measurements and current-voltage relations in the wildtype and $SUR1^{-/-}$ islets. Fura-2 Ca^{2+} measurements from wildtype (A) and $SUR1^{-/-}$ islets (B) at 11 mM glucose. The change in Ca^{2+} is expressed as the Fura-2 340/380 ratio. (C) Comparison of I-V curves from wild-type (black) and $SUR1^{-/-}$ (red) β-cells. The wild-type recording is representative from n=6 islets from 4 mice. The $SUR1^{-/-}$ recording is representative from n=8 islets from 5 mice. The $SUR1^{-/-}$ islets exhibit significant inward rectification at lower potentials compared to wild-type islets.

Our collaborators (Satin lab at the University of Michigan) have recently reported that the level of Kir2.1 channel protein is increased in islets that were isolated from $SUR1^{-/-}$ mice (manuscript in preparation). To verify the electrophysiological functionality of these channels in the β-cell membrane of KO islets, we explored the difference between the current-voltage relations of wild-type and KO cells by using the perforated patch-clamp technique to monitor current in peripheral islet β-cells. Figure 3.3C shows current recordings made by applying voltage ramp commands to wild-type islets (black) and KO islets (red), where cells were voltage-clamped to a holding potential of -60 mV, and a 2-second voltage ramp from -120 to -50 mV was applied. Evoked currents were then digitized at 10 kHz after filtering at 2.9 kHz for analysis. In both cases, there is a switch from current clamp to voltage clamp mode during the silent phases of bursts and a two-second voltage ramp from a holding potential of -120 mV to -50 mV was applied.

In wild-type islets, the current-voltage relation exhibited a linear relation at voltages above -110 mV (Fig. 3.3C, black) (n=6 islets from 4 mice), while in the KO-cells the evoked current exhibited a nonlinear response to the voltage ramp (Fig. 3.3C, red). In these cells, significant inward rectification was observed at voltages below -90 mV (n=8 islets from 5 mice). The strong inward rectification observed at the more hyperpolarized voltages in KO cells is likely due to the upregulated Kir2.1 inward-rectifying K^+ current, supporting a functional role for the upregulated Kir2.1 channel protein.

3.4 Ca^{2+}- and AMP-dependent Regulation of cAMP

In the model, Ca^{2+} affects the cAMP concentration in three ways. First, it directly activates the enzymes AC and PDE, as several forms of Ca^{2+}-activated AC and PDE enzymes are expressed in β-cells (Cooper et al. 1995; Han et al. 1999; Pyne and Furman 2003). Second, elevations in intracellular Ca^{2+} invoke ATP hydrolysis via Ca^{2+}-ATPase pumps in the plasma membrane and the endoplasmic reticulum, leading to an increase in ADP and, through the actions of adenylate kinase, AMP. The AMP in turn inhibits adenylyl cyclase (Blume and Foster 1975; Londos and Preston 1977; Johnson et al. 1989). Third, Ca^{2+} activates mitochondrial dehydrogenases (Denton 2009), increasing ATP production at the expense of ADP and AMP.

In Figure 3.4 we show a voltage step simulation to illustrate the effect of Ca^{2+} and AMP on the cAMP concentration. Stepping voltage from a holding potential of -75 mV to -60 mV (Fig. 3.4C) increases *c* somewhat (Fig. 3.4A), by activating a small fraction of Ca^{2+} channels. At low *c,* cAMP production is greater than its degradation since AC has a higher affinity to Ca^{2+} than PDE with the affinity parameters used in this simulation. Therefore, cAMP concentration is increased at this step. Depolarizing the membrane to -45 mV increases *c* to ~0.15 μM. AC is saturated at this level of Ca^{2+} and PDE is significantly activated. In addition, increased Ca^{2+} influx activates Ca^{2+}-ATPase pumps in the plasma and ER membranes, which are powered by the hydrolysis of ATP. The subsequent increase in the AMP concentration (Fig. 3.4B) leads to inhibition of AC. As a result, degradation of cAMP exceeds its production and the cAMP concentration declines. Stepping voltage to -30 mV and higher levels increases *c* further. This

saturates PDE and further increases the AMP, which significantly inhibits AC. Therefore, the cAMP concentration is reduced to lower levels at these steps.

In summary, the cAMP concentration responds to increases in Ca^{2+} concentration in different ways. At low *c*, production exceeds the degradation and increases the cAMP concentration. At higher *c*, AMP inhibits the production and degradation dominates, reducing the cAMP concentration.

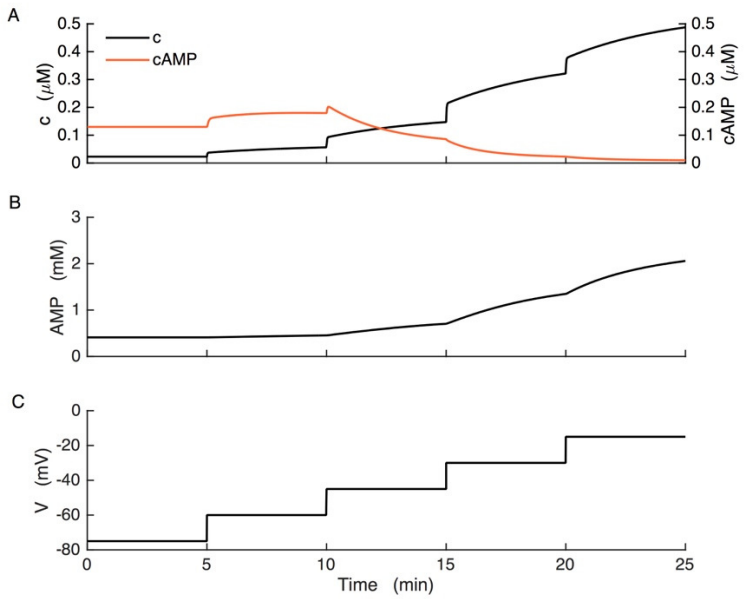

Figure 3.4. Ca^{2+}- and AMP-dependent regulation of cAMP. A voltage step protocol shows the effects of Ca^{2+} and AMP on cAMP. (A) Ca^{2+} rises as the cell is depolarized, but cAMP rises at the beginning and then falls. (B) AMP rises with depolarization, inhibiting cAMP. (C) The voltage step protocol.

3.5 Bursting in the Model KO Cells

Figure 3.5 illustrates slow bursting produced by the model for the case of wild-type cells. The oscillations in the free Ca^{2+} concentration observed here (Fig. 3.5A) result from the bursting electrical activity described earlier. The burst timing in this case is controlled by the slow glycolytic oscillations, which are reflected by the FBP time course as shown (Fig. 3.5E). FBP

oscillations in turn cause oscillations in downstream metabolic components, including cytosolic ATP and AMP (Fig. 3.5C, D). The conductance of K(ATP) channels ($g_{K(ATP)}$) is dependent on ADP and ATP levels, and oscillations in the concentrations of these nucleotides cause K(ATP) conductance (Fig. 3.5B) and concomitantly K(ATP) current to oscillate and drive slow busting. The slow cAMP oscillations are modulated by Ca^{2+} and AMP, but in the model of the wild-type β-cells cAMP has no impact on the cell's electrical activity.

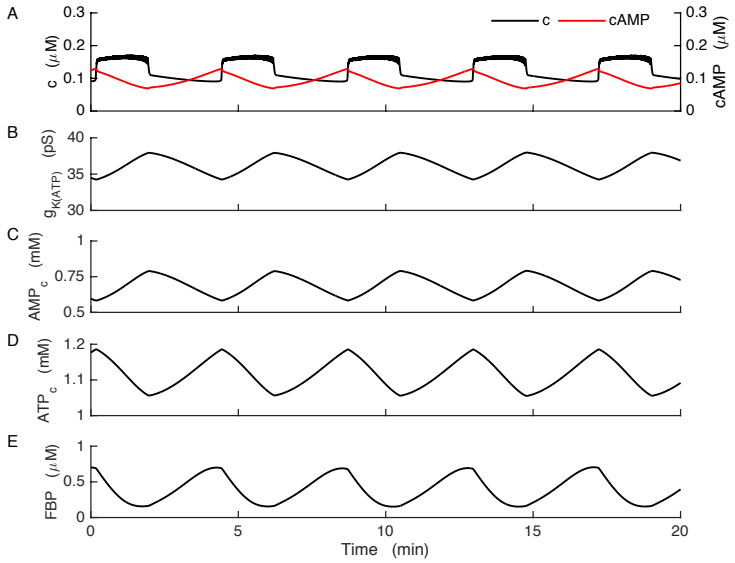

Figure 3.5. Bursting in the model wild-type cells. Slow glycolytic oscillations drive bursting through actions on the K(ATP) current. (A) cAMP declines at the start of each Ca^{2+} plateau. (B) K(ATP) channel conductance. (C-D) Adenine nucleotide concentrations in the cytosol. (E) Slow glycolytic oscillations are reflected in the FBP time course.

If the key K(ATP) channels are removed, the model cell spikes continuously, as is seen experimentally when a K(ATP) channel blocker like tolbutamide is applied to a wild-type islet (Fig. 2.7) (Larsson et al. 1996; Gomis and Valdeolmillos 1998; Ren et al. 2013). The upregulated Kir2.1 conductance shown in Fig. 3.3C would be expected to also provide hyperpolarizing current, but can it rescue the bursting oscillations that are normally driven by K(ATP) current? To answer this, we replaced K(ATP) current in the model with Kir2.1 current to simulate the case for KO cells. The properties of this model current are discussed in the Section 3.2 and are shown in Fig. 3.2. A key feature of the Kir2.1 channels is their activation by cAMP (Fakler et al. 1994; Brugada et al. 2013; Zhang L et al. 2013).

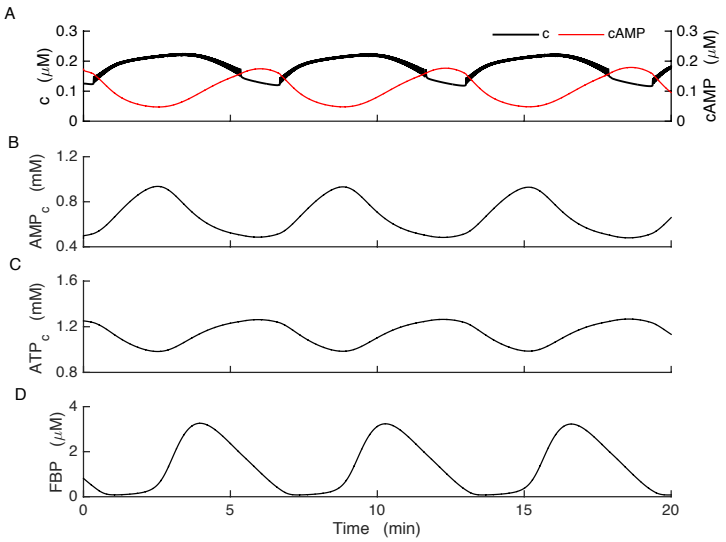

Figure 3.6. Bursting in the model KO cells, where K(ATP) current is replaced with Kir2.1 current. Glycolytic oscillations drive bursting through a cAMP-dependent pathway. (A) Ca^{2+} and cAMP concentrations oscillate in anti-phase. (B) AMP_c oscillations contribute to the production of cAMP oscillations. (C) ATP_c oscillates due to oscillations in glycolysis. (D) FBP is the product of the PFK enzyme that is responsible for glycolytic oscillations. For this simulation, the glucokinase reaction rate was increased from 0.09 μM/ms to 0.14 μM/ms and k_{FBP} was increased from 0.8 to 0.95.

In Figure 3.6 we show that if Kir2.1 up-regulation is sufficiently large, it can rescue slow bursting in the model KO cells that lack K(ATP). In the model of the KO condition, slow glycolytic oscillations now drive slow AMP_c oscillations (Fig. 3.6B) that cause cAMP concentration to oscillate (Fig. 3.6A, red). cAMP in turn activates the Kir2.1 channels and results in oscillations in the Kir2.1 conductance. This causes the membrane potential to switch between active and silent phases and drives bursting and Ca^{2+} oscillations as in the wild type case (Fig. 3.6A, black). The cAMP concentration peaks during the silent phase in the KO model cells, unlike the wild-type model cells where cAMP peaks at the beginning of the active phase. Although the ATP concentration also oscillates (Fig. 3.6C), it does not affect the membrane potential in this case since there are no K(ATP) channels.

In the wild-type cells, cAMP was only a readout and had no effect on the membrane potential or any other model components. However, in the model we made of the KO cells, cAMP, acting through Kir2.1 channels, is now the key to slow bursting. To further understand this mechanism, we show a slow burst in more detail in Fig. 3.7. To facilitate this, voltage is

averaged over the duration of each spike to illustrate the mean voltage trace (Fig. 3.7A, red). This allows us to focus on the slower burst waveform. The figure begins in the silent phase, where there is elevated Kir2.1 conductance (Fig. 3.7D) due to elevated cAMP concentration (Fig. 3.7B, red) and a relatively hyperpolarized voltage (Fig. 3.7A, red). As glycolytic activity declines near the end of the silent phase AMP_c slowly increases (Fig. 3.7B, black). This, in turn, reduces the cAMP concentration by inhibiting adenylyl cyclase, thereby reducing Kir2.1 channel activation (Fig. 3.7C, red). The resulting decline in Kir2.1 conductance initiates an active phase of electrical activity, further reducing Kir2.1 conductance due to voltage-dependent channel blockade (Fig. 3.7C, black). The Ca^{2+} concentration now increases due to influx through voltage-dependent Ca^{2+} channels and this activates Ca^{2+}-ATPase pumps that further increase the AMP_c concentration due to ATP hydrolysis. This causes cAMP to decline rapidly. By the middle of the active phase AMP reaches its peak and starts to decline. This decline, despite the continued rise in c, is due to the glycolytic oscillator. Decreased AMP_c disinhibits adenylyl cyclase and cAMP again starts to increase. The cytosolic Ca^{2+} concentration starts to decrease only after cAMP is elevated enough to significantly activate Kir2.1 current (Fig. 3.7C, red), eventually terminating the active phase.

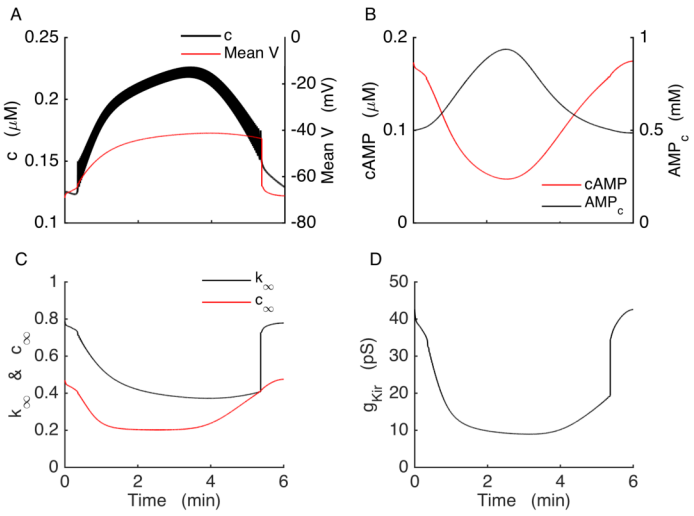

Figure 3.7. Bursting mechanism in the Kir model cell. In the model KO cells, bursting is driven by the Kir2.1 current, which is regulated by voltage and the cAMP concentration. Voltage is averaged over each spike in panel A.

3.6 Fast/Slow Analysis of the Kir Model

To better understand the dynamics of the bursting mechanism, and to facilitate the design of new experiments, we performed a fast/slow analysis of the Kir2.1 model (Rinzel and Ermentrout 1989). This method separates system variables into fast and slow subsystems based on their time scales. The slow variables are almost constant when shown on the time scale of changes in the fast variables. Therefore, these variables can be treated as slowly-varying parameters of the fast subsystem. In our model, the fast variables are voltage (V), the activation variable for voltage-gated K^+ current (n) and cytosolic Ca^{2+} (c). The variables that change on slower time scales are fructose 6-phosphate ($F6P$), fructose 1,6-bisphosphate (FBP), ATP_c, AMP_c, $cAMP$ and Ca^{2+} concentration in the ER (c_{er}). We start by setting c_{er} to its mean value, since it is not a part of the primary oscillatory mechanism. The slow variables other than c_{er} interact according to the following scheme:

$$\mathrm{F6P} \rightarrow \mathrm{FBP} \rightarrow \mathrm{ATP} \rightarrow \mathrm{AMP} \rightarrow \mathrm{cAMP}$$

and only cAMP directly affects the fast subsystem, through the cAMP-dependent activation variable of I_{Kir} (c_∞). We now generate a bifurcation diagram of the fast subsystem with c_∞ as the bifurcation parameter (Fig. 3.8B). For small values of c_∞ the system is at a depolarized steady state, since the Kir2.1 current is largely turned off. These stable steady states make up the initial segment of the upper branch of the z-shaped curve (solid line), which we refer to as the z-curve. As c_∞ is increased two branches of periodic solutions, one stable (bold solid curve) and one unstable (bold dashed curve), emerge at a saddle node of periodics (SNP) bifurcation. The branch of unstable limit cycles is created at a subcritical Hopf Bifurcation (HB), at which point the branch of stable steady states becomes unstable (dashed curve). The branch of unstable steady states turns at a saddle-node bifurcation (SN1), forming the middle branch of the z-curve. This branch turns at another saddle-node bifurcation (SN2) and forms the stable lower branch of the z-curve. The stable branch of periodic solutions reflects tonic spiking, and the minimum and maximum voltage values during a spike are shown as two separate curves. This branch terminates at the left knee of the z-curve at a saddle-node on invariant circle (SNIC) bifurcation.

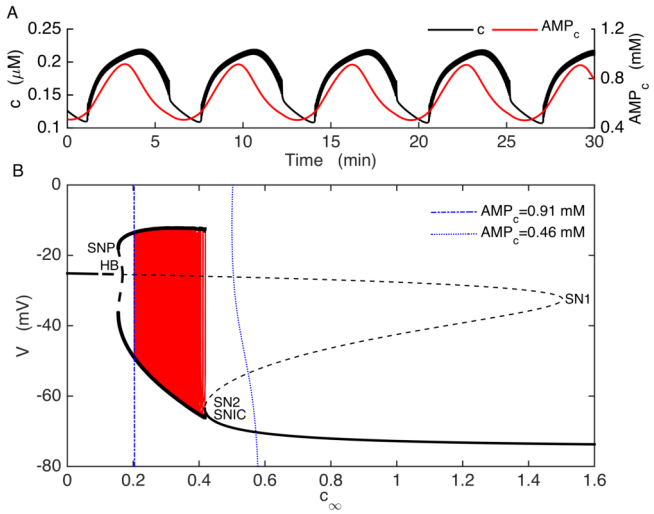

Figure 3.8. Fast/slow analysis of the Kir model. Glycolytic oscillations drive bursting in the model KO cell. (A) c (black) oscillates reflecting bursting electrical activity, while AMP_c oscillates reflecting glycolytic oscillations. (B) Fast/slow analysis of the system shows that glycolytic oscillations drive bursting by shifting the c_∞curve back and forth. HB=Hopf bifurcation, SN=saddle-node bifurcation, SNP=saddle-node of periodics bifurcation. Solid and dashed curves represent stable and unstable steady states, respectively, while bold solid and bold dashed curves are for stable and unstable limit cycles, respectively. The c_∞ curve is shown for AMP_c at its minimum (dotted blue) and maximum (dot-dashed blue) during a burst. The burst trajectory (red) is superimposed.

We now incorporate the slow dynamics by adding the c_∞ curve (Eq. 3.11). This depends on the cAMP concentration, which has the following steady state function:

$$cAMP_{ss} = \frac{k_{PDEcamp} V_{AC}}{\overline{v}_{PDE}\left(\alpha_{PDE} + \beta_{PDE} \frac{{c_{iss}}^3}{{c_{iss}}^3 + K_{PDEca}^3}\right) - V_{AC}} \tag{3.12}$$

where V_{AC} is the adenylyl cyclase production rate and is inhibited by AMP_c (Eq. 3.2). AMP_c changes slowly during a burst (Fig. 3.8A, red) due to the glycolytic oscillator. The steady-state cytosolic Ca^{2+} concentration in Eq. 3.12 (c_{iss}) is given by:

$$c_{iss} = \frac{\alpha I_{Ca} + k_{leak} c_{er}}{k_{pmca} + k_{leak} + k_{SERCA}} \tag{3.13}$$

where I_{Ca} is a function of V and c_{er} is clamped at its mean value. This gives the voltage dependence to the c_∞ curve.

The intersection of the z-curve and the c_∞ curve is the 'quasi-steady state' of the system. This intersection will be at different locations during the burst as the glycolytic oscillator moves the c_∞ curve back and forth. Figure 3.8 shows a fast/slow analysis of a burst, with the c_∞ curve plotted when AMP_c is at its minimum (dotted blue curve) and maximum (dot-dashed blue curve) during a burst (Fig. 3.8A, red trace). The burst trajectory is shown in red (Fig. 3.8B).

During a burst AMP_c moves between these minimum and maximum values and shifts the c_∞ curve back and forth. For small values of AMP_c, the c_∞ curve is shifted to the right (dotted blue curve), intersecting the z-curve on the bottom stationary branch. At this point the system is in its hyperpolarized silent phase. As the glycolytic oscillator slowly increases AMP_c, the c_∞ curve shifts to the left and the phase point follows it. When the curve passes the knee, the phase point is attracted to the periodic spiking branch, starting the active phase. The phase point follows the periodic branch to the left until AMP_c reaches its maximum (dot-dashed blue curve). At its maximum, AMP_c starts declining and shifts the c_∞ curve rightward, bringing the phase point with it. The c_∞ curve eventually reaches SN2 again and intersects the stable stationary branch initiating a silent phase. It keeps moving rightward as AMP_c continues to decline, bringing the phase point with it. Eventually AMP_c begins to rise, restarting the cycle. This is parabolic bursting since the spike frequency during a burst follows a parabolic time course, low at the beginning and the end as the phase point passes near the infinite-period SNIC bifurcation (Rinzel and Lee 1987). The fast subsystem bifurcation diagram lacks a bistable region, so the glycolytic oscillations are necessary for bursting in the Kir2.1 model.

3.7 An Alternate Burst Mechanism for KO Cells

Can upregulation of other types of K^+ channels yield effects similar to those of Kir2.1? To address this question, we examined the effects of replacing K(ATP) current with a hyperpolarizing constant-conductance or "leak" K^+ current, instead of Kir2.1 current, and increased the K(Ca) channel conductance (Fig. 3.9). With these modifications, bursting resulted from the Ca^{2+} feedback onto K(Ca) channels (Fig. 3.9A). In this model ER Ca^{2+}, which played little role in bursting with the Kir2.1 model, becomes absolutely essential in driving the burst.

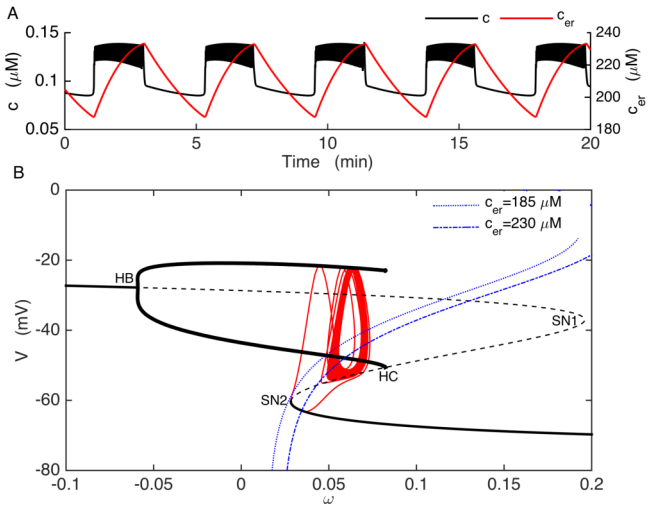

Figure 3.9. Fast/slow analysis of the ER bursting model. The model KO cell can produce bursting with upregulation of a constant-conductance (leak) K^+ current and a K(Ca) conductance. $g_{leak} = 32.5$ pS, $g_{K(Ca)} = 90$ pS. (A) Negative feedback of c (black) on the membrane potential and slow c_{er} (red) oscillations drive bursting. (B) Fast/slow analysis shows that the oscillations in c_{er} turn bursts of activity on and off by translating the ω curve left and right. Labels are defined as in Fig. 3.8B. ω curves are generated at the minimum (dotted blue) and maximum (dot-dashed blue) c_{er} values during a burst.

In this model, the glycolytic oscillations are irrelevant since they do not change the membrane potential or contribute to burst generation in any way. The fast subsystem consists of two variables in this case, V and n. The slow variables are c and c_{er}, which we consider as slowly-varying parameters of the fast subsystem. Rather than using c as the primary bifurcation parameter of the fast subsystem, we use the K(Ca) channel activation variable ω, which is related to c by Eq. 3.8. The fast-subsystem bifurcation diagram again is z-shaped (Fig. 3.9B), but now it has a region of bistablity between the periodic spiking branch and the lower stationary branch. (The diagram is extended to negative ω values for illustration purposes; only positive ω values are possible.)

We now add the Ca^{2+} dynamics into our analysis by superimposing the ω-curve. This uses Eq. 3.8, with c at its equilibrium for each value of V (Eq. 3.13). The phase point moves to the left when it is below the ω-curve and it moves to the right above the ω-curve. The intersection of the ω-curve and the z-curve is the quasi-steady state of the system. If the intersection occurs deep in the periodic branch, the system exhibits spikes and if the intersection

occurs at the bottom stationary branch of the z-curve then the system is at rest at a hyperpolarized silent state. Here, c_{er} plays a significant role by slowly changing the position of the ω-curve through its actions on c_{iss} (Eq. 3.13). ω-curves generated for the maximum and minimum c_{er} values during a burst are given by dot-dashed and dotted blue curves, respectively (Fig. 3.9B). For high values of c_{er} the ω-curve is shifted to the right (dot-dashed blue curve) and intersects the z-curve on the bottom branch (as well as the periodic branch), allowing the system to enter the silent phase. For low values of c_{er} the ω-curve is left-shifted so that it intersects the periodic branch only, resulting in continuous spiking. During the silent phase c_{er} declines, shifting the ω-curve slowly to the left and the phase point follows it. When the ω-curve reaches the knee, the phase point escapes from the stationary branch and jumps to the periodic branch, which is now the only remaining stable structure. This starts an active phase and each spike brings in more Ca^{2+} and increases c and c_{er}. Increased c_{er} shifts the ω-curve slowly to the right and eventually the phase point escapes from the periodic branch and returns to the bottom stationary branch, restarting the cycle. This is an example of phantom bursting with c_{er} playing the role of the second slow variable (Bertram and Sherman 2004).

3.8 Experimental Tests for Distinguishing the Two Models

We have thus far described two possible ways in which the upregulation of hyperpolarizing K^+ channels can rescue bursting in $SUR1^{-/-}$ β-cells. How can we determine which mechanism is most likely correct? Is there an experimental test that can be performed to discount one of the two mechanisms? One clear difference between the two mechanisms is their dependence on ER Ca^{2+} concentration. This difference motivated us to explore the consequences of manipulating ER Ca^{2+} concentration. This can be done experimentally by blocking the Ca^{2+} pumps on the ER membrane (the SERCA pumps) using the agent thapsigargin (Inesi and Sagara 1992).

In the model, the parameter k_{SERCA} is the Ca^{2+} pumping rate into the ER from the cytosol. To mimic the effect of thapsigargin we reduce k_{SERCA} by a factor of 4. In the ER bursting model, this reduces c_{er} (Fig. 3.10A, red trace) and converts bursting into continuous spiking (Fig. 3.10A, black trace). In terms of the fast/slow analysis, this is because the reduced c_{er} shifts the ω-curve

leftward, where it intersects the z-curve only on the periodic branch (Fig. 3.10B, dotted blue curve). Since the Ca^{2+} flux into the ER is mostly blocked, the ER does not refill and thus the ω-curve does not be move back to the right. Therefore, the cell remains in the spiking state and bursting is terminated.

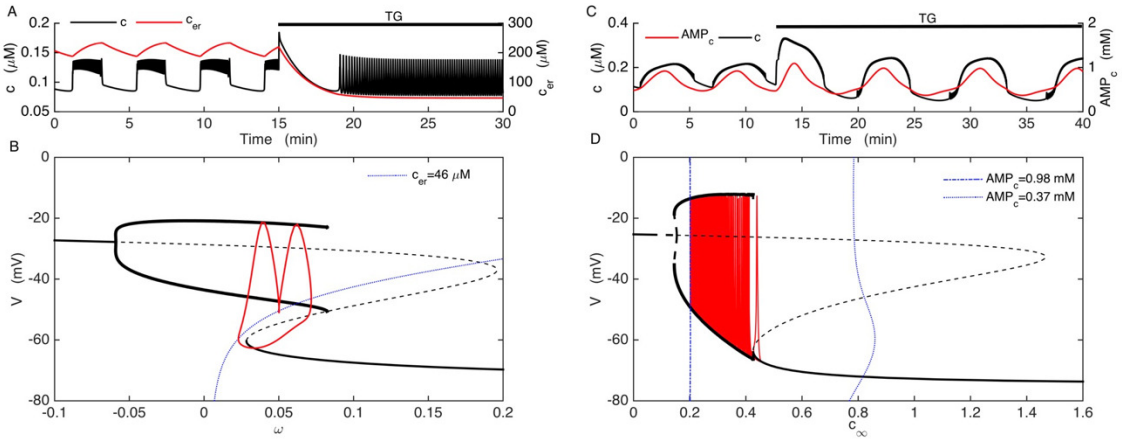

Figure 3.10. The two model predict different outcomes from the partial blockade of SERCA pumps with thapsigargin (TG). (A) In the model where bursting is driven by oscillations in the ER calcium concentration simulation of TG application reduces the c_{er} (red) and terminates c oscillations (black). (B) In this model, TG shifts the ω curve (dotted blue) to left where it intersects the z-curve deep in the periodic branch. (C) In the model in which bursting is driven by oscillations in the Kir2.1 current, bursting continues after TG application (black) because the AMP_c oscillations (red) persist. (D) In this model, TG increases the amplitude of the AMP_c oscillations, which shifts the c_∞ curve further to the right and increases the period of oscillations, but the burst mechanism is unaltered.

When we perform the same procedure with the Kir2.1 model, bursting persists (Fig. 3.10C, black). This is because bursting in this case is driven by the glycolytic oscillator. The procedure lowers mean c_{er}, which affects the cytosolic Ca^{2+} level, but this only modulates the slow bursting pattern. Indeed, the fast/slow analysis illustrates that the burst mechanism is very similar to what it was before the reduction in k_{SERCA} (Fig. 3.10D). The main difference is that the period is now increased, since the c_∞ curve moves further to the right during the silent phase (Fig. 3.10D, dotted blue curve) because more Kir2.1 conductance, and hence more cAMP, is needed to make up for the lack of K(Ca) conductance.

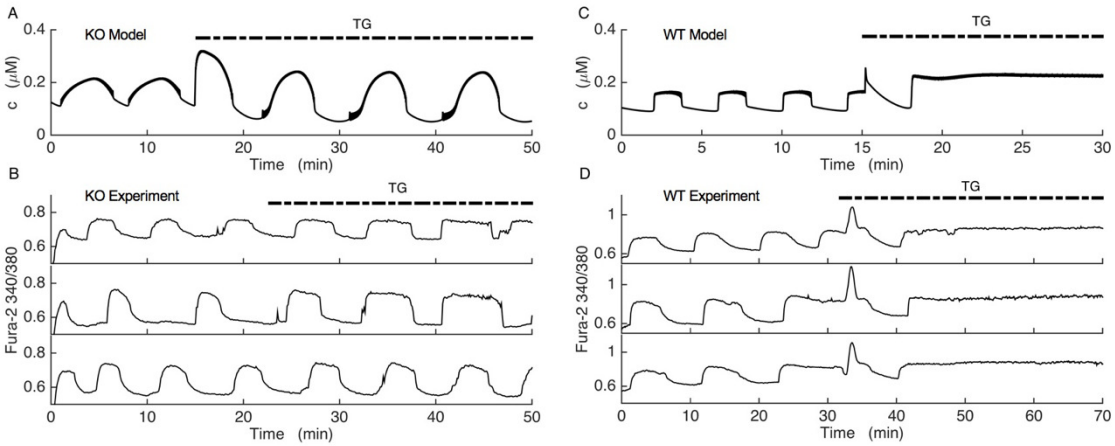

Figure 3.11. Experimental tests for distinguishing the two models. Fura-2 Ca^{2+} measurements of $SUR1^{-/-}$ and wild-type islets compared with model simulations. In the experiments, the change in Ca^{2+} is expressed as the Fura-2 340/380 fluorescence ratio. (A) In the Kir2.1 model, the parameter k_{SERCA} is reduced by a factor of 4 to mimic application of the SERCA pump blocker thapsigargin (TG). (B) Fura-2 Ca^{2+} measurements from 3 representative $SUR1^{-/-}$ islets. Islets were maintained in 11 mM glucose, and the irreversible SERCA pump blocker TG was applied as indicated. Slow Ca^{2+} oscillations persisted after TG application in all 10 KO islets tested, as predicted by the model. (C) In the wild-type model, parameter k_{SERCA} was reduced by a factor of 4 to simulate TG application. D) Fura-2 Ca^{2+} measurements from 3 representative wild-type islets maintained in 11 mM gluocse. TG was applied as indicated. Slow Ca^{2+} oscillations were replaced by sustained elevation in Ca^{2+} in 13 of 14 wild-type islets tested, as predicted.

These simulations make a testable prediction that can eliminate one or the other of the compensation models. Our model predictions were subsequently tested in the lab, by treating $SUR1^{-/-}$ and wild type islets with the drug thapsigargin (TG), which blocks sarco/endoplasmic reticulum Ca^{2+}-ATPase pumps (SERCA pumps) on the ER membrane and depletes the ER. Figure 3.11 shows the model prediction made using the Kir2.1 model on the top row and the results of the experiments on the bottom three rows (3 $SUR^{-/-}$ islets and 3 wild-type islets). TG application does not terminate slow bursting in any of the $SUR1^{-/-}$ islets shown and Ca^{2+} oscillations persist (Fig. 3.11B), as predicted by the Kir2.1 model (Fig. 3.11A). In fact, Ca^{2+} oscillations persisted in all 10 KO islets tested. The slow Ca^{2+} decline that occurs at the end of each active phase prior to TG application was eliminated during TG application, as expected (Arredouani et al. 2002a; Arredouani et al. 2002b), demonstrating that the TG is in fact having an effect on the Ca^{2+} dynamics. The persistence of oscillations is in contrast with the wild-type model (the model with K(ATP) current) and the wild-type islets, where in most of the wild-type

islets tested TG converted slow oscillations to continuous spiking with an elevated cytosolic Ca^{2+} level (in 13 of 14 islets tested) (Fig. 3.11C, D). A similar effect of TG on slow Ca^{2+} oscillations was observed previously in islets (Dula et al. 2010). Since the response to TG confirms the prediction from the Kir2.1 model, but not that of the ER bursting model, we conclude that the Kir2.1 model is the more likely candidate for the compensation that occurs in $SUR1^{-/-}$ islets. That is, the data support the hypothesis that the rescue of bursting observed in the KO islets is due to the upregulation of Kir2.1 channels.

3.9 Discussion and Concluding Remarks

The primary aim of the modeling study presented in this chapter was to help understand how islet β-cells can compensate for the knockout of K(ATP) channels in $SUR1^{-/-}$ mice. One focus was on Kir2.1 channels, which our collaborators recently found to be upregulated in the KO-mice (manuscript in preparation). We showed that upregulation in the expression of these channels can rescue bursting, even though the K(ATP) channels that normally couple metabolic oscillations to plasma membrane channel activity are missing in this case. This requires that the Kir channels have a dependence on cAMP, as has been reported previously for Kir2.1 channels (Fakler et al. 1994; Ruppersberg and Fakler 1996; Brugada et al. 2013; Zhang L et al. 2013). It has also been reported that cAMP exhibits slow oscillations in wild-type mouse islets (Dyachok et al. 2008), a behavior which could reflect oscillations in the nucleotide AMP (Peercy et al. 2015). Indeed, we were not able to rescue bursting in simulations of KO-islets if the AMP regulation of cAMP were omitted (not shown). We did, however, discover an alternative mechanism for bursting in the KO islets that is independent of Kir2.1 current. The two alternate models made very different predictions for the effects of blocking Ca^{2+} pumps in the ER membrane, and subsequent experiments with the SERCA pump blocker thapsigargin supported the Kir2.1 model over the alternate model.

One prediction of the Kir2.1 model is that the Ca^{2+} and cAMP oscillations should be 180^{o} out of phase with one another in the KO cells (Fig. 3.6A). This differs considerably from the wild-type case, where cAMP has a saw-tooth pattern and declines during the burst active phase and then rises during the silent phase (Fig. 3.5A). While cAMP levels have been measured

simultaneously with Ca^{2+} in wild-type islets and the time course is in general agreement with the model (Dyachok et al. 2008), such measurements have not yet been made in $SUR1^{-/-}$ islets.

Glycolytic oscillations are well established in yeast (Richard 2003), but until recently there was no direct evidence that they occur in islet β-cells. However, recent studies using a FRET sensor for the glycolytic enzyme pyruvate kinase provided direct evidence for the existence of glycolytic oscillations in islets (Merrins et al. 2013; Merrins et al. 2016). These metabolic oscillations are readily transmitted to the membrane potential through the cyclic activity of K(ATP) channels (McKenna et al. 2016)(Fig. 3.5), and we have now illustrated how these can drive bursting even in the absence of K(ATP) channels by utilizing the cAMP dependence of upregulated Kir2.1 channels.

CHAPTER 4

Ca^{2+} FREQUENCY SENSITIVE COMPENSATION MECHANISM

The results presented in this chapter are submitted to the Bulletin of Mathematical Biology for publication (Yildirim and Bertram).

4.1 Introduction

The work presented in this chapter was motivated by the finding that in SUR1 KO mouse islets there is an upregulation of the Kir2.1 isoform of inward-rectifying K^+ channels (manuscript in preparation) and the modeling work presented in Chapter 3 that demonstrates the resulting Kir2.1 current can effectively compensate for the loss of K(ATP) current and rescue slow bursting oscillations. This rescue only occurs, however, if the level of upregulated conductance is right. This raises the question that motives the work presented in this chapter: how does the cell know the appropriate level of compensation? The most likely answer is that it sets the compensation level so that Ca^{2+} oscillations with frequency similar to the wild-type cells are restored. But how does it do that? We demonstrate here that a model containing two Ca^{2+}-dependent enzymes with opposing actions can achieve this. These enzymes effectively decode the frequency of Ca^{2+} oscillations and regulate the activity of a target transcription factor. By coupling the activity-dependent compensation mechanism with a well-studied β-cell model (Bertram and Sherman 2004), we show that the paradoxical bursting electrical activity, and Ca^{2+} and insulin oscillations observed in KO islets, could result from compensation by another ion channel whose expression is regulated by intracellular Ca^{2+} dynamics. The optimal expression level of this channel is achieved naturally by the Ca^{2+}-dependent enzymes. Unlike prior theoretical studies that made use of a target average Ca^{2+} level to achieve appropriate conductance levels (LeMasson et al. 1993; O'Leary et al. 2014), this mechanism naturally achieves the target activity pattern due to properties of the Ca^{2+}-dependent enzymes controlling transcription of the compensating channel protein.

This chapter has two main parts. The first part focuses on how Ca^{2+}-dependent enzymes can discriminate between Ca^{2+} signals of different frequencies. It ends by demonstrating that

transcription factor activation by two Ca^{2+}-dependent enzymes with opposing actions can be adjusted to increase monotonically with the frequency of Ca^{2+} pulse application, or decrease monotonically, or exhibit a bell-shaped response. The second part of this chapter combines the transcription model to a model of the activity of the pancreatic β-cell. The β-cell model sets the Ca^{2+} dynamics that in turn regulate the activity of the transcription factor, thereby closing the loop. This combined model is then used to illustrate the compensation mechanism that is triggered by the removal of the key K(ATP) current. It demonstrates that compensation at the appropriate level to rescue slow Ca^{2+} oscillations associated with electrical bursting can be achieved through the actions of Ca^{2+} on two opposing enzymes, provided that the compensating gene product, an ion channel, feeds back onto the membrane potential and contributes to the patterning of electrical activity (Fig. 4.1).

4.2 Ca^{2+} Oscillation Frequency Decoding Gene Transcription Model

The Ca^{2+} frequency-decoding network (Fig. 4.1) consists of a Ca^{2+}-dependent activator enzyme (A) and an inhibitor enzyme (I), both of which regulate the activity of the target transcription factor. These enzymes could be either kinases or phosphatases, which regulate the activity of proteins by phosphorylating and dephosphorylating them, respectively. Both enzyme families have Ca^{2+}-dependent members (Rosen et al. 1995) and studies have shown that some Ca^{2+}-frequency sensitive transcription factors are activated when phosphorylated (Segil et al. 1991; Oeckinghaus and Ghosh 2009) where others are activated when dephosphorylated (Rao et al. 1997). Therefore, we avoid using terms kinase and phosphatase and use activator and inhibitor instead. In the model, we assume that the total concentration of the enzymes and the transcription factor do not change over time and we represent the activation of these proteins by the fractions of their active forms. Studies show that Ca^{2+} binds and activates several Ca^{2+} dependent enzymes cooperatively (Stemmer and Klee 1994; Bradshaw et al. 2003; Falcke and Malchow 2003; Swulius and Waxham 2013). Taking the nonlinearity induced by cooperativity into account, we employ a simple mechanism for enzyme activation kinetics that is easy to analyze and yet encapsulates the

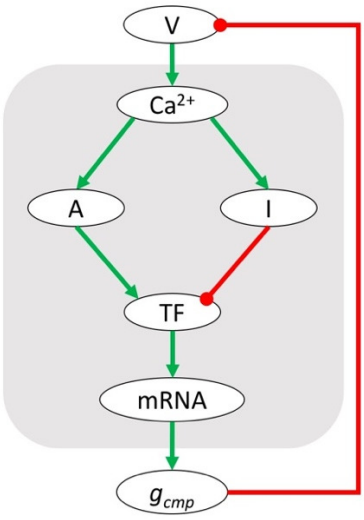

Figure 4.1: Ca^{2+} frequency decoding gene transcription network. Green arrows are for stimulatory and red circles are for inhibitory pathways. The model consists of a Ca^{2+}-dependent activator enzyme (A) and an inhibitor enzyme (I), both of which regulate the activity of the target transcription factor (TF). The activated transcription factor accelerates compensating ion channel mRNA synthesis, which increases the maximal conductance (g_{cmp}) of the compensating current. By providing negative feedback on the membrane potential (V), g_{cmp} completes the feedback loop that underlies activity-dependent homeostasis.

kinetic properties of many Ca^{2+}-dependent enzymes (Falcke and Malchow 2003). The fraction of activator enzyme that is activated by Ca^{2+}, A_a, changes with time according to:

$$\frac{dA_a}{dt} = p_A \frac{c^{n_A}}{c^{n_A} + K_{cA}^{n_A}}(1 - A_a) - d_A A_a \tag{4.1}$$

where p_A and d_A are the activation and deactivation rate constants, respectively. The activation rate is a Hill function of the free intracellular Ca^{2+} concentration (c), with Hill coefficient n_A and dissociation constant K_{cA}. The fraction of inhibitor enzyme that is activated by Ca^{2+}, I_a, changes over time according to:

$$\frac{dI_a}{dt} = p_I \frac{c^{n_I}}{c^{n_I} + K_{cI}^{n_I}}(1 - I_a) - d_I I_a \quad . \tag{4.2}$$

Parameters for the inhibitor enzyme are analogous to those for the activator.

The rate of change of the fraction of activated transcription factor, TF_a, is given by the difference between its activation and inhibition rates in the following form:

$$\frac{dTF_a}{dt} = A_\infty(1 - TF_a) - I_\infty TF_a \quad . \tag{4.3}$$

The activation rate of the transcription factor is given by the A_a-dependent second-order Hill function A_∞:

$$A_\infty = \frac{\alpha_A {A_a}^2}{{A_a}^2 + {K_A}^2} \tag{4.4}$$

where the maximal activation rate is α_A and K_A is A_a fraction for half maximal activation. The inactivation rate of the transcription factor is given by the I_a-dependent Hill function I_∞:

$$I_\infty = \frac{\beta_I I_a}{I_a + K_I} \tag{4.5}$$

where β_I is the maximal inhibition rate and K_I is the I_a fraction for half maximal inhibition (we assume a Hill coefficient of 1).

In the initial studies of the Ca^{2+} frequency decoding mechanism we simulate changes in the intracellular free Ca^{2+} concentration with a periodic square wave:

$$c(t) = \begin{cases} c_0 = 0.1\,, & \mathrm{mod}(t,T) \le D \\ 0\,, & \mathrm{mod}(t,T) > D \end{cases} \tag{4.6}$$

where c_0 is the amplitude of the Ca^{2+} signal during a pulse, T is the oscillation period, and D is the pulse duration. Periodic piecewise continuous Ca^{2+} signals were used in previous experimental (De Koninck and Schulman 1998; Dolmetsch et al. 1998) and computational (Dupont et al. 2003; Schuster et al. 2005; Salazar et al. 2008) studies. Ca^{2+} signals of this type are easy to manipulate in terms of amplitude and frequency in the experiments, and allow derivation of analytical solutions for kinetic equations in computational studies.

4.3 Long-Term Enzyme Response to Square-Wave Ca^{2+} Oscillations

Our first goal is to determine the long-term dynamics of an enzyme with Ca^{2+}-dependent activation described by a Hill function. This enzyme could either activate or repress a gene transcription factor. As described with Eqs. 4.1-4.2, the form we use is:

$$\frac{dE_a}{dt} = p_E \frac{c^{n_E}}{c^{n_E} + K_E^{n_E}} (1 - E_a) - d_E E_a \tag{4.7}$$

where E_a is the fraction of an enzyme that is in its activated state. Assuming that all enzyme molecules are initially in an inactive form, and that the enzyme is subject to a periodic square-wave Ca^{2+} signal (Eq. 4.6), we can derive an analytical solution to Eq. 4.7 during periods where the Ca^{2+} input is on (top) or off (bottom):

$$E_a(t) = \begin{cases} E_{ss}(1 - e^{-(p_E^* + d_E)t}), & t < D \\ E_a(D)e^{-d_E t}, & D \le t \le T \end{cases} \tag{4.8}$$

where

$$p_E^* = p_E \frac{c_0^{n_E}}{c_0^{n_E} + K_E^{n_E}} \tag{4.9}$$

is the Ca^{2+}-dependent activation rate of the enzyme, and

$$E_{ss} = \frac{1}{1 + \frac{d_E}{p_E^*}} \tag{4.10}$$

is the steady state fraction of activated enzyme with Ca^{2+} concentration c_0. Equation 4.8 shows that the characteristic response time of the enzyme to the stimulus is $1/d_E$. Thus, if d_E is large then the response time is fast and E_{ss} is small. In this case, the activated enzyme concentration closely follows the c time course. However, many enzymes respond to a stimulus slowly due to the conformational changes and/or phosphorylation necessary for their activation (Frieden 1970; Frieden 1979). The rate-limiting slow activation dynamics serve as a low-pass filter against noise

in the input and also enable the enzyme to have an optimal response to certain stimulus frequencies (Wu and Xing 2012). Our aim is to construct a signaling model that will exhibit such a response to the periodic Ca^{2+} stimulus, so we tune d_E and p_E so that the characteristic response time of the enzyme is comparable to the period of the square-wave Ca^{2+} stimulus.

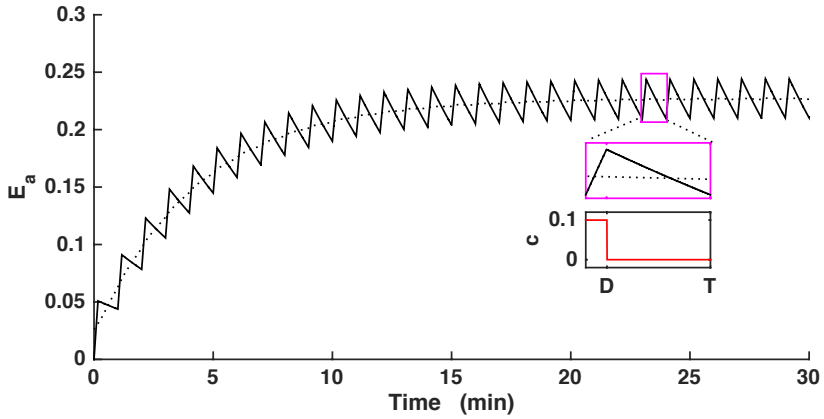

Figure 4.2: Long-term enzyme response to square wave Ca^{2+} stimulus. Time course of the fraction of the activated enzyme (black solid curve) with a representative square wave Ca^{2+} signal (red curve, inset). The enzyme integrates the Ca^{2+} signal over time. The mean fraction of activated enzyme (black dotted curve) initially increases and reaches an equilibrium once the activated enzyme level becomes periodic.

Figure 4.2 shows one period of a representative Ca^{2+} stimulus (inset, red) and the resulting activated enzyme time course (black solid) over many periods of the stimulus. The time-varying mean value of the fraction of activated enzyme over the i^{th} stimulus cycle, $\bar{E}_{a,i}$ is:

$$\bar{E}_{a,i} = \frac{1}{T}\int_{iT}^{(i+1)T} E_a(t)dt \tag{4.11}$$

and is shown by the dashed curve in the figure. This eventually settles to a value $\bar{E}_a$. The formula for this steady-state mean activated enzyme fraction is derived in Appendix B, and is given by:

$$\bar{E}_a = E_{ss}\left(\frac{D}{T} + \frac{E_{ss}}{d_E T}\frac{\left(1-e^{-D(p_E^*+d_E)}\right)\left(1-e^{-d_E(T-D)}\right)}{1-e^{-(p_E^* D+d_E T)}}\right) \quad . \tag{4.12}$$

This provides a manageable expression for $\bar{E}_a$ in terms of the Ca^{2+} pulse duration (D) and the period (T) of the periodic square-wave Ca^{2+} stimulus.

4.4 Oscillation Efficiency

Is Ca^{2+} more effective at activating an enzyme when it is delivered as periodic square pulses? To answer this question, we compare the long-term activated enzyme level with a square-wave stimulus to that obtained with a constant stimulus of the same mean value of Ca^{2+}. This value, c_c, is:

$$c_c = c_0 \frac{D}{T} \quad . \tag{4.13}$$

Substituting c_c for c in the equilibrium activated enzyme function Eq. 4.10 yields, after some algebra,

$$\bar{E}_{a,c} = \frac{1}{1+\frac{d_E}{P_E}\left(1+\left(\frac{K_E}{c_c}\right)^{n_E}\right)} \tag{4.14}$$

which gives the steady state fraction of the activated enzyme with constant Ca^{2+}. We now compare $\bar{E}_{a,c}$ with the long-term average activated enzyme level with a square-wave stimulus, $\bar{E}_a$, using what we call the 'Oscillation Efficiency':

$$\text{Oscillation Efficiency} = \frac{\bar{E}_a - \bar{E}_{a,c}}{\bar{E}_{a,c}} \quad . \tag{4.15}$$

Figure 4.3 shows the oscillation efficiency over a range of values of the oscillation period T and the Ca^{2+} dissociation constant for the enzyme, K_E, using three different levels of cooperativity n_E. In each case $D = 10$ sec. When $T \to D$ in Eqs. 4.12 and 4.14, both $\bar{E}_a \to E_{ss}$ and $\bar{E}_{a,c} \to E_{ss}$ and consequently the oscillation efficiency approaches zero independent of n_E. That is, the responses of the enzyme to the square wave and constant stimuli are similar when there is little time between stimuli, regardless of the cooperativity (leftmost portions of each panel in Fig. 4.3).

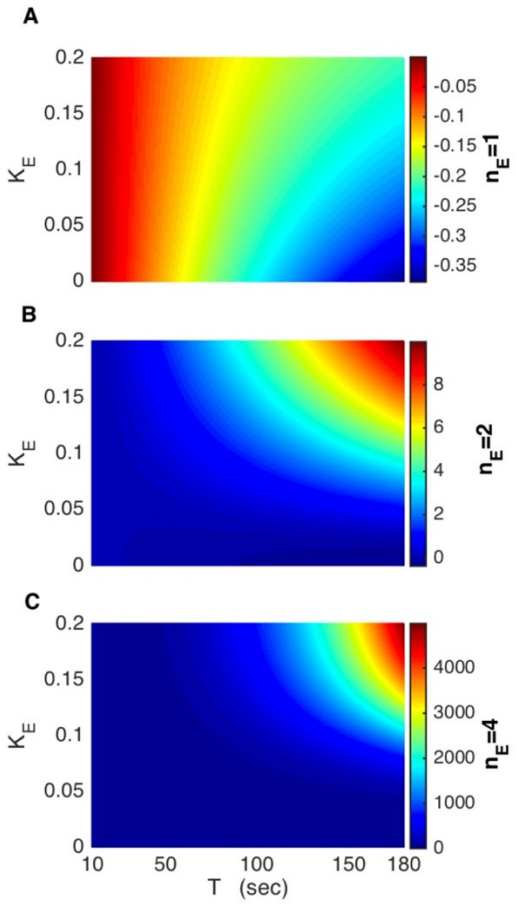

Figure 4.3: Oscillation efficiency. Cooperativity increases the oscillation efficiency (Eq. 4.15) at low frequencies when Ca^{2+} binds to enzyme with low affinity (larger K_E). (A) When n_E=1, the oscillation efficiency is negative for all K_E values, indicating that a constant Ca^{2+} stimulus is more effective than a square wave stimulus. (B, C) With increasing Ca^{2+} binding cooperativity the square wave Ca^{2+} stimulus becomes more effective, particularly at low frequencies.

Figure 4.3A shows that when $n_E = 1$, oscillation efficiency is negative ($\bar{E}_a \leq \bar{E}_{a,c}$) for all values of K_E shown. That is, when Ca^{2+} binds to the enzyme non-cooperatively, a constant Ca^{2+} stimulus is more effective than a square wave Ca^{2+} stimulus. However, with positive cooperativity ($n_E > 1$), the oscillation efficiency increases with longer periods T and larger values of K_E ($\frac{d\bar{E}_a}{dT} > \frac{d\bar{E}_{a,c}}{dT}$) due to the exponential dependence of $\bar{E}_{a,c}$ on n_E. Thus, the periodic square wave Ca^{2+} becomes more effective at activating the enzyme than constant Ca^{2+} at lower frequencies (Fig. 4.3B, C). Since K_E multiplies T in Eq. 4.14, when K_E is small T must be large for this effect to be seen (the efficiency is highest in the upper right portions of panels B and C).

How does Ca^{2+} cooperativity affect the activated enzyme level? This depends on whether Ca^{2+} is constant or delivered as periodic square pulses. For the case of a constant Ca^{2+} stimulation this is simple; Eq. 4.14 shows that if $c_c > K_E$ then cooperativity increases the activated enzyme level, while if $c_c < K_E$ it decreases it. If the Ca^{2+} signal is a periodic square wave, then the influence of cooperativity on the long-term mean activated enzyme concentration, $\bar{E}_a$ (Eq. 4.12), is determined by

$$\frac{d\bar{E}_a}{dn_E} = \frac{d\bar{E}_a}{dp_E^*}\frac{dp_E^*}{dn_E} \quad . \tag{4.16}$$

It can be shown that $\frac{d\bar{E}_a}{dp_E^*} > 0$ and,

$$\frac{dp_E^*}{dn_E} = \frac{c_0^{n_E} K_E^{n_E} \left(\ln\frac{c_0}{K_E}\right)}{\left(c_0^{n_E} + K_E^{n_E}\right)^2} \tag{4.17}$$

which is positive if the argument of the natural log is greater than 1, so $\frac{d\bar{E}_a}{dn_E} > 0$ if $K_E < c_0$. Therefore, for a periodic square wave Ca^{2+} signal, Ca^{2+} cooperativity increases the activated enzyme level if the amplitude of the Ca^{2+} pulse is greater than the dissociation constant, else it decreases the activated enzyme level.

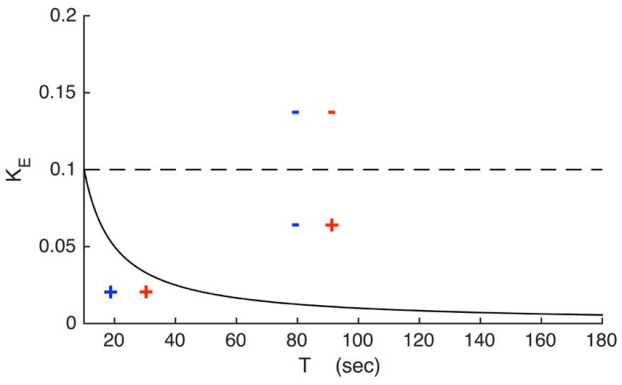

Figure 4.4: Cooperativity effects. The K_E values where cooperative Ca^{2+} binding enhances or reduces the enzyme activation are indicated by + or -, respectively. Blue symbols are for a constant Ca^{2+} stimulus, and red symbols are for a square wave stimulus with the same mean

Figure 4.4 continued: level. The solid curve satisfies $K_E = c_0 \frac{D}{T} = c_c$, while the dashed line satisfies $K_E = c_0$. Oscillations increase the range of the parameter space where cooperativity has a positive impact on the enzyme activation.

The cooperativity effects are illustrated in Fig. 4.4. Below the curve $K_E = c_0 \frac{D}{T}$ cooperativity increases activated enzyme if the Ca^{2+} level is constant (Fig. 4.4, blue +). Below the dashed line $K_E = c_0$ cooperativity increases activated enzyme if the Ca^{2+} level is a square wave (Fig. 4.4, red +). Since the latter area is larger, the range of $K_E$values where cooperativity increases the activated enzyme level is greater with a square wave Ca^{2+} stimulus than with a constant stimulus with the same average Ca^{2+} level.

4.5 Frequency Decoding Capabilities of the Enzymes

It is clear that the activated enzyme level increases with the frequency of the square wave Ca^{2+}. However, it is ambiguous whether increased activation is due to the increased average Ca^{2+} concentration with frequency or due to the increased frequency itself. To what extent is the activation responding to the frequency of the oscillations? To answer this question, it is necessary to fix the average Ca^{2+} as the oscillation frequency is varied. We do this while keeping the duty cycle, $\gamma = \frac{D}{T}$, fixed. Consequently, as T is varied, the average Ca^{2+} remains constant. Figure 4.5 shows the fraction of activated enzyme as T and K_E are varied, with $\gamma = 0.25$ and $n_E = 4$. For all K_E values, the activated enzyme concentration decreases with the period of the square wave (Fig. 4.5A), so short Ca^{2+} pulses separated by small intervals are more effective at activating the enzyme. How does the frequency decoding capability of the enzyme depend on its affinity to Ca^{2+}? To find out, for each K_E value, we calculate the fraction of activated enzyme obtained for a short-period stimulus, $T = 10$ sec, and a long-period stimulus, $T = 180$ sec. We denote these by $\bar{E}_{a,10}(K_E)$ and $\bar{E}_{a,180}(K_E)$, respectively. The effect of frequency for each K_E value is reflected in the difference between these two. Normalizing this with respect to $\bar{E}_{a,180}(K_E)$ yields the following K_E-dependent estimate for the 'Decoding Capacity' of the enzyme:

$$\text{Decoding Capacity} = 100 \cdot \frac{\bar{E}_{a,10}(K_E) - \bar{E}_{a,180}(K_E)}{\bar{E}_{a,180}(K_E)} \quad . \tag{4.18}$$

The frequency decoding capacity of the enzyme decreases as K_E increases (Fig. 4.5B). Thus, enzymes with higher Ca^{2+} affinity are better able to decode the frequency of oscillations.

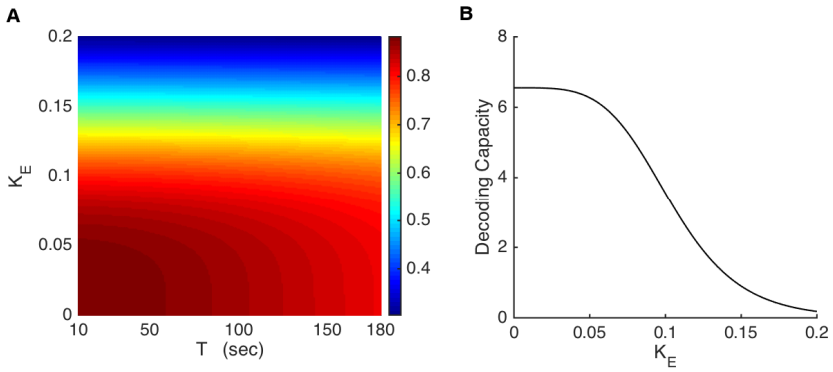

Figure 4.5: Frequency decoding capabilities of the enzymes. The enzyme is capable of decoding the Ca^{2+} oscillation frequency when the average Ca^{2+} is held constant. In Eq. 4.12 we set $D=\gamma T$ and γ=0.25. (A) Fraction of activated enzyme is color coded with dark red being the highest and dark blue being the lowest values. Enzyme activation is higher when short square wave Ca^{2+} pulses are separated by short intervals. (B) Frequency decoding capacity of the enzyme declines as K_E increases. The decoding capacity is defined in Eq. 4.18.

4.6 Frequency Response Regime of the Transcription Factor

In this section, we investigate the frequency-dependent regulation dynamics of the transcription factor, subject to Ca^{2+}-dependent activator (A) and inhibitor (I) enzymes. The time-dependent activation of enzymes is governed by Eqs. 4.1 and 4.2, and Eq. 4.3 describes the effect of the activated form of the enzymes (A_a and I_a) on the fraction of activated transcription factor (TF_a). For a periodic square-wave Ca^{2+} stimulus, the long-term mean values of A_a and I_a (denoted by $\bar{A}_a$ and $\bar{I}_a$, respectively) are described by Eq. 4.12. Inserting these into Eqs. 4.4 and 4.5, respectively, yields $\bar{A}_\infty$ and $\bar{I}_\infty$ (Fig. 4.6A). These long-term activator and inhibitor actions determine the approximate long-term or steady-state fraction of activated transcription factor:

$$\overline{TF}_{ss} = \frac{\bar{A}_\infty}{\bar{A}_\infty + \bar{I}_\infty} \quad . \tag{4.19}$$

In the model, the sensitivity of the transcription factor to activator and inhibitor enzymes is determined by K_A and K_I, respectively. Changes in these parameters shift the $\bar{A}_\infty$ and $\bar{I}_\infty$ curves left/right when plotted versus stimulus period as in Fig. 4.6A and, for each T value, the vertical distance between the curves is the primary determinant of the long-term transcription factor activation level (Eq. 4.19). That means the relative positions of these curves gives the fraction of activated transcription factor at each T value. Therefore, we explore frequency dependent transcription factor dynamics by fixing $\bar{I}_\infty$ and shifting $\bar{A}_\infty$ horizontally by varying K_A (Fig. 4.6B). For small values of K_A, increasing frequency by moving from right to left reduces $\overline{TF}_{ss}$ (Fig. 4.6B, bottom portion), while for large K_A values increasing frequency increases $\overline{TF}_{ss}$ (Fig. 4.6B, top portion). For moderate K_A values, the frequency response of $\overline{TF}_{ss}$ is bell shaped. Thus, for moderate K_A values there exists an optimum frequency for which $\overline{TF}_{ss}$ is maximized (Fig. 4.6B, middle portion). To understand these relationships, we compare the rate of change of $\bar{A}_\infty$ with respect to period T to that of $\bar{I}_\infty$ as K_A is varied. Both $\bar{A}_\infty$ and $\bar{I}_\infty$ are decreasing functions of T, but in the brown region of Fig. 4.6C the rate of change of $\bar{A}_\infty$ with respect to T is greater than the rate of change of $\bar{I}_\infty$. Therefore, in this region, as the frequency is increased (or as T is decreased) $\bar{A}_\infty$ grows less than $\bar{I}_\infty$ and inhibition dominates. Consequently, for small K_A values, increasing frequency reduces $\overline{TF}_{ss}$. In the blue region, this relation is reversed and increased frequency leads to a greater increase in $\bar{A}_\infty$. Therefore, for large K_A values, increasing frequency increases $\overline{TF}_{ss}$. For moderate K_A values, there is a transition from one region to the other as frequency is increased. Therefore, increasing frequency initially has a greater impact on $\bar{A}_\infty$ then $\bar{I}_\infty$ (blue region), which leads to a net increase in $\overline{TF}_{ss}$. Once in the brown region, further increasing frequency causes $\overline{TF}_{ss}$ to decrease. In summary, depending on their sensitivities to the Ca^{2+} regulated enzymes, the transcription factor activity may increase or decrease with the frequency of the Ca^{2+} signal. If the sensitivity of the transcription factor to the inhibitor is greater than its sensitivity to the activator, then increased frequency increases transcription factor activation. When sensitivity of the transcription factor to the activator and the inhibitor are relatively similar, then the frequency response curve of the transcription factor is bell shaped and has an optimum range for stimulus frequency.

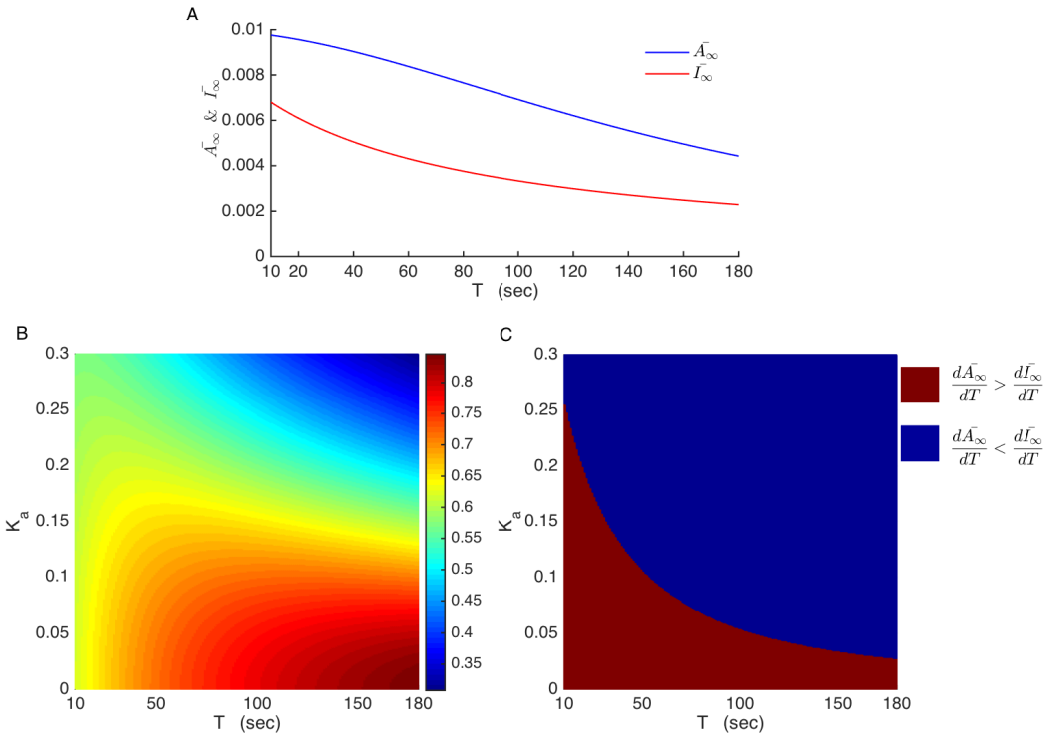

Figure 4.6: Frequency response regimes of the transcription factors. Relative sensitivity of the transcription factor to the activator and inhibitor enzymes determines the frequency response regime. (A) Representative $\bar{A}_\infty$ (blue) and $\bar{I}_\infty$ (red) curves. Relative positions of these curves determine the transcription factor activation level. (B) Approximate asymptotic fraction of the activated transcription factor ($\overline{TF}_{ss}$) over a range of values of T and K_a. (C) The rates of changes of $\bar{A}_\infty$ and $\bar{I}_\infty$ with respect to T determines the frequency response. In the blue region $\bar{A}_\infty$ declines faster than $\bar{I}_\infty$ as T is increased. In the brown region this relation is reversed.

The transcription factor is assumed to be an activator, so that its activated form, TF_a, increases the mRNA concentration. In the model, we describe the mRNA level with a dimensionless variable M, which changes in time according to:

$$\frac{dM}{dt} = p_M \frac{TF_a}{TF_a + K_{mRNA}} - d_M M \tag{4.20}$$

where p_M is the maximal transcription rate, K_M is the TF_a for half maximal transcription and d_M is the degradation rate. From the analysis above, it is clear that the level of activated transcription factor, and from Eq. 4.20 the level of mRNA, will be different with different patterns of square-wave input. This is shown in the red and blue traces of Fig. 4.7, where the stimulus frequency

and amplitudes are different, but the mean levels of Ca^{2+} are the same. In this case, the blue pattern evokes a larger response in the mRNA level (panel B). This is also true for the response to sinusoidal (violet and green) versus square (blue and red) wave stimuli. Clearly, both the shape of the pulses and their frequency influence the mRNA level.

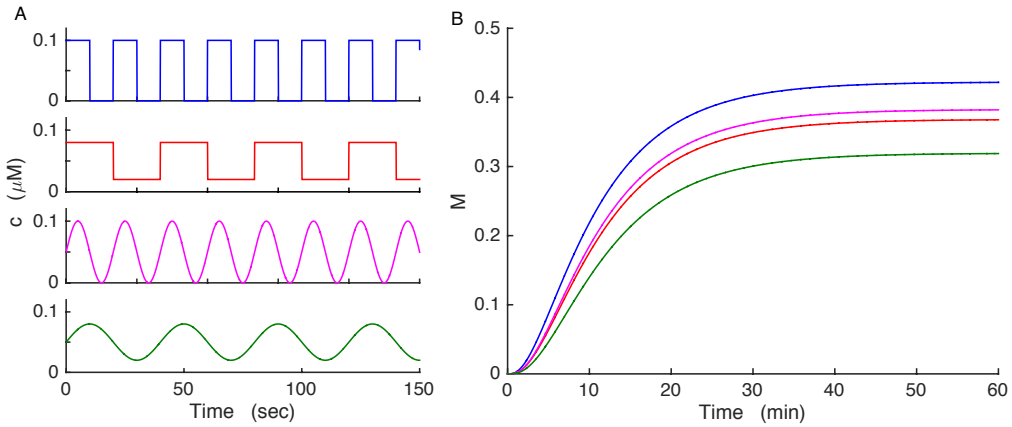

Figure 4.7: Pattern of the Ca^{2+} signal determines the mRNA level. Different periodic Ca^{2+} signals produce different levels of gene expression, even though the average Ca^{2+} level is the same. (A) Two square wave and two sinusoidal Ca^{2+} signals, each with the same average of 0.05 μM. (B) The mRNA level in response to the four Ca^{2+} stimuli.

4.7 Ca^{2+} Frequency-Dependent Compensation in the Model KO Cells

We now ask whether, in a β-cell model adopted from (Bertram and Sherman 2004), knockout of the key K(ATP) ion channel can induce compensating upregulation of a different K^+ ion channel to the correct level so that bursting electrical activity is rescued? In other words, can the Ca^{2+}-dependent transcription described above act as a homeostatic mechanism to return the system to its original pattern of activity? An illustration of the model that shows the pathways regulating membrane potential is given in Fig. 4.8A. The model wild-type cell can produce bursting electrical activity by coupling a Hodgkin-Huxley type membrane potential model with intracellular Ca^{2+} and nucleotide dynamics. It is equipped with voltage-gated Ca^{2+} and K^+ currents (I_{Ca}, I_K), ATP- and Ca^{2+}-sensitive K^+ currents (I_{KATP}, I_{KCa}), a leak current (I_l) and an inward-rectifying K^+ current (I_{cmp}). I_{cmp} is the compensating current which has a very small

influence on the electrical activity of the wild-type cells and will gain importance during compensation. The differential equations for the electrical potential change across the plasma membrane, V, delayed-rectifying K^+ current activation, n, the cytosolic ADP/ATP ratio, a, and the free cytosolic Ca^{2+} concentration, c, and free endoplasmic reticulum (ER) Ca^{2+} concentration, c_{er}, are as follows:

$$\frac{dV}{dt} = -(I_{Ca} + I_K + I_{K_{ATP}} + I_{K_{Ca}} + I_l + I_{cmp})/C_m \quad (4.21)$$

$$\frac{dn}{dt} = (n_\infty(V) - n)/\tau_n \quad (4.22)$$

$$\frac{dc}{dt} = f_{cyt}(J_{mem} + J_{er}) \quad (4.23)$$

$$\frac{dc_{er}}{dt} = -f_{er}\frac{V_{cyt}}{V_{er}}J_{er} \quad (4.24)$$

$$\frac{da}{dt} = (a_\infty(c) - a)/\tau_a \quad (4.25)$$

where C_m is the constant membrane capacitance. $n_\infty(V)$ and $a_\infty(c)$ are the equilibrium functions for activation variables *n* and *a* respectively, τ_n and τ_a are activation time constants, J_{mem} is the Ca^{2+} flux across the membrane, and f_{cyt} is the ratio of unbound Ca^{2+} to the total Ca^{2+} concentration. J_{er} is the Ca^{2+} flux across the ER membrane and f_{er} is the ratio of unbound Ca^{2+} to the total Ca^{2+} concentration in the ER. V_{cyt} and V_{er} are the volumes of cytosolic and ER compartments, respectively. The details of the equilibrium activation functions, ionic currents and fluxes are given in Appendix B.

When exposed to stimulatory glucose levels, pancreatic β-cells exhibit bursting electrical activity and Ca^{2+} oscillations. The model cell can produce bursting for moderate maximal conductance values of the ATP-sensitive K^+ current (Fig. 4.8B). In the model, the fast activation of depolarizing Ca^{2+} current and delayed activation of hyperpolarizing K^+ current produces action potentials. Episodes of action potentials are separated by slow negative feedback provided by Ca^{2+} on the membrane potential and ATP production. In the model the endoplasmic reticulum (ER) acts as a Ca^{2+} sink during active phases of spiking and as a Ca^{2+} source during silent phases. The impact that this buffering has on the cytosolic Ca^{2+} ultimately sets the period of bursting; during an active phase c_{er} slowly rises as it uptakes Ca^{2+}, thereby removing some of

the Ca^{2+} from the cytosol that would otherwise terminate a burst quickly through actions on Ca^{2+}-activated K^+ channels. During a silent phase c_{er} slowly declines as it releases Ca^{2+} into the cytosol, thereby delaying the decline of c that will ultimately allow spiking to restart by deactivation of the same K(Ca) channels (Fig. 4.8C). A detailed analysis of this bursting mechanism is given in the following section where we discuss the compensation dynamics.

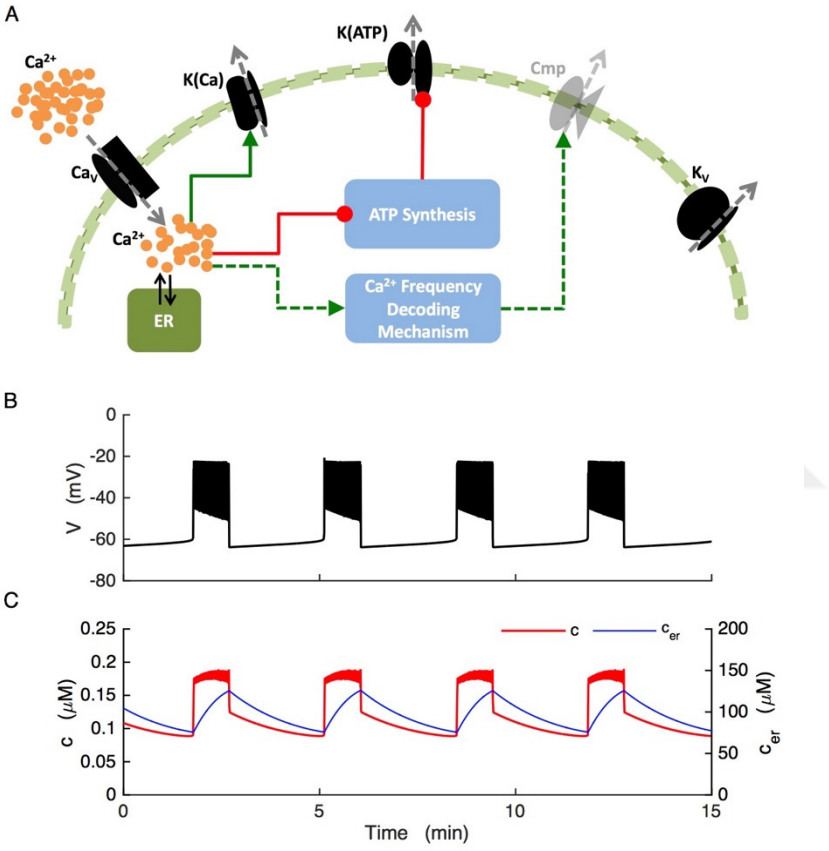

Figure 4.8: Key components of the β-cell model and bursting. The model β-cell produces bursts of electrical activity accompanied by oscillations in the free cytosolic Ca^{2+} concentration (c) and the free ER Ca^{2+} concentration (c_{er}). (A) An illustration of the β-cell model. Green arrows represent stimulatory and red circles represent inhibitory pathways. Solid lines represent pathways that regulate the membrane potential where dashed lines represent pathways regulating activity-dependent ion channel expression. (B) The model cell produces bursts of electrical activity with a period of ~3 minutes. (C) Bursts of electrical activity are accompanied by square-wave c oscillations (red) and slow sawtooth- shaped c_{er} oscillations (blue).

We assume that the maximal conductances of all ionic currents are constant, with the exception of that of the compensating current (g_{cmp}). We assume that the maximal conductance

of this current is proportional to the compensating channel expression and dynamically regulated by Ca^{2+}-dependent gene transcription with the following equation:

$$\frac{dg_{cmp}}{dt} = p_g \frac{M}{M+K_g} - d_g \tag{4.26}$$

where M is the mRNA level, whose dynamics are governed by Eq. 4.20, p_g is the maximal rate of production, K_g is the mRNA level for half-maximal production and d_g represents the saturated degradation rate (Drengstig et al. 2008; He et al. 2013; O'Leary et al. 2014). Dynamical regulation of g_{cmp} by Ca^{2+}-dependent transcription completes the feedback loop illustrated in Fig. 4.1.

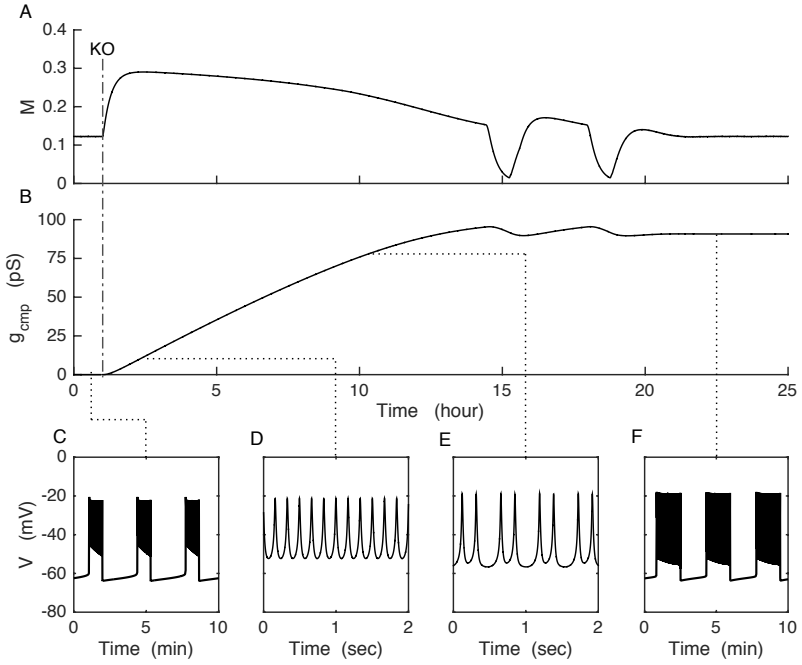

Figure 4.9: Homeostatic compensation. K(ATP) channel knockout changes the pattern of activity and leads to an increase in the expression of the compensating ion channel, eventually rescuing the bursting pattern. (A, B) Frequency decoding mechanism regulates *M*, which regulates g_{cmp}, according to the pattern of activity. Prior to the K(ATP) knockout (KO) the cell is in a homeostatic state with *M* and g_{cmp} at equilibrium levels. Once compensation is complete, a new homeostatic state is reached. (C-F) Voltage traces show patterns of activity before KO (C), during compensation (D and E) and at the completion of compensation (F).

We next examine the effect of K(ATP) channel knockout. Can the model cell successfully compensate for this and restore slow bursting? Prior to the knockout (KO) of K(ATP) channels (to the left of the dot-dashed line in Fig. 4.9), the cell is in a homeostatic state. The cell bursts with a period about 3 minutes (Fig. 4.9C) and this pattern leads to a certain level of M (Fig. 4.9A, left of the KO). Parameter values are set so that at this homeostatic state g_{cmp} is low and constant (Fig. 4.9B, left of the KO). Since the burst pattern generated in this state is the behavior of the wild-type cell in the homeostatic state we refer to it as 'the target pattern of activity'. Following the knockout, the complete loss of hyperpolarizing K(ATP) current puts the cell into a continuously spiking depolarized state (Fig. 4.9D). This change in the pattern of activity alters the Ca^{2+} signal and consequently gene expression (Fig. 4.9A, right of the KO). Since the cytosolic Ca^{2+} level is now higher than before, both the mRNA level, M, of the compensating ion channel and the channel conductance, g_{cmp}, increase (Fig. 4.9B, right of the KO). Since the compensating current is a hyperpolarizing K^+ current, increased maximal conductance hyperpolarizes the cell membrane and slowly changes the pattern of activity (Fig. 4.9E). The hyperpolarization is accompanied by decreased Ca^{2+} concentration, which slows down production of M. At about hour 14 following the knockout, there is a sharp decrease in the mRNA. This is due to the overexpression of the compensating current, which puts the cell into a transient silent state, where the Ca^{2+} level is low. As a result, both M and g_{cmp} decline. The latter decline causes electrical activity to re-emerge and the process continues as before. Within several more hours a new homeostatic state is reached, and in this new state the cell is once again bursting with a period close to that of the target pattern of activity (Fig. 4.9F). There is a difference between burst periods and between the burst duty cycles, but this is to be expected since the properties of the compensating ion channel are not the same as those of the K(ATP) channel in the wild-type cell. In fact, electrophysiological recordings from wild-type and KO-mice islets also show noticeable differences in the bursting patterns (Düfer et al. 2004).

4.8 The Evolution of Dynamics in the Model β-Cell During Compensation

To understand the way the dynamics of the model β-Cell evolve throughout compensation, we performed a fast/slow analysis (Rinzel and Ermentrout 1989; Bertram and

Rubin 2016). In the β-cell model that we use, the fast variables are voltage (V) and the activation variable for the voltage-gated K^+ current (n). The slow variables are the cytosolic Ca^{2+} (c), Ca^{2+} concentration in the ER (c_{er}) and the cytosolic *ATP/ADP* ratio (a). If we set a to its mean value over a burst period, the cell continues to burst with almost the same pattern. Therefore, we start our analysis by setting a to its mean over a burst period, which reduces the number of slow variables and simplifies the analysis. The remaining slow variables, c and c_{er}, act on the fast subsystem through the activation variable of the K(Ca) current, ω.

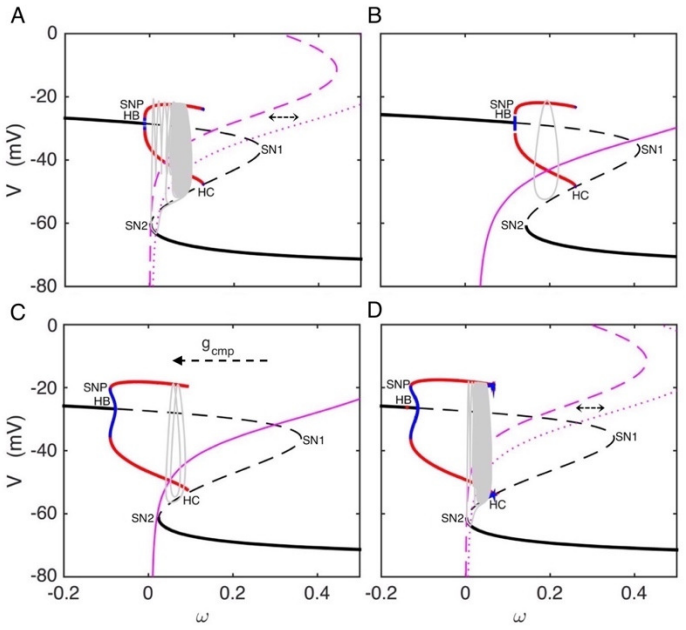

Figure 4.10: Fast/slow analysis of the model β-cell dynamics throughout the compensation process. The black curve represents stationary solutions of the fast subsystem, while the red curves are the minimum and maximum voltage branches of periodic spiking solutions. The purple curves are described by Eq. 4.29 with different values of the ER Ca^{2+} concentration. The gray curve is the burst trajectory. (A) Before K(ATP) channel knockout. (B-C) At different points in the compensation process. (D) After completion of compensation. Panels A, B, C and D correspond to the time courses shown in Fig. 4.9, panels C, D, E and F, respectively.

We now use bifurcation analysis to explore the dynamics of the fast subsystem of the model wild-type cell, using ω as the bifurcation parameter (Fig. 4.10A). Although only positive ω values are biologically meaningful, the diagram starts with negative ω values. For small values of ω, the fast subsystem is at rest at a depolarized steady state. These depolarized stable steady states constitute the initial portion of the upper branch of the z-shaped manifold (solid

black), which we refer to as the z-curve. Increasing ω increases the K(Ca) current and destabilizes the stationary branch (dashed black curve) at a subcritical Hopf bifurcation (HB). This gives rise to a branch of unstable periodic solutions that gains stability at a saddle node of periodics bifurcation (SNP). This periodic branch, reflecting tonic spiking of action potentials, continues for higher values of ω until it terminates at a homoclinic bifurcation (HC). The stationary branch goes through two saddle node bifurcations (SN1 and SN2) and regains stability at SN2. Between SN2 and HC there is a region of bi-stability between the spiking branch and the lower stationary branch, which is key to the bursting.

As mentioned above, the slow subsystem acts on the fast subsystem through the action of Ca^{2+} on the activation variable of the K(Ca) current, ω. This relation is given with the following equation:

$$\omega = \frac{c^5}{c^5 + K_\omega^5} \quad . \tag{4.27}$$

Setting the slow variable c to its steady state yields

$$c_{ss} = \frac{\alpha I_{Ca} + k_{erout} c_{er}}{k_{pmca} + k_{erout} + k_{erin}} \quad , \tag{4.28}$$

where the ionic current I_{Ca} is a function of V and gives the relation between V and c_{ss}. Substituting c_{ss} for c in Eq. 4.27:

$$\omega_{ss} = \frac{c_{ss}^5}{c_{ss}^5 + K_\omega^5} \quad . \tag{4.29}$$

We now add in the dynamics of the slow subsystem to the fast subsystem bifurcation diagram by superimposing two ω_{ss}-curves, calculated for either the minimum or maximum values that c_{er} takes on during a burst (Fig. 4.10A, dashed and dotted purple curves, respectively). Finally, we complete the picture by adding a burst trajectory (gray). At the beginning of a burst active phase c_{er} is small and the ω_{ss}-curve intersects the z-curve deep in the

periodic branch. Therefore, the full system exhibits spiking. This results in an influx of Ca^{2+} and a subsequent slow increase in c_{er} that shifts the ω_{ss}-curve rightward and the phase point follows after it. Eventually the rightward shift of the ω_{ss}-curve allows the phase point to leave the periodic branch as it approaches the homoclinic orbit HC, ending the active phase and initiating the silent phase of the burst as the phase point moves to the bottom stationary branch. The Ca^{2+} influx is now greatly reduced, so both the cytosolic and ER Ca^{2+} concentrations decline, shifting the ω_{ss}-curve leftward. When the ω_{ss}-curve passes the lower knee of the z-curve, the only remaining stable structure is the periodic branch. Therefore, the phase point jumps back to the periodic branch and restarts a burst active phase. The dynamics described above corresponds to the bursting pattern in Fig. 4.9C.

The K(ATP) channel knockout shifts the z-curve rightward (Fig. 4.10B) so that the ω_{ss}-curve intersects the z-curve deep in the periodic branch. Hence, the cell spikes tonically (Fig. 4.9D). Meanwhile, the compensation mechanism increases the expression of the compensating channel, which shifts the z-curve leftward by hyperpolarizing the cell membrane (Fig. 4.10C). The shift in the z-curve is accompanied by the widening of the periodic branch, which increases the spike amplitude (Fig. 4.9E). Finally, compensation restores bursting with a dynamic mechanism essentially the same as in the wild-type cell (Fig. 4.10D).

4.9 The Effect of Prolonged Pharmacological Blockade of K(ATP) Channels

Experimental evidence suggests that pharmacological long term blockade of the K(ATP) channels could lead to increased gene expression (Sjöholm 1995). Thus, upregulation of the compensating current may result from long term pharmacological blockade of K(ATP) channels. Unlike the genetic knockout, the pharmacological blockade of the K(ATP) channels with an agent such as tolbutamide would be transient and reversible.

Figure 4.11 shows the effects of simulated blockade of K(ATP) channels. The model cell is initially bursting, but when K(ATP) channels are blocked (red dashed line) the cell immediately begins to spike continuously, leading to an elevated cytosolic Ca^{2+} level (Fig. 4.11B), which causes increased expression of the compensating channel and consequent increase in the channel conductance (Fig. 4.11A). The sharp rise in c after K(ATP) blockade, is followed

by a gradual decay, which is due to the slow rise in the compensating current that hyperpolarizes the cell membrane. After removal of the K(ATP) channel blocker, (vertical green dashed line) the cell remains silent for roughly an hour, which results in a sustained low value of c. This prolonged silent period is due to the combination of the restored K(ATP) current and the compensating K^+ current, I_{cmp}. With the low value of c, however, g_{cmp} declines and after some time I_{cmp} is small enough that bursting resumes, although initially with a lower frequency. The longer the application of K(ATP) channel blocker, the longer the silent phase after its removal. The prolonged hyperpolarized phase that follows K(ATP) channel restoration is a testable model prediction.

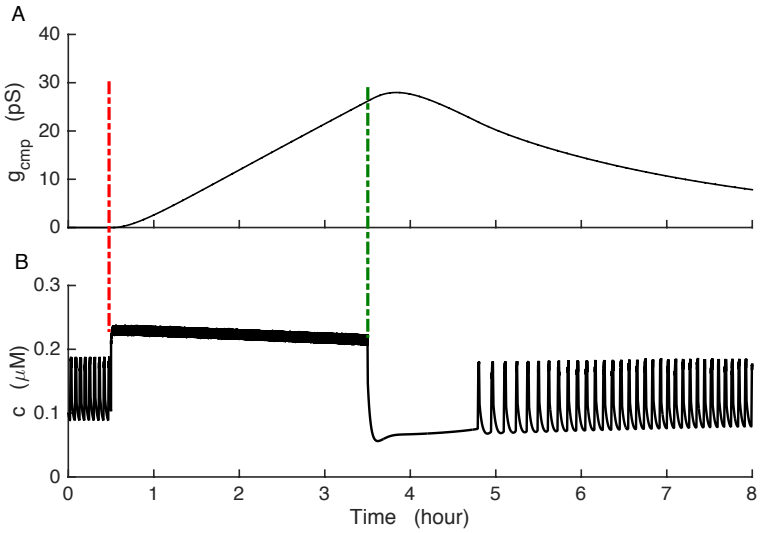

Figure 4.11: The effect of transient K(ATP) blockade on compensation. K(ATP) current is transiently turned off at the vertical red dashed line and turned back on at the vertical green dashed line. (A) The compensating current conductance. (B) The c time course, showing a transient silencing after K(ATP) current is added back.

4.10 Discussion and Concluding Remarks

In this chapter, we introduced an activity-dependent homeostatic compensation mechanism to explain the rescue of bursting electrical activity observed in K(ATP) channel deficient pancreatic mouse β-cells (Fig. 4.9). The mechanism for compensation is based on Ca^{2+} activation of two opposing enzymes that control the level of gene expression of the

compensating channel, and which is altered when the K(ATP) channels are removed. It is well established that long-term changes in the activity of an excitable cell can regulate the expression of ion channels (31, 40, 43,). This may result from the increased intracellular Ca^{2+} concentration, which is a well-documented regulator of gene expression (Barish 1998; West et al. 2001). One safety aspect of the feedback mechanism is that it prevents the cytosolic Ca^{2+} concentration from remaining persistently elevated, which leads to excitotoxicity and ultimately cell death (Efanova et al. 1998; Iwakura et al. 2000; Maedler et al. 2005; Pinton et al. 2008). Our model responds to the K(ATP) channel knockout by regulating the expression of a compensating inward-rectifier K^+ channel. Such channels, Kir2.1, have been shown to be upregulated in K(ATP) knockout cells by our collaborators and in Chapter 3 we demonstrated that the upregulated channels are functional (Fig. 3.3C), providing inward-rectifying current. In the model, the key elements are two opposing Ca^{2+}-dependent enzymes, which decode the frequency of the Ca^{2+} oscillations and regulate the activity of a target transcription factor. These enzymes could be either kinases or phosphatases, both of which have Ca^{2+}-dependent isoforms (Rosen et al. 1995; Li et al. 2011; Swulius and Waxham 2013). Studies have shown that some Ca^{2+}-frequency sensitive transcription factors are activated when phosphorylated (Segil et al. 1991; Oeckinghaus and Ghosh 2009) where others are activated when dephosphorylated (Rao et al. 1997).

It was previously shown that Ca^{2+} is more effective at regulating gene expression when delivered in an oscillatory fashion (Dolmetsch et al. 1998; Tsien et al. 1998). This amplifying effect of Ca^{2+} oscillations was subsequently studied with mathematical models (Dupont et al. 2003; Schuster et al. 2005; Salazar et al. 2008). These studies show that the efficiency of the oscillatory signals arises primarily from the non-linear dependence of the components of the pathway to the upstream events, which may result from cooperative Ca^{2+} binding, zero-order ultra-sensitivity, homo-dimerization or -trimerization and cooperative activation through multiple pathways (Zhang Q et al. 2013). These prior modeling studies either focused on the transcription factors which are regulated by a single Ca^{2+}-dependent enzyme (Salazar et al. 2008) or focus on the activation of the enzymes themselves (Dupont et al. 2003). However, activity of several transcription factors are modulated by multiple pathways that involve Ca^{2+}-dependent components (Berridge et al. 2003). We show that regulation of a transcription factor by two opposing Ca^{2+}-dependent enzymes yields qualitatively different frequency response regimes.

Depending on the relative affinities of the transcription factor to the activator and inhibitor enzymes, transcription factor activation may increase with the frequency of the stimulus or decrease. If the transcription factor's sensitivity to the activator and inhibitor enzymes are comparable then there is bell-shaped response function with an optimum frequency for which the activation of the transcription factor is maximized (Fig. 4.6), as has been observed experimentally (Tsien et al. 1998; Zhu et al. 2008).

The compensation mechanism that we employed differs fundamentally from the mechanism described in (O'Leary et al. 2014). In that study, gene expression evolved to a point such that the time-averaged Ca^{2+} concentration matched a target level. In the mechanism that we employed, there is no explicit target, and the Ca^{2+} pattern, not its time average, sets the expression level of the compensating gene (Fig. 4.7). Parameter values were set so that the interaction of the activator and inhibitor enzymes push the system to a point such that the Ca^{2+} concentration oscillates and the pattern is similar to that of wild-type cells. We speculate that in the actual cells this choice of affinity values would be set through natural selection, given the importance of pulsatile insulin secretion in glucose homeostasis (Matthews et al. 1983b; Paolisso et al. 1991; Hellman 2009; Matveyenko et al. 2012).

While we have considered compensation through a single gene, the reality is much more complicated. Studies have shown that the expression levels are altered for tens or hundreds of genes in response to genetic knockout of a single gene (Liu et al. 2007; Eraly 2014; Wang et al. 2015). The difficulty comes in determining which of these changes are the most important for the behavior of the cell. In the case of K(ATP) channel knockout in pancreatic β-cells, we know that Kir2.1 channels are upregulated (Vadrevu et al., in preparation), but there are likely many other changes in protein levels, some of which could be ion channels. Mathematical modeling can be useful here, in determining which channels can potentially compensate for the K(ATP) channel in the preservation of electrical bursting activity. In Chapter 3, we showed that Kir2.1 has the right properties to do this, but we gave no explanation for how the cell would know how much Kir2.1 conductance was needed to rescue bursting. How would the appropriate level of expression of this compensating channel be determined? That question motivated the work presented in this chapter, where we have shown that the appropriate level of compensation can

occur quite naturally provided that the transcription factor is activated by Ca^{2+}-dependent enzymes whose levels of activation are different for Ca^{2+} signals of different frequencies. That is, Ca^{2+}-frequency regulated enzymes. This process would of course be much more complex if the expression levels of multiple ion channel proteins or modulating enzymes are affected by the compensation process, but the same underlying principle should apply. Indeed, having several degrees of freedom should make it easier to achieve a target pattern that is similar to that of the wild-type cell.

It has been shown that long-term blockade of K(ATP) channels by pharmacological agents in insulin secreting cell lines results in increased DNA synthesis (Sjöholm 1995). The same study showed that blocking Ca^{2+} influx, while K(ATP) channels are blocked, suppressed the DNA synthesis. This is direct evidence for Ca^{2+}-dependent compensatory gene expression in response to the removal of K(ATP) current. We simulated transient K(ATP) blockage and found that the cell is silenced for an extended period of time after the channel blocker is removed (Fig. 4.11). The duration of the silent phase increases with the length of time that K(ATP) channels remain blocked. While K(ATP) channel blockers such as tolbutamide have been used in many studies (for example, (Larsson et al. 1996; Ren et al. 2013)), the exposure time is typically in the seconds to minutes range. A recent study applied tolbutamide to islets overnight, but the behavior of the islets immediately after removal of the channel blocker was not examined (Glynn et al. 2016). Thus, our finding of cell silencing after hours-long blockade of K(ATP) channels is a testable, but to our knowledge untested, prediction.

CHAPTER 5

CONCLUSION

5.1 Summary

In this dissertation, using a systems biology approach, we investigated the mechanisms through which genetic defects in the expression of a key ion channel, the K(ATP) channel, can be compensated in mouse pancreatic β-cells. In humans, genetic defects in the expression of K(ATP) channels leads to spontaneous β-cell activity and excessive insulin secretion even when blood glucose is low, which results in persistent hyperinsulinemic hypoglycemia of infancy (PHHI). However, mice overcome the same defects by engaging alternative mechanisms. The paradoxical bursting electrical activity and Ca^{2+} oscillations observed in the K(ATP) channel deficient mouse pancreatic β-cells were the motivation behind this study. This surprising phenomenon has been observed by several different labs over the past decades but no underlying mechanism has been identified until today. Our primary aim was solving this mystery by explaining the mechanisms driving slow oscillations in these cells.

Our collaborators (the Satin lab at the Brehm Center for Diabetes Research at the University of Michigan) have recently demonstrated that Kir2.1 channel protein levels are upregulated in mice β-cells when K(ATP) channels are genetically knocked out (manuscript in preparation). Does this upregulated channel protein have an actual effect on the membrane potential? Current-voltage recordings from the Satin lab (Fig. 3.3C) demonstrate that in KO islets an inward rectifying K^+ current, which is not present at significant levels in the wild type islets, is upregulated. This demonstrated that the upregulated channels could provide hyperpolarization, but could the ionic current through the channels take over the role that K(ATP) current played in the wild type β-cells and restore oscillations in the KO cells? We answered this question with mathematical modeling and showed that upregulated Kir2.1 current was capable of driving bursting electrical activity through a cAMP dependent pathway in the model KO cells (Fig. 3.6A). We also investigated the possibility of upregulation of other ion channel types that could drive slow oscillations. Even though we demonstrated that upregulation

of other K^+ channel types could drive slow oscillations through a distinct mechanism (Fig. 3.9), an experimental test verified that the Kir2.1 channel upregulation is the more likely mechanism for the bursting electrical activity observed in the KO cells (Fig 3.11).

We then made a theoretical exploration of the mechanism that controls the level of upregulation of the compensating channel. Previous studies show that a well-tuned control element is required for homeostatic compensation and computational studies suggest that this element could be cytosolic Ca^{2+}. We proposed a mathematical model for a Ca^{2+} frequency sensitive gene transcription network (Fig. 4.1) and showed that this network can decode the pattern of the Ca^{2+} signal and naturally define a target pattern of activity for compensation (Fig. 4.7). By incorporating this gene transcription network into a well-studied β-cell model we showed that it can dynamically set the compensating channel conductance to the right level and restore oscillations when K(ATP) channels are genetically knocked out (Fig. 4.9). We demonstrated that defining the homeostatic target with a pattern of activity ensures oscillations to be restored in β-cells, which is important for normal blood glucose regulation.

5.2 Future Work and Conclusion

One study of RINm5F insulinoma cell lines shows that long-term blockade of K(ATP) channels with pharmacological agents leads to altered gene expression through a Ca^{2+} dependent mechanism in these cells. The same approach can be implemented to investigate the effect of a transient long term blockade of the K(ATP) channels on compensation. Our compensation model predicts that a long-term blockade of K(ATP) channels with sulfonylureas in the wild type cells should be followed by a long hyperpolarized silent phase when the drug is washed-out (Fig. 4.11B). This prediction is in contrast with the effects of a short-term sulfonylurea treatment, where electrical activity reemerges right after the wash-out. Therefore, this makes a very testable prediction. Testing this prediction is a future goal.

In order to verify the role that Ca^{2+} plays in compensation, the long term β-cell membrane depolarization approach can be employed in combination with manipulating cytosolic Ca^{2+}. These experiments can directly verify the role that cytosolic Ca^{2+} plays in compensation and can

give a better understanding about the dynamics of the process. In principle, this can be done by blocking voltage-gated Ca^{2+} channels with drugs like verapamil while cell membrane is depolarized with sulfonylureas. However, blocking Ca^{2+} influx would also affect membrane depolarization in β-cells. Therefore, instead of sulfonylurea treatment, in these experiments, membrane depolarization can be induced by activating K(ATP) channels with the drug diazoxide and increasing extracellular K^+ concentration by adding KCl to the medium. KCl will increase the K^+ reversal potential by increasing extracellular K^+ concentration. Therefore, K^+ will flow down the concentration gradient in the inward direction through activated K(ATP) channels and will depolarize the cell membrane. Thus, membrane depolarization will be achieved while Ca^{2+} influx is detained.

Another way of manipulating cytosolic Ca^{2+} during this experiments could be accompanying sulfonylurea treatment with Ca^{2+} buffers, such as EGTA and BAPTA. This way Ca^{2+} influx will be preserved but its cytosolic action will be prevented. The benefit of these set of experiments is that BAPTA and EGTA have different affinities for Ca^{2+}, which means each will allow Ca^{2+} to be diffused to a different distance from the channel pores before it gets buffered inside the cell. BAPTA has high affinity for Ca^{2+} and buffers Ca^{2+} within the close vicinity of the channel pores as soon as it enters the cell. In the other hand, EGTA has a lower affinity for Ca^{2+} and consequently allows Ca^{2+} to be diffused further away from inside the cell. Therefore, these experiments can demonstrate possible co-localization of the Ca^{2+}-dependent enzymes and Ca^{2+} channels. That is, if treatment with BAPTA and EGTA leads different results, then Ca^{2+} binding enzymes are most likely co-localized with voltage-gated Ca^{2+} channels, which indicates another mechanism that β-cells employ to increase the efficiency of Ca^{2+}-dependent gene expression. However, it must be noted that these approaches are challenging since pancreatic islets do not survive under severe Ca^{2+} deficient conditions for a long time.

In conclusion, the mechanism that we propose in this dissertation is the likely mechanism that is responsible for the paradoxical bursting electrical activity observed in the K(ATP) channel deficient mouse pancreatic β-cells. One of the long-term goals of this study is identifying possible targets for persistent hyperinsulinemic hypoglycemia of infancy or congenital hypoglycemia therapies. According to our model, one such target could be cAMP dependent

pathways in these cells. A further study that focuses on the different gene regulatory mechanisms that mice and humans employ when subject to genetic defects is needed to understand why human β-cells do not accomplish compensation like mice β-cells. It is obvious that such experiments can't be performed on human subjects to see whether their β-cells can overcome K(ATP) channel defects over time. However, even though a clinical approach can't be used, *in vitro* experiments performed by long-term blockade of K(ATP) channels with pharmacological agents in human islets can be significantly helpful. These experiments can show whether or not human β-cells possess similar regulatory mechanisms that mice employ for homeostatic compensation.

APPENDIX A

THE DUAL OSCILLATOR MODEL

A.1 The Glycolytic and Mitochondrial Model

The glycolytic model explains the dynamics of the metabolic oscillations, which result from the allosteric activity of the enzyme phosphofructokinase (PFK) (for details see (Smolen 1995)). A complete mathematical and biophysical description of the model can be found in (Bertram et al. 2004; Watts et al. 2014; McKenna et al. 2016). In the model the glycolytic output is given by the output of the PFK reaction, which phosphorylates fructose 6-phosphate (F6P) to fructose 1,6-bisphosphate (FBP). FBP is then assumed to be proportional to the substrate concentration for the enzyme pyruvate dehydrogenase (PDH), described by the following flux rate:

$$J_{PDH} = k_{PDH}\left(\frac{c_m}{c_m + k_{PDHcm}}\right)\sqrt{FBP/1\mu M} \tag{A.1.1}$$

where k_{PDH} is the rate constant, $c_m = 5c$ is mitochondrial Ca^{2+} concentration (Merrins et al. 2016). The rate of change of F6P and FBP concentrations are given by:

$$\frac{dF6P}{dt} = k_{F6P}(J_{GK} - J_{PFK}) \tag{A.1.2}$$

$$\frac{dFBP}{dt} = k_{FBP}(J_{PFK} - 0.5J_{PDH}) \tag{A.1.3}$$

where k_{F6P} and k_{FBP} are the proportionality constants derived from a series of reactions upstream and downstream of PFK (for derivation see (McKenna et al. 2016)), and J_{GK} is the constant flux through glucokinase. This rate would be determined by factors such as the glucose concentration, the expression and the activity of the glucose transporters (GLUT2), and the expression of the glucokinase enzyme itself. The different J_{GK} values used in the model wild-type and KO cell simulations may be regarded as a result of altered gene expression.

The mitochondrial metabolism model is from (Watts et al. 2014). It is assumed that the sum of the mitochondrial ADP (ADP_m) and ATP (ATP_m) concentrations is constant: $A_{mtot}= ADP_m+ ATP_m$. ADP_m is in rapid equilibrium with J_{PDH} according to:

$$ADP_m = \frac{k_{ADPm}}{\exp\left(\frac{J_{PDH}}{k_{ADPmPDHP}}\right)} \quad . \tag{A.1.4}$$

The ATP produced in the mitochondria enters the cytosol via the adenine nucleotide translocator (ANT) with flux rate:

$$J_{ANT} = \frac{v_{ANT}}{1+k_{ANT}\frac{ADP_m}{ATP_m}} \exp\left(\frac{FRT}{2}\psi_m\right) \tag{A.1.5}$$

where $FRT= F/RT$ is Faraday's constant divided by the gas constant and temperature, and ψ_m is the mitochondrial membrane potential. The rate of change of the cytosolic ATP concentration, ATP_c, is determined by ATP translocation and hydrolysis:

$$\frac{dATP_c}{dt} = V_{mc}J_{ANT} - J_{hyd} \tag{A.1.6}$$

where V_{mc} is the ratio of the volume of the mitochondria to the volume of the cytosol. J_{hyd} is the ATP hydrolysis due to cellular activity, given by:

$$J_{hyd} = \left(k_{hyd}c + J_{hyd,bas}\right)ATP_c \tag{A.1.7}$$

where the first term represents the ATP hydrolysis due to the fueling of Ca^{2+} pumps on the plasma and endoplasmic reticulum membranes and depends on c, and the second term is ATP utilization for other processes. Cytosolic AMP and ADP concentrations (AMP_c and ADP_c, respectively) are in rapid equilibrium with ATP and are given as in (Peercy et al. 2015):

$$ADP_c = \frac{ATP_c}{2K_a}\left(\sqrt{1 - 4K_a\left(\frac{1-A_{tot}}{ATP_c}\right)} - 1\right) \tag{A.1.8}$$

$$AMP_c = K_a \frac{{ADP_c}^2}{ATP_c} \quad \text{(A.1.9)}$$

where A_{tot} is the total cytosolic adenosine nucleotide concentration, assumed to be constant.

A.2 Ca^{2+} Handling and Membrane Potential Modules

Equations for this module of the model are from (Bertram et al. 2004). The rate of change of the membrane potential is given by the following Hodgkin-Huxley type equation:

$$\frac{dV}{dt} = -\left(I_K + I_{Ca} + I_{K(Ca)} + I_{K(ATP)}\right)/C_m \quad \text{(A.2.10)}$$

where, C_m is the membrane capacitance, I_K is the delayed rectifier K^+ current, I_{Ca} is voltage-sensitive Ca^{2+} current, $I_{K(Ca)}$ is Ca^{2+}-activated K^+ current, and $I_{K(ATP)}$ is ATP-sensitive K^+ current.

$$I_K = g_K n(V - V_K) \quad \text{(A.2.11)}$$

$$I_{Ca} = g_{Ca} m_\infty (V - V_{Ca}) \quad \text{(A.2.12)}$$

$$I_{K(Ca)} = g_{K(Ca)} \omega (V - V_K) \quad \text{(A.2.13)}$$

$$I_{K(ATP)} = g_{K(ATP)} s_{K(ATP)} (V - V_K) \quad \text{(A.2.14)}$$

where each g_i is the maximal conductance of the current. n is the activation variable of the delayed rectifier K^+ current with dynamics given by:

$$\frac{dn}{dt} = \frac{n_\infty - n}{\tau_n} \quad \text{(A.2.15)}$$

where τ_n is the time constant and the steady state function n_∞ is given by:

$$n_\infty = \frac{1}{1+\exp\left(\frac{V - V_{kv}}{5}\right)} \quad . \quad \text{(A.2.16)}$$

For simplicity, we assume that the Ca^{2+} channel activation is instantaneous, described by:

$$m_\infty = \frac{1}{1+\exp\left(\frac{V-V_{cv}}{12}\right)} \quad . \tag{A.2.17}$$

Activation of the Ca^{2+}-activated K^+ channels is given by the variable ω, defined as:

$$\omega = \frac{c^2}{c^2+K_c^2} \tag{A.2.18}$$

where k_c is the affinity constant for Ca^{2+}. The K(ATP) conductance is assumed to respond instantaneously to changes in the concentrations of the cytosolic adenine nucleotides ADP^{3-}, ATP^{4-} and $MgADP^-$. This relation is given by the activation function $s_{K(ATP)}$, which is taken from (Magnus and Keizer 1998):

$$s_{K(ATP)} = \frac{0.08\left(1+\frac{2MgADP^-}{17mM}\right)+0.89\left(\frac{MgADP^-}{17mM}\right)^2}{\left(1+\frac{MgADP^-}{17mM}\right)^2\left(1+\frac{ADP^{3-}}{26mM}+\frac{ATP^{4-}}{1mM}\right)} \tag{A.2.19}$$

where the binding nucleotide concentrations are given as $MgADP^- = 165ADP_c$, $ADP^{3-} = 135ADP_c$, and $ATP^{4-} = 50ATP_c$.

In the case of $SUR1^{-/-}$ model cells the K(ATP) current is replaced by an inward rectifying K^+ current:

$$I_{Kir} = g_{Kir}k_\infty c_\infty (V - V_K) \quad . \tag{A.2.20}$$

Here g_{Kir} is the maximal Kir2.1 channel conductance, k_∞ is voltage-dependent inactivation and c_∞ is cAMP-dependent activation of the channels. $k_\infty$is described by:

$$k_\infty = \frac{1}{1+\exp\left(\frac{V-V_{kir}}{s_{kir}}\right)} \tag{A.2.21}$$

where V_{kir} is the half-activation potential and s_{kir} is the slope factor. cAMP-dependent and -independent components of the Kir2.1 activation are described by:

$$c_\infty = \alpha_{camp} + \beta_{camp}\frac{cAMP^4}{cAMP^4+K_{camp}^4} \tag{A.2.22}$$

where α_{camp} is the cAMP-independent component, and the Hill function in the second term is the cAMP-dependent component. The constant-conductance leak K^+ current used in the ER bursting model is defined by:

$$I_{K,leak} = g_{K,leak}(V - V_K) \tag{A.2.23}$$

The rate of change of free cytosolic Ca^{2+} concentration is given by:

$$\frac{dc}{dt} = f_{cyt}\left(\overbrace{-\alpha I_{Ca} - k_{pmca}c}^{J_{mem}} + \overbrace{k_{leak}(c_{er} - c) - k_{SERCA}c}^{J_{ER}}\right) \tag{A.2.24}$$

where J_{mem} and J_{ER}represent the Ca^{2+} flux across the plasma membrane and net flux out of the endoplasmic reticulum (ER), respectively. Here, f_{cyt} is the fraction of free to total cytosolic Ca^{2+}, α_c converts current to flux, k_{pmca} is the Ca^{2+} pumping rate from the cytosol, k_{leak} is the leak rate of Ca^{2+} from the ER, and k_{SERCA} is the Ca^{2+} pumping rate into the ER by SERCA pumps. The ER Ca^{2+} concentration changes in time according to:

$$\frac{dc_{er}}{dt} = -f_{er}V_{cte}(k_{leak}(c_{er} - c) - k_{SERCA}c) \tag{A.2.25}$$

where f_{er} is the ratio of the concentration of free to total Ca^{2+} in the ER and V_{cte} is the ratio of the volume of the cytosol to the volume of the ER compartment.

Equations for the dynamics of cAMP are from (Peercy et al. 2015), where the cAMP concentration is given by the difference between its production by adenylyl cyclase (V_{AC}) and degradation by phosphodiesterases (V_{PDE}):

$$\frac{dcAMP}{dt} = V_{AC} - V_{PDE} \tag{A.2.26}$$

where,

$$V_{AC} = \bar{v}_{AC}\left(\alpha_{AC} + \beta_{AC}\frac{c^3}{c^3 + K_{ACca}^3}\right)\left(\beta_{amp}\frac{K_{amp}^2}{AMP_c^2 + K_{amp}^2}\right) \tag{A.2.27}$$

$$V_{PDE} = \bar{v}_{PDE}\left(\alpha_{PDE} + \beta_{PDE}\frac{c^3}{c^3 + K_{PDEca}^3}\right)\frac{cAMP}{cAMP + K_{PDEcamp}} \quad . \tag{A.2.28}$$

The free cytosolic Ca^{2+} stimulates both production and degradation of cAMP by acting on adenylyl cyclase and phosphodiesterases with different affinities, K_{ACca} and K_{PDEca}, respectively. AMP inhibits the cAMP production by inhibiting adenylyl cyclase. α_{AC} and α_{PDE} are basal cAMP production and degradation rates, respectively. All model parameter values are given in Table A.1.

Table A.1: Dual Oscillator Model Parameters

k_{PDH}	0.00037 μMms^{-1}	k_{leak}	4.14x10^{-5} ms^{-1}
k_{PDHcm}	0.1 μM	α_c	0.0414 ms^{-1}
J_{GK}	0.09 or 0.14μMms^{-1}	V_k	-75 mV
k_{F6P}	0.136	g_K	486 pS
k_{FBP}	0.8 or 0.95	v_{kv}	-16 mV
A_{mtot}	15 mM	h_{kv}	0.2
k_{ADPm}	12.5	τ_{kv}	1000/9 ms
v_{ANT}	0.00007245 μMms^{-1}	$g_{K(Ca)}$	18
k_{ANT}	2	k_c	0.5 μM
FRT	0.037 mV^{-1}	$g_{K(ATP)}$	2960 pS
A_{ctot}	2.5 mM	K_{ACca}	0.08 μM
K_a	0.8	β_{AC}	3
ψ_m	164 mV	α_{AC}	0.5
V_{mc}	39/532	K_{PDEca}	0.1 μM
k_{hyd}	0.0000234 μM^{-1}ms^{-1}	$\bar{v}_{AC}$	0.00018 μMms^{-1}
$J_{hyd,bas}$	0.0000081 ms^{-1}	$\bar{v}_{PDE}$	0.0024 μMms^{-1}
C_m	5300 fF	α_{PDE}	0.4
f_{cyt}	0.0086	β_{PDE}	1.2
V_{Ca}	25 mV	$k_{PDEcamp}$	3 μM
g_{Ca}	180 pS	k_{ACamp}	0.2 mM
v_{cv}	-20 mV	β_{amp}	1.9
h_{cv}	1/12	K_{camp}	0.22
α_c	5.17x10^{-6} fA^{-1}μMms^{-1}	α_{camp}	0.2
k_{pmca}	0.0414 ms^{-1}	β_{camp}	0.8
V_{cte}	620/23	g_{Kir}	110 pS
f_{er}	0.01	v_{kir}	-49 mV
k_{SERCA}	0.0828 ms^{-1}	s_{kir}	15 mV

APPENDIX B

FREQUENCY DECODING COMPENSATION MODEL

B.1 Derivation of Equation for the Long-Term Enzyme Response to Square Wave Ca^{2+}

The linear differential equation (Eq. 4.7) that governs the rate of change of the fraction of an activated enzyme has the following form:

$$\frac{dE_a}{dt} = p_E \frac{c^{n_E}}{c^{n_E} + K_E^{n_E}}(1 - E_a) - d_E E_a \quad . \tag{B.1.1}$$

This can be solved in response to the following square wave Ca^{2+} stimulus:

$$c(t) = \begin{cases} c_0 = 0.1\,, & \mathrm{mod}(t, T) \le D \\ 0\,, & \mathrm{mod}(t, T) > D \end{cases} \tag{B.1.2}$$

Derivation of the solution is similar to what was done in prior studies (Schuster et al. 2005; Salazar et al. 2008). The solution during the i^{th} oscillation cycle is:

$$E_{a,i}(\theta) = \begin{cases} E_{ss} + \xi_i e^{-(p_E^* + d_E)\theta}, & 0 \le \theta < D \\ \psi_i e^{-d_E \theta} \quad , & D \le \theta \le T \end{cases} \tag{B.1.3}$$

where $E_{a,i}$ is the solution of Eq. B.1.1 for the i^{th} stimulus cycle with the internal time $\theta \in [0, T]$, and E_{ss} and p_E^* are given by:

$$p_E^* = p_E \frac{c_0^{n_E}}{c_0^{n_E} + K_E^{n_E}} \quad , \tag{B.1.4}$$

$$E_{ss} = \frac{1}{1 + \frac{d_E}{p_E^*}} \quad . \tag{B.1.5}$$

For consecutive oscillation cycles $i - 1$ and i,

$$E_{a,i-1}(T) = E_{a,i}(0) \tag{B.1.6}$$

and $E_{a,i}$ is continuous at D. Therefore, these relations yield the following difference equations for coefficients ξ_i and ψ_i:

$$\xi_{i+1} = E_{ss}\left(e^{-d_E(T-D)} - 1\right) + e^{-(p_E^* D + d_E T)}\xi_i \tag{B.1.7}$$

$$\psi_i = e^{-p_E^* D}\xi_i + E_{ss}e^{-d_E D} \quad . \tag{B.1.8}$$

Assuming that enzyme is completely in its inactive form at the beginning, $E_{a,0}(0) = 0$, we get $\xi_0 = -E_{ss}$. The difference equation in Eq. B.1.7 has the form,

$$x_{i+1} = ax_i + b \tag{B.1.19}$$

and with initial condition x_0:

$$\begin{aligned} x_i &= ax_{i-1} + b \\ &= a(ax_{i-2} + b) + b \\ &= a^2 x_{i-2} + ab + b \\ &= a^2(ax_{i-3} + b) + ab + b \\ &= a^3 x_{i-3} + a^2 b + ab + b \\ &\cdots \\ x_i &= a^i x_0 + b\underbrace{(a^{i-1} + \cdots a^2 + a + 1)}_{\frac{(a^i - 1)}{a-1}} \end{aligned}$$

Hence,

$$x_i = a^i x_0 + \frac{b(a^i - 1)}{a-1} \quad . \tag{B.1.10}$$

Therefore, the solution to Eq. B.1.7 is:

$$\xi_i = -e^{-(p_E^* D + d_E T)i}E_{ss} + \frac{E_{ss}(e^{-d_E(T-D)} - 1)(e^{-(p_E^* D + d_E T)i} - 1)}{e^{-(p_E^* D + d_E T)} - 1} \tag{B.1.11}$$

For $i \longrightarrow \infty$,

$$\xi_i \longrightarrow \xi_\infty = -E_{ss}\frac{e^{-d_E(T-D)} - 1}{e^{-(p_E^* D + d_E T)} - 1} \tag{B.1.12}$$

and consequently,

$$\psi_i \longrightarrow \psi_\infty = E_{ss}\frac{e^{d_E D}-e^{-p_E^* D}}{1-e^{-(p_E^* D+d_E T)}} \quad . \tag{B.1.13}$$

Thus, over many stimulus cycles the solution to Eq. B.1.3 approaches:

$$E_{a,\infty}(\theta) = \begin{cases} E_{ss}+\xi_\infty e^{-(p_E^*+d_E)\theta}, & 0 \le \theta < D \\ \psi_\infty e^{-d_E\theta} \quad , & D \le \theta \le T \end{cases} \quad . \tag{B.1.14}$$

The mean fraction of activated enzyme concentration during this stimulus cycle is then given by:

$$\bar{E}_a = \frac{1}{T}\int_0^T E_{a,\infty}(\theta)\, d\theta \quad , \tag{B.1.15}$$

or upon integration:

$$\bar{E}_a = E_{ss}\left(\frac{D}{T}+\frac{1}{d_E T}E_{ss}\frac{\left(1-e^{-D(d_E+p_E^*)}\right)\left(1-e^{-d_E(T-D)}\right)}{1-e^{-(p_E^* D+d_E T)}}\right) \quad . \tag{B.1.16}$$

B.2 Auxiliary Equations for the ER Based β-Cell Model

The β-Cell model is from (Bertram and Sherman 2004) with the following ionic currents:

$$I_{Ca} = g_{Ca} m_\infty (V - V_{Ca}) \quad , \tag{B.2.1}$$

$$I_K = g_K n (V - V_K) \quad , \tag{B.2.2}$$

$$I_{K_{ATP}} = g_{K_{ATP}} a (V - V_K) \quad , \tag{B.2.3}$$

$$I_{K_{Ca}} = g_{K_{Ca}} \omega (V - V_K) \quad , \tag{B.2.4}$$

$$I_l = g_l (V - V_l) \quad , \tag{B.2.5}$$

$$I_{cmp} = g_{cmp} k_{\infty}(V - V_K) \quad . \tag{B.2.6}$$

For each ionic current I_i, g_i is the maximal conductance, V_i is the reversal potential and $(V - V_i)$ is the driving force. The rates of changes of the delayed rectifier K^+ current activation, n, and the K(ATP) current activation, a, are:

$$\frac{dn}{dt} = (n_{\infty}(V) - n)/\tau_n \quad , \tag{B.2.7}$$

$$\frac{da}{dt} = (a_{\infty}(c) - a)/\tau_a \quad , \tag{B.2.8}$$

where τ_n and τ_a are the time constants. Steady state activation functions, m_{∞}, n_{∞}, a_{∞} and k_{∞}, are:

$$m_{\infty}(V) = \frac{1}{1+e^{(-20-V)/12}} \quad , \tag{B.2.9}$$

$$n_{\infty}(V) = \frac{1}{1+e^{(-16-V)/5}} \quad , \tag{B.2.10}$$

$$k_{\infty}(V) = \frac{1}{1+e^{(-49-V)/15}} \quad , \tag{B.2.11}$$

$$a_{\infty}(c) = \frac{1}{1+e^{(0.14-c)/0.1}} \quad , \tag{B.2.12}$$

where m_{∞}, n_{∞}, a_{∞} and k_{∞} are sigmoidal functions of V and c. ω is the Ca^{2+}-dependent activation variable of $I_{K_{Ca}}$ and given with the following Hill equation:

$$\omega = \frac{c^5}{c^5 + K_{\omega}^5} \quad , \tag{B.2.13}$$

where K_{ω} is the dissociation constant. Ca^{2+} fluxes across the plasma and endoplasmic reticulum (ER) membranes are:

$$J_{mem} = -(\alpha I_{Ca} + k_{pmca} c) \quad , \tag{B.2.14}$$

$$J_{er} = p_{leak}(c_{er} - c) - k_{serca} c \quad , \tag{B.2.15}$$

where parameter α converts ionic current to flux and provides Ca^{2+} influx through voltage gated Ca^{2+} channels and k_{pmca} is the plasma membrane Ca^{2+}-ATPase pumping rate and mediates Ca^{2+} efflux from the cytosol. Ca^{2+} leaks from the ER with a rate proportional to p_{leak}. k_{serca} is the Ca^{2+} pumping rate into the ER by SERCA pumps.

Table B.1: Frequency Dependent Compensation Model Parameters

p_A	0.1 s^{-1}	C_m	5300 fF
n_A	4	τ_n	16 ms
K_{cA}	0.4	f_{cyt}	0.01
d_A	0.004 s^{-1}	f_{er}	0.01
p_I	0.1 s^{-1}	V_{cyt}/V_{er}	5
n_I	4	τ_a	300 s
K_{cI}	0.4	V_{Ca}	25 mV
d_I	0.004 s^{-1}	V_K	-75 mV
α_A	0.03 s^{-1}	g_{Ca}	1200 pS
K_a	0.8	g_K	3000 pS
β_I	0.03 s^{-1}	$g_{K_{ATP}}$	142 pS
K_i	0.1	$g_{K_{Ca}}$	400 pS
c_0	0.1 μM	g_l	170 pS
p_M	0.001 s^{-1}	K_ω	0.3 μM
K_m	0.8	α	4.5x10^{-6} ms^{-1}
d_M	0.001 s^{-1}	k_{pmca}	0.2 ms^{-1}
p_g	0.02 pSs^{-1}	p_{leak}	0.0005 ms^{-1}
K_g	0.8	k_{serca}	0.4 ms^{-1}
d_g	0.00265 s^{-1}		

APPENDIX C

SOURCE CODES

C.1 Source Codes for the Wild-Type and KO β-cell Models

Simulations for the wild type and KO β-cell models used in Chapter 3 were done using the cvode numerical integrator in XPPAUT (http://www.math.pitt.edu/~bard/xpp/xpp.html). Figures were generated from exported data using Matlab (http://www.mathworks.com/products/matlab/). The XPPAUT source code for the wild type and KO models used in Chapter 3 are given below.

```
#The default setup is for the wild type model. In order to
#switch between models, in XPP go to File>Get_par_set
#units: V=mV; t=ms; g=pS; I=fA

# Glycolytic component
# glucokinase (GK)
p jgk=9.45e-5
# glucose 6-phosphate isomerase (GPI)
p kgpi=6.3

# phosphofructokinase (PFK), adapted from Smolen 1995
p vpfk=9e-4, kpfkbas=.06
p kpfkamp=.04, kpfkfbp=1, kpfkf6p=5e4, kpfkatp=2.5e-4
p famp=.02, fmt=20, ffbp=.2, fbt=20, fatp=20
pow[0..63]=mod(flr(flr([j]/4)*2^(mod([j],4)-3)),2)\
w[0..15]=\
(amp/kpfkamp)^shift(pow0,4*[j])*\
(fbp/kpfkfbp)^shift(pow0,4*[j]+1)*\
(f6p^2/kpfkf6p)^shift(pow0,4*[j]+2)*\
(atpc^2/kpfkatp)^shift(pow0,4*[j]+3)/\
famp^(shift(pow0,4*[j])*shift(pow0,4*[j]+2))/\
fmt^(shift(pow0,4*[j])*shift(pow0,4*[j]+3))/\
ffbp^(shift(pow0,4*[j]+1)*shift(pow0,4*[j]+2))/\
fbt^(shift(pow0,4*[j]+1)*shift(pow0,4*[j]+3))/\
fatp^(shift(pow0,4*[j]+2)*shift(pow0,4*[j]+3))
jpfk=vpfk*((1-kpfkbas)*w14 + \
kpfkbas*(w2+w3+w6+w7+w10+w11+w14+w15)) \
/(sum(0,15)of(shift(w0,i')))

# lower glycolysis (LG)
p sumkp=.5
klg=.5*sumkp

# pyruvate dehydrogenase (PDH)
```

```
p vpdh=3.7e-4, kpdhcam=.1, kca=5,alpha1=0, fixx=0.866
cam=kca*cac
jpdh=vpdh*(alpha1*fixx + (1-alpha1)*cam/(cam+kpdhcam))*sqrt(fbp)

# ATP production/hydrolysis component
!volmtoc=39/532
p actot=2.5, amtot=15

#AMP and ADP terms are taken from Peercy et al. 2015.
ddd=1-4*ka1*(1-(actot/atpc))
adpc=(atpc/(2*ka1))*(sqrt(ddd)-1)

atpm=amtot-adpm
aux adpc=adpc

#AMP component
p ka1=0.8, ka2=1
amp=ka1*(adpc^2)/atpc
aux amp=amp

# adenine nucleotide translocator (ANT)
p FRT=.037, vant=7.245e-5, kantam=2, kadpm=12.5, kadpmpdh=.0047
p psim=164
adpm=kadpm/exp(jpdh/kadpmpdh)
jant=vant/(1+kantam*adpm/atpm)*exp(FRT/2*psim)

# hydrolysis (hyd)
p khyd=2.34e-5, khydbas=8.1e-6
jhyd=(khyd*cac+khydbas*atpc

# Ionic current component
p cm=5300

# Ca channels/pumps
p fc=0.0086 vca=25

# voltage-activated Ca (Ca(V)) current
p gcav=180, vcav=-20
!hcav=1/12
scavinf=1/(1+exp(vcav-v)^hcav)
icav=gcav*scavinf*(v-vca)

# plasma membrane Ca ATPase (PMCA) flux
!F=20000000/207
p kpmca=.0414
jmem=-(icav/2/F + kpmca*cac)

# endoplasmic reticulum (ER) flux
```

```
!volctoer=620/23
p fer=.01 kerout=4.14e-5, kerin=.0828
jerout=kerout*(caer-cac)
jerin=kerin*cac
jer=jerout-jerin

# K+ channels
p vk=-75

# voltage-activated K (K(V)) current
p gkv=486, vkv=-16, hkv=.2
!taukv=1000/9
skvinf=1/(1+exp(vkv-v)^hkv)
ikv=gkv*skv*(v-vk)

# Ca-activated K (K(Ca)) current
p gkca=18, kkcaca=.5, hkcaca=2
skcainf=1/(1+(kkcaca/cac)^hkcaca)
ikca=gkca*skcainf*(v-vk)

#Leak current
p gl=0
il=gl*(v-vk)

# K(ATP), adapted from Magnus and Keizer, 1998
p dz=0, gkatp=2960, kdd=17, ktd=26, ktt=1
mgadp=165*adpc
adp3m=135*adpc
atp4m=50*atpc

skatpinf=\
(.08*(1+2*mgadp/kdd) + .89*(mgadp/kdd)^2)/\
((1+mgadp/kdd)^2 * (1+adp3m/ktd+atp4m/ktt))

ikatp=(1-dz)*gkatp*skatpinf*(v-vk)+dz*gkatp*(v-vk)

# cAMP component (uM and uM/ms)
p beta_ac=3, p=3, Kacca=0.08, Kpdeca=0.1
num Kacatp=1400
p vacbar=0.00018, alpha_ac=0.5, vpdebar=0.0024
par alpha_pde=0.4, beta_pde=1.2, Kpdecamp=3, Kacamp=0.2
num fixATP=0

# Adenylyl kinase is inhibited by AMP
par alpha_amp=0, beta_amp=1.9, pa=2
vac=vacbar*(alpha_ac+beta_ac*cac^p/(cac^p+Kacca^p)*(alpha_amp +\
beta_amp*kacamp^pa/(kacamp^pa+amp^pa))
vpde=vpdebar*(alpha_pde+beta_pde*cac^p/(cac^p+Kpdeca^p)*cAMP/\
```

```
(cAMP+Kpdecamp)

# Kir current is voltage and cAMP sensitive
par Kcamp=0.22, nc=4, acamp=0.2,bcamp=0.8
cinf = acamp + bcamp*cAMP^nc/(Kcamp^nc+cAMP^nc)

p gkir=0, vkir=-49, skir=15, gleak=0
kinf = 1/(1+exp((v-vkir)/skir))
ikir = kinf*gkir*cinf*(v-vk)
ileak=gleak*(v-vk)

# Switch between models (Kir_M=Kir Model, WT_M=Wild Type Model,
# ER_M=Er Bursting Model)
set Kir_M {gkir=110, gkatp=0, jgk=0.000145, sumkp=.1 ,gl=0,\
gkca=18}
set WT_M {gkir=0, gkatp=2960, jgk=9.45e-5, sumkp=.5 ,gl=0,\
gkca=18}
set ER_M {gkir=0, gkatp=0, jgk=9.45e-5, sumkp=.5, gl=32,\
gkca=90}

# Differential Equations
v'=-(ikv+icav+ikca+il+ikatp+ikir)/cm
skv'=(skvinf-skv)/taukv
cac'=fc*(jmem+jer)
caer'=-fer*volctoer*jer
f6p'=1/(1+kgpi)*(jgk-jpfk)
fbp'=1/(1+klg)*(jpfk-.5*jpdh)
atpc'=volmtoc*jant-jhyd
camp'=vac-vpde

# Initial conditions
v(0)=-66.1141887342
skv(0)=.0000443655
cac(0)=.1092530273
caer(0)=284.1574308548
f6p(0)=248.3759439254
fbp(0)=0.1741876845
atpc(0)=1.0579152042

@ meth=cvode, toler=1.0e-10, atoler=1.0e-10, dt=20.0
@ total=1800000
@ maxstor=20000001,bounds=10000000, bell=0,
@ nplot=2 xp1=tmin, yp1=camp, xp2=tmin, yp2=cac
@ xlo=0, xhi=30, ylo=0, yhi=0.4
@ BUT=QUIT:fq
aux tmin=t/60000
done
```

C.2 Source Codes for the Frequency Decoding Compensation Model

Simulations of the frequency decoding compensation model, which are presented in Chapter 4, were performed by using the cvode numerical integrator in XPPAUT (http://www.math.pitt.edu/~bard/xpp/xpp.html). The figures were generated from the exported data using Matlab (http://www.mathworks.com/products/matlab/). Analytical solutions of the enzyme and transcription factor response equations were implemented in Matlab, where the corresponding figures were generated. The XPPAUT and Matlab source codes used in Chapter 4 are given below.

```
#Compensation mechanism with the ER-calcium based Beta-cell
model used in Chapter 4

#units: V=mV; t=ms; g=pS; I=fA

#Ica- calcium current
#Ik- delayed rectifier K+ current
#Ik(Ca)- Ca2+ dependent K+ current
#Ik(ATP)- nucleotide-sensitive K+ current
#Ikir- Inward rectifier K+ current (Compensating Current)
#c - cytosolic free Ca2+ concentration
#cer - ER Ca2+ concentration
#Aa- fraction of activated activator
#Ia- fraction of activated inhibitor
#TFa- fraction of active transcription factor
#mr- mRNA concentration
#gcmp- compensating channel conductance

#Ionic current parameters
par gca=1200, gkca=400, gk=3000
par vca=25, vk=-75, cm=5300
par taun=16, alpha=4.5e-6
par fcyt=0.01, kpmca=0.2, kd=0.3
par vn=-16, vm=-20, sn=5, sm=12
par kserca=0.4, dact=0.35, dinact=0.4
par fer=0.01, pleak=0.0005, dip3=0.5, vcytver=5
par ip3=0, gkatp=142, sa=0.1, r=0.14 taua=300000
par epser=1, freezeatp=0, astar=0.46

# ionic currents
ica(v)=gca*minf(v)*(v-vca)
ik(v)=gk*n*(v-vk)
ikca(v)=gkca*w*(v-vk)
ikatp(v)=gkatp*a*(v-vk)
```

```
#activation functions
minf(v)=1.0/(1.0+exp((vm-v)/sm))
ninf(v)=1.0/(1.0+exp((vn-v)/sn))
aainf(c)=1.0/(1.0+exp((r-c)/sa))

#fraction of K(Ca) channels activated by cytosolic Ca2+
w=c^5/(c^5+kd^5)

#flux of Ca2+ through the membrane
jmem=-(alpha*Ica(v)+kpmca*c)

#Ca2+ influx into the ER via SERCA
jserca=kserca*c

#efflux out of the ER has two components
# 1. Ca2+ leak is proportional to gradient between Ca2+ and ER
jleak=pleak*(cer-c)

#net Ca2+ efflux from the ER
jer=jleak-jserca

# Leak current
p gl=170
il(v)=gl*(v-vk)

# Nucleic mRNA Production and Transcriptional Regulation
%Activator and Inhibitor Enzyme Parameters
p  nA=4,  KcA=0.4,  pA=0.1,  dA=0.004,  nI=4,  KcI=0.4,  pIn=0.1,
dI=0.004

% TF Parameters
p alphaA=0.03, betaI=0.03, KA=0.8, KI=0.1

% mRNA Parameters
p KmRNA=0.8, pM=0.001, dM=0.001

%gkir parameters
p pg=0.02, dg=0.002655, Kg=0.8

%Time Constants
p tauAc=1000, tauI=1000, tauTF=1000, tauM=1000, taug=1000

Aa'=(pA*(c^nA)/(c^nA+KcA^nA)*(1-Aa)-dA*Aa)/tauAc
Ia'=(pIn*(c^nI)/(c^nI+KcI^nI)*(1-Ia)-dI*Ia)/tauI

Ainf=(alphaA*Aa^2)/(KA^2+Aa^2)
Iinf=(betaI*Ia)/(KI+Ia)
TFa'=(Ainf*(1-TFa)-Iinf*TFa)/tauTF
```

```
mr'=(pM*TFa/(TFa+KmRNA)-dM*mr)/tauM
gcmp'=(pg*mr/(mr+Kg)-dg)/taug

#Compensating Current
params vkir=-49, skir=15
kinf(v) = 1.0/(1.0+exp((v-vkir)/skir))
icmp(v) =gcmp*kinf(v)*(v-vk)

#differential equations
v'=-(ica(v)+ik(v)+ikca(v)+ikatp(V)+il(v)+icmp(v))/cm
n'=(ninf(v)-n)/taun
c'=fcyt*(jmem+epser*jer)
cer'=-epser*fer*(vcytver)*jer
a'=(aainf(c)-a)/taua

#initial cond.
Aa(0)=0.0493
Ia(0)=0.0493
TFa(0)=0.0685
mr(0)=1.0206
gcmp(0)=0
v(0)=-38.82
n(0)=0.0064
c(0)=0.1695
cer(0)=85.3492
a(0)=0.4441

aux tsec=t/1000.0
aux tmin=t/60000

@  meth=cvode,  dtmax=1,  dt=20,  total=18e5,  maxstor=1000000,
delay=2000,
@ bounds=100000000, xp=tmin,  yp=v, toler=1.0e-7, atoler=1.0e-7
@ xlo=0, xhi=30, ylo=-80, yhi=0
done


% Matlab code for Oscillation Efficiency (Fig. 4.3) for 3
%different cooperativity values (nnE)

% Cooperativity vector
nnE=[1,2,4];
for i=1:3;
    nE=nnE(i);

%Enzyme parameters
pE=0.09; dE=0.003;
D=10;
```

```
T=D:1:180;

KE=0:0.001:0.2;
[T,KE]=meshgrid(T,KE);

%Response to Oscillatory Ca
%Ebar represents the mean fractions of an activeted Enzyme
%During on times Ca is 0.1 and inbetween it is set to 0;

c0=0.1;

%activation rate during on times
pEstar=pE*(c0^nE)./(c0^nE+KE.^nE);

%steady state fractions of active enzymes
E_ss=pEstar./(pEstar+dE);

%Activated enzyme franction (Eq. 4.12)
Ebar=E_ss.*(D./T+((pEstar./((pEstar+dE).*dE.*T)).*…
(1-exp(-D.*(pEstar+dE)))).*(1-exp(-dE.*(T-D))).…
/(1-exp(-(pEstar.*D+dE.*T))));

%Non-Oscillatory Ca with the same concentration
%subsrcipt c (_c) is used for indicating constant Ca (Eq. 4.14)
cc=c0*D./T;
E_c_ss=pE.*((cc.^nE)./(cc.^nE+KE.^nE))./(pE.*((cc.^nE).…
/(cc.^nE+KE.^nE))+dE);

%Oscillation Efficiency (Eq. 4.15)
Os_Ef=(Ebar-E_c_ss)./E_c_ss;

%Figure 4.3
figure()
subplot(3,1,i)
mesh(T,KE,Os_Ef)
end

% Matlab code for Fig. 4.6B,C
%Activator and inhibitor enzyme equations are described by
%Eq. 4.12 (Eq. 4.12).

%Enzyme Parameters
nA=4; KcA=0.2; nI=4; KcI=0.2;
pA=0.09; dA=0.003; pI=0.09; dI=0.003;

%TF parameters
alphaA=0.01; betaI=0.01;
```

```
D=10;
T=D:1:180;

KA=0:0.001:0.3;
KI=0.4;

[T,KA]=meshgrid(T,KA);

%Response to Oscillatory Ca
%Abar and Ibar represent the mean fractions of active activator
%and inhibitor concentrations after sufficiently large
%oscillation cycles, respectively.

% During on times Ca is 0.1 and inbetween it is set to 0;
c0=0.1;

%activation rates during on times
pAstar=pA*(c0^nA)/(c0^nA+KcA^nA);
pIstar=pI*(c0^nI)/(c0^nI+KcI^nI);

%steady state fractions of active enzymes
A_ss=pAstar./(pAstar+dA);
I_ss=pIstar./(pIstar+dI);

%Activated enzyme franctions
Abar=A_ss.*(D./T+((pAstar./((pAstar+dA).*dA.*T)).*…
(1-exp(-D.*(pAstar+dA)))).*(1-exp(-dA.*(T-D))./…
(1-exp(-(pAstar.*D+dA.*T))));
Ibar=I_ss.*(D./T+((pIstar./((pIstar+dI).*dI.*T)).*…
(1-exp(-D.*(pIstar+dI)))).*(1-exp(-dI.*(T-D))./…
(1-exp(-(pIstar.*D+dI.*T))));

Ainf=alphaA*(Abar.^2)./(KA.^2+Abar.^2);
Iinf=betaI*(Ibar.^1)./(KI.^1+Ibar.^1);

TFbar=Ainf./(Ainf+Iinf);

%Rates of Changs of infinity functions versus T
d_Abar_dT=A_ss*(-D./(T.^2)-(pAstar./(dA*(T.^2).*(pAstar+dA))).*…
((1-exp(-D.*(pAstar+dA)))).*(1-exp(-dA.*(T-D))./…
(1-exp(-(pAstar.*D+dA.*T)))+…
(pAstar./((pAstar+dA).*dA.*T)).*…
(1-exp(-D*(pAstar+dA)))*dA.*(exp(-dA*(T-D))-…
exp(-(pAstar*D+dA*T))./((1-exp(-(pAstar*D+dA*T))).^2));

d_Ibar_dT=I_ss*(-D./(T.^2)-(pIstar./(dI*(T.^2).*(pIstar+dI))).*…
((1-exp(-D.*(pIstar+dI)))).*(1-exp(-dI.*(T-D))./…
(1-exp(-(pIstar.*D+dI.*T)))+…
```

```
(pIstar./((pIstar+dI).*dI.*T)).*…
(1-exp(-D*(pIstar+dI)))*dI.*(exp(-dI*(T-D))-…
exp(-(pIstar*D+dI*T))./((1-exp(-(pIstar*D+dI*T))).^2));

d_Ainf_dT=2*(KA.^2).*(Abar.^…
(-2-1)).*d_Abar_dT./((1+(KA.^2).*(Abar.^-2)).^2);
d_Iinf_dT=1*(KI.^1).*(Ibar.^…
(-1-1)).*d_Ibar_dT./((1+(KI.^1).*(Ibar.^-1)).^2);

Diff=(d_Ainf_dT)-(d_Iinf_dT);
Sign_Diff=0.5*sign(Diff);

%Figure 4.6 panels B and C
figure()
subplot(1,2,1)
mesh(T,KA,TFbar)
subplot(1,2,2)
mesh(T,KA,Sign_Diff)
```

APPENDIX D

COPYRIGHT PERMISSIONS

ELSEVIER LICENSE
TERMS AND CONDITIONS

Feb 01, 2017

This Agreement between Vehpi Yildirim ("You") and Elsevier ("Elsevier") consists of your license details and the terms and conditions provided by Elsevier and Copyright Clearance Center.

License Number	4031450388028
License date	Jan 17, 2017
Licensed Content Publisher	Elsevier
Licensed Content Publication	Biophysical Journal
Licensed Content Title	The Ca2+ Dynamics of Isolated Mouse β-Cells and Islets: Implications for Mathematical Models
Licensed Content Author	Min Zhang,Paula Goforth,Richard Bertram,Arthur Sherman,Leslie Satin
Licensed Content Date	May 2003
Licensed Content Volume Number	84
Licensed Content Issue Number	5
Licensed Content Pages	19
Start Page	2852
End Page	2870
Type of Use	reuse in a thesis/dissertation
Portion	figures/tables/illustrations
Number of figures/tables/illustrations	1
Format	both print and electronic
Are you the author of this Elsevier article?	No
Will you be translating?	No
Order reference number	
Original figure numbers	figure 4
Title of your thesis/dissertation	Mathematical Modeling and Analysis of Gene Knockout Compensation in Pancreatic Beta-Cells
Expected completion date	Feb 2017
Estimated size (number of pages)	110
Elsevier VAT number	GB 494 6272 12
Requestor Location	

JOHN WILEY AND SONS LICENSE TERMS AND CONDITIONS

Feb 01, 2017

This Agreement between Vehpi Yildirim ("You") and John Wiley and Sons ("John Wiley and Sons") consists of your license details and the terms and conditions provided by John Wiley and Sons and Copyright Clearance Center.

License Number	4031450659998
License date	Jan 17, 2017
Licensed Content Publisher	John Wiley and Sons
Licensed Content Publication	British Journal of Pharmacology
Licensed Content Title	Regulation by tolbutamide and diazoxide of the electrical activity in mouse pancreatic β-cells recorded in vivo
Licensed Content Author	Ana Gomis,Miguel Valdeolmillos
Licensed Content Date	Feb 3, 2009
Licensed Content Pages	6
Type of use	Dissertation/Thesis
Requestor type	University/Academic
Format	Print and electronic
Portion	Figure/table
Number of figures/tables	1
Original Wiley figure/table number(s)	Figure 2
Will you be translating?	No
Title of your thesis / dissertation	Mathematical Modeling and Analysis of Gene Knockout Compensation in Pancreatic Beta-Cells
Expected completion date	Feb 2017
Expected size (number of pages)	110
Requestor Location	
Publisher Tax ID	EU826007151
Billing Type	Invoice
Billing Address	
Total	0.00 USD

REFERENCES

Adams F (1856) The extant works of Arataeus the Cappadocian. The Sydenham Society, London.

Ahmed AM (2002) History of diabetes mellitus. Saudi Med. J. 23:373–378.

Alberts B, Johnson A, Lewis J, Raff M, Roberts K, Walter P (2008) Molecular Biology of the Cell. New York: Garland Science. Classic Text Book 5th Eddition.

Arredouani A, Guiot Y, Jonas JC, Liu LH, Nenquin M, Pertusa JA, Rahier J, Rolland JF, Shull GE, Stevens M, Wuytack F, Henquin JC, Gilon P (2002a) SERCA3 ablation does not impair insulin secretion but suggests distinct roles of different sarcoendoplasmic reticulum Ca^{2+} pumps for Ca^{2+} homeostasis in pancreatic β-cells. Diabetes 51:3245–3253.

Arredouani A, Henquin JC, Gilon P (2002b) Contribution of the endoplasmic reticulum to the glucose-induced Ca^{2+} response in mouse pancreatic islets. Am J Physiol 282:E982-991.

Atwater I, Dawson CM, Scott A, Eddlestone G, Rojas E (1980) The nature of the oscillatory behaviour in electrical activity from pancreatic β-cell. Horm Metab Res Suppl Suppl 10:100–107.

Barish ME (1998) Intracellular calcium regulation of channel and receptor expression in the plasmalemma: Potential sites of sensitivity along the pathways linking transcription, translation, and insertion. J Neurobiol 37:146–157.

Bergsten P, Grapengiesser E, Gylfe E, Tengholm A, Hellman B (1994) Synchronous oscillations of cytoplasmic Ca^{2+} and insulin release in glucose-stimulated pancreatic islets. J Biol Chem 269:8749–8753.

Berridge MJ, Bootman MD, Roderick HL (2003) Calcium signalling: dynamics, homeostasis and remodelling. Nat Rev Mol Cell Biol 4:517–529.

Bertram R, Rubin JE (2016) Multi-timescale systems and fast-slow analysis. Math Biosci. doi: 10.1016/j.mbs.2016.07.003

Bertram R, Satin L, Zhang M, Smolen P, Sherman A (2004) Calcium and glycolysis mediate multiple bursting modes in pancreatic islets. Biophys J 87:3074–3087.

Bertram R, Sherman A (2004) A calcium-based phantom bursting model for pancreatic islets. Bull Math Biol 66:1313–1344.

Bertram R, Sherman A, Satin LS (2007) Metabolic and electrical oscillations: Partners in controlling pulsatile insulin secretion. Am J Physiol 293:E890-900.

Blume AJ, Foster CJ (1975) Mouse neuroblastoma adenylate cyclase. Adenosine and adenosine analogues as potent effectors of adenylate cyclase activity. J Biol Chem 250:5003–5008.

Bradley KK, Jaggar JH, Bonev AD, Heppner TJ, Flynn ER, Nelson MT, Horowitz B (1999) Kir2.1 encodes the inward rectifier potassium channel in rat arterial smooth muscle cells. J Physiol 515 Pt 3:639–651.

Bradshaw JM, Kubota Y, Meyer T, Schulman H (2003) An ultrasensitive Ca^{2+}/calmodulin-dependent protein kinase II-protein phosphatase 1 switch facilitates specificity in postsynaptic calcium signaling. Proc Natl Acad Sci U S A 100:10512–10517.

Bruel-Jungerman E, Davis S, Laroche S (2007) Brain plasticity mechanisms and memory: A party of four. Neuroscientist 13:492–505.

Brugada P, Brugada R, Campuzano O, Sarquella-Brugada G, Brugada P, Brugada V, Brugada J (2013) Brugada syndrome 1992-2012: Twenty years of scientific progress. In *Cardiac Electrophysiology: From Cell to Bedside*, pp. 925-934. Elsevier-Saunders, Philadelphia, 2014.

Cha CY, Nakamura Y, Himeno Y, Wang J, Fujimoto S, Inagaki N, Earm YE, Noma A (2011) Ionic mechanisms and Ca^{2+} dynamics underlying the glucose response of pancreatic β-cells: a simulation study. J Gen Physiol 138:21–37.

Chay TR, Keizer J (1983) Minimal model for membrane oscillations in the pancreatic β-cell. Biophys J 42:181–190.

Cole KS (1972) Membranes, ions and impulses: A chapter of classical biophysics. Univ of California Press, Berkley, California

Collins TJ, Lipp P, Berridge MJ, Bootman MD (2001) Mitochondrial Ca^{2+} uptake depends on the spatial and temporal profile of cytosolic Ca^{2+} signals. J Biol Chem 276:26411–26420.

Cooper DM, Mons N, Karpen JW (1995) Adenylyl cyclases and the interaction between calcium and cAMP signalling. Nature 374:421–424.

Davis GW (2006) Homeostatic control of neural activity: From phenomenology to molecular design. Annu Rev Neurosci 29:307–323.

De Koninck P, Schulman H (1998) Sensitivity of CaM kinase II to the frequency of Ca^{2+} oscillations. Science 279:227–230.

Deisseroth K, Tsien RW (2002) Dynamic multiphosphorylation passwords for activity-dependent gene expression. Neuron 34:179–182.

Denton RM (2009) Regulation of mitochondrial dehydrogenases by calcium ions. Biochim Biophys Acta - Bioenerg. 1787:1309–1316.

Detimary P, Gilon P, Henquin JC (1998) Interplay between cytoplasmic Ca^{2+} and the ATP/ADP ratio: A feedback control mechanism in mouse pancreatic islets. Biochem J 333Pt 2:269–274.

Dolmetsch RE, Xu K, Lewis RS (1998) Calcium oscillations increase the efficiency and specificity of gene expression. Nature 392:933–936.

Drengstig T, Ueda HR, Ruoff P (2008) Predicting perfect adaptation motifs in reaction kinetic networks. J Phys Chem B 112:16752–16758.

Düfer M, Haspel D, Krippeit-Drews P, Aguilar-Bryan L, Bryan J, Drews G (2004) Oscillations of membrane potential and cytosolic Ca^{2+} concentration in $SUR1^{-/-}$ β-cells. Diabetologia 47:488–498.

Dula SB, Jecmenica M, Wu R, Jahanshahi P, Verrilli GM, Carter JD, Brayman KL, Nunemaker CS (2010) Evidence that low-grade systemic inflammation can induce islet dysfunction as measured by impaired calcium handling. Cell Calcium 48:133–142.

Dupont G, Goldbeter A (1998) CaM kinase II as frequency decoder of Ca^{2+} oscillations. BioEssays 20:607–610.

Dupont G, Houart G, De Koninck P (2003) Sensitivity of CaM kinase II to the frequency of Ca^{2+} oscillations: A simple model. Cell Calcium 34:485–497.

Dyachok O, Idevall-Hagren O, Sågetorp J, Tian G, Wuttke A, Arrieumerlou C, Akusjärvi G, Gylfe E,Tengholm A (2008) Glucose-induced cyclic AMP oscillations regulate pulsatile insulin secretion. Cell Metab 8:26–37.

Dyachok O, Isakov Y, Sagetorp J, Tengholm A (2006) Oscillations of cyclic AMP in hormone-stimulated insulin-secreting β-cells. Nature 439:349–352.

Efanova IB, Zaitsev S V., Zhivotovsky B, Köhler M, Efendić S, Orrenius S, Berggren PO (1998) Glucose and tolbutamide induce apoptosis in pancreatic β-cells: A process dependent on intracellular Ca^{2+} concentration. J Biol Chem 273:33501–33507.

Eisenbarth GS, Gardner J, Anderson M (2011) Immunoendocrinology: Scientific and clinical aspects. Immunoendocrinology Sci Clin Asp 95-113–113.

Eraly SA (2014) Striking differences between knockout and wild-type mice in global gene expression variability. PLoS One. doi: 10.1371/journal.pone.0097734

Fakler B, Brändle U, Glowatzki E, Zenner HP, Ruppersberg JP (1994) Kir2.1 inward rectifier K^+ channels are regulated independently by protein kinases and ATP hydrolysis. Neuron 13:1413–1420.

Falcke M, Malchow D (2003) Understanding calcium dynamics: experiments and theory. Springer-Verlag, Berlin, Germany.

Fridlyand LE, Tamarina N, Philipson LH (2003) Modeling of Ca^{2+} flux in pancreatic β-cells: Role of the plasma membrane and intracellular stores. Am J Physiol 285:E138–E154.

Frieden C (1970) Kinetic aspects of regulation of metabolic processes. The hysteretic enzyme concept. J Biol Chem 245:5788–5799.

Frieden C (1979) Slow transitions and hysteretic behavior in enzymes. Annu Rev Biochem 48:471–489.

Gadsby DC (2009) Ion channels versus ion pumps: the principal difference, in principle. Nat Rev Mol Cell Biol 10:344–352.

Ganguly K, Poo M ming (2013) Activity-dependent neural plasticity from bench to bedside. Neuron 80:729–741.

Gilon P, Ravier MA, Jonas JC, Henquin JC (2002) Control mechanisms of the oscillations of insulin secretion *in vitro* and *in vivo*. Diabetes 51:S144–S151.

Gilon P, Shepherd RM, Henquin JC (1993) Oscillations of secretion driven by oscillations of cytoplasmic Ca^{2+} as evidenced in single pancreatic islets. J Biol Chem 268:22265–22268.

Glynn E, Thompson B, Vadrevu S, Lu S, Kennedy RT, Ha J, Sherman A, Satin LS (2016) Chronic glucose exposure systematically shifts the oscillatory threshold of mouse islets: Experimental evidence for an early intrinsic mechanism of compensation for hyperglycemia. Endocrinology 157:611–623.

Gomis A, Valdeolmillos M (1998) Regulation by tolbutamide and diazoxide of the electrical activity in mouse pancreatic β-cells recorded in vivo. Br J Pharmacol 123:443–448.

Grayson DR (2011) Laboratory of molecular neurobiology (1988-1994). Pharmacol Res 64:339–343.

Hajnóczky G, Robb-Gaspers LD, Seitz MB, Thomas AP (1995) Decoding of cytosolic calcium oscillations in the mitochondria. Cell 82:415–424.

Han P, Werber J, Surana M, Fleischer N, Michaeli T (1999) The calcium/calmodulin-dependent phosphodiesterase PDE1C down-regulates glucose-induced insulin secretion. J Biol Chem 274:22337–22344.

He F, Fromion V, Westerhoff HV (2013) (Im)Perfect robustness and adaptation of metabolic networks subject to metabolic and gene-expression regulation: Marrying control engineering with metabolic control analysis. BMC Syst Biol 7:131.

Hellman B (2009) Pulsatility of insulin release - A clinically important phenomenon. Ups J Med Sci 114:193–205.

Henquin JC (2009) Regulation of insulin secretion: A matter of phase control and amplitude modulation. Diabetologia 52:739–751.

Hille B (2001) Ion channels of excitable membranes. Edition 3. Sunderland, MA: Sinauer.

Hodgkin AL, Huxley AF (1952a) The components of membrane conductance in the giant axon of Loligo. J Physiol 116:473–496.

Hodgkin AL, Huxley AF (1952b) Currents carried by sodium and potassium ions through the membrane of the giant axon of Loligo. J Physiol 116:449–472.

Hodgkin AL, Huxley AF (1990) A quantitative description of membrane current and its application to conduction and excitation in nerve. Bull Math Biol 52:25–71.

Hunter T, Karin M (1992) The regulation of transcription by phosphorylation. Cell 70:375–387.

Huopio H, Otonkoski T, Vauhkonen I, Reimann F, Ashcroft FM, Laakso M (2003) A new subtype of autosomal dominant diabetes attributable to a mutation in the gene for sulfonylurea receptor 1. Lancet 361:301–307.

Inesi G, Sagara Y (1992) Thapsigargin, a high affinity and global inhibitor of intracellular Ca^{2+} transport ATPases. Arch Biochem Biophys 298:313–317.

Iwakura T, Fujimoto S, Kagimoto S, Inada A, Kubota A, Someya Y, Ihara Y, Yamada Y, Seino Y (2000) Sustained enhancement of Ca^{2+} influx by glibenclamide induces apoptosis in RINm5F cells. Biochem Biophys Res Commun 271:422–428.

Jia JM, Chen Q, Zhou Y, Miao S, Zheng J, Zhang C, Xiong ZQ (2008) Brain-derived neurotrophic factor-tropomyosin-related kinase B signaling contributes to activity-dependent changes in synaptic proteins. J Biol Chem 283:21242–21250.

Johnson RA, Yeung SM, Stübner D, Bushfield M, Shoshani I (1989) Cation and structural requirements for P site-mediated inhibition of adenylate cyclase. Mol Pharmacol 35:681–688.

Kane C, Shepherd RM, Squires PE, Johnson PR, James RF, Milla PJ, Aynsley-Green A, Lindle KJ, Dunne MJ (1996) Loss of functional K_{ATP} channels in pancreatic β-cells causes persistent hyperinsulinemic hypoglycemia of infancy. Nat Med 2:1344–1347.

Keizer J, Magnus G (1989) ATP-sensitive potassium channel and bursting in the pancreatic β-cell. A theoretical study. Biophys J 56:229–242.

Kidd JG (1971) Eugene Lindsay Opie, MD, 1873-1971. Am J Pathol 65:483–92.

Laios K, Karamanou M, Saridaki Z, Androutsos G (2012) Aretaeus of Cappadocia and the first description of diabetes. Hormones 11:109–113.

Larsson O, Kindmark H, Brandstrom R, Fredholm B, Berggren PO (1996) Oscillations in K_{ATP} channel activity promote oscillations in cytoplasmic free Ca^{2+} concentration in the pancreatic beta cell. Proc Natl Acad Sci U S A 93:5161–5165.

Leibiger IB, Leibiger B, Berggren P (2008) Insulin signaling in the pancreatic β-cell. Annu Rev Nutr 28:233–251.

LeMasson G, Marder E, Abbott LF (1993) Activity-dependent regulation of conductances in model neurons. Science 259:1915–1917.

Li H, Rao A, Hogan PG (2011) Interaction of calcineurin with substrates and targeting proteins. Trends Cell Biol. 21:91–103.

Li L, Stefan MI, Le Novère N (2012) Calcium input frequency, duration and amplitude differentially modulate the relative activation of calcineurin and CaMKII. PLoS One. doi: 10.1371/journal.pone.0043810

Liu DY-T, Liu C-H, Lai M-T, Lin HK, Hseu TH (2007) Global gene expression profiling of wild type and *lysC* knockout *Escherichia Coli* W3110. FEMS Microbiol Lett 276:202–206.

Liu Z, Golowasch J, Marder E, Abbott LF (1998) A model neuron with activity-dependent conductances regulated by multiple calcium sensors. J Neurosci 18:2309–2320.

Londos C, Preston MS (1977) Regulation by glucagon and divalent cations of inhibition of hepatic adenylate cyclase by adenosine. J Biol Chem 252:5951–5956.

Lopatin AN, Makhina EN, Nichols CG (1994) Potassium channel block by cytoplasmic polyamines as the mechanism of intrinsic rectification. Nature 372:366–369.

Lyford GL, Yamagata K, Kaufmann WE, Barnes CA, Sanders LK, Copeland NG, Gilbert DJ, Jenkins NA, Lanahan AA, Worley PF (1995) Arc, a growth factor and activity-regulated gene, encodes a novel cytoskeleton-associated protein that is enriched in neuronal dendrites. Neuron 14:433–445.

MacDonald PE, Rorsman P (2006) Oscillations, intercellular coupling, and insulin secretion in pancreatic β-cells. PLoS Biol. 4:167–171.

Maedler K, Carr RD, Bosco D, Zuellig RA, Berney T, Donath MY (2005) Sulfonylurea induced β-cell apoptosis in cultured human islets. J Clin Endocrinol Metab 90:501–506.

Maffei A, Bucher D, Fontanini A (2012) Homeostatic plasticity in the nervous system. Neural Plast 2012:97–107.

Magnus G, Keizer J (1998) Model of β-cell mitochondrial calcium handling and electrical activity. I. Cytoplasmic variables. Am J Physiol 274:C1158–C1173.

Marks F, Klingmüller U, and Müller-Decker K (2009) Cellular Signal Processing: An Introduction to the Molecular Mechanisms of Signal Transduction. New York: Garland Science.

Matsuda H, Saigusa A, Irisawa H (1987) Ohmic conductance through the inwardly rectifying K^+ channel and blocking by internal Mg^{2+}. Nature 325:156–159.

Matthews DR, Lang DA, Burnett MA, Turner RC (1983a) Control of pulsatile insulin secretion in man. Diabetologia 24:231–237.

Matthews DR, Naylor BA, Jones RG (1983b) Pulsatile insulin has greater hypoglycemic effect than continuous delivery. Diabetes 37:617–621.

Matveyenko AV, Liuwantara D, Gurlo T, Kirakossian D, Dalla Man C, Cobelli C, White MF, Copps KD, Volpi E, Fujita S, Butler PC (2012) Pulsatile portal vein insulin delivery enhances hepatic insulin action and signaling. Diabetes 61:2269–2279.

Matveyenko AV, Veldhuis JD, Butler PC (2008) Measurement of pulsatile insulin secretion in the rat: direct sampling from the hepatic portal vein. Am J Physiol 295:E569–E574.

McKenna JP, Ha J, Merrins MJ, Satin LS, Sherman A, Bertram R (2016) Ca^{2+} effects on ATP production and consumption have regulatory roles on oscillatory islet activity. Biophys J 110:733–742.

Merrins MJ, Poudel C, McKenna JP, Ha J, Sherman A, Bertram R, Satin LS (2016) Phase analysis of metabolic oscillations and membrane potential in pancreatic islet β-cells. Biophys J 110:691–699.

Merrins MJ, Van Dyke AR, Mapp AK, Rizzo MA, Satin LS (2013) Direct measurements of oscillatory glycolysis in pancreatic islet β-cells using novel fluorescence resonance energy transfer (FRET) biosensors for pyruvate kinase M2 activity. J Biol Chem 288:33312–33322.

Moody WJ, Bosma MM (2005) Ion channel development, spontaneous activity, and activity-dependent development in nerve and muscle cells. Physiol Rev 85:883–941.

Morrison H (1937) Contributions to the microscopic anatomy of the pancreas by Paul Langerhans (Berlin 1869). Bull Inst Hist Med 5:259–297.

Nenquin M, Szollosi A, Aguilar-Bryan L, Bryan J, Henquin JC (2004) Both triggering and amplifying pathways contribute to fuel-induced insulin secretion in the absence of sulfonylurea receptor-1 in pancreatic β-cells. J Biol Chem 279:32316–32324.

Nichols CG (2006) K_{ATP} channels as molecular sensors of cellular metabolism. Nature 440:470–476.

Nunemaker CS, Zhang M, Wasserman DH, McGuinness OP, Powers AC, Bertram R, Sherman A, Satin LS (2005) Individual mice can be distinguished by the period of their islet calcium oscillations: Is there an intrinsic islet period that is imprinted in vivo? Diabetes 54:3517–3522.

O'Leary T, Williams AH, Franci A, Marder E (2014) Cell types, network homeostasis, and pathological compensation from a biologically plausible ion channel expression model. Neuron 82:809–821.

O'Rahilly S, Turner RC, Matthews DR (1988) Impaired pulsatile secretion of insulin in relatives of patients with non-insulin-dependent diabetes. N Engl J Med 318:1225–30.

Oeckinghaus A, Ghosh S (2009) The NF-κB family of transcription factors and its regulation. Cold Spring Harb. Perspect. Biol. 1:a000034.

Olokoba AB, Obateru OA, Olokoba LB (2012) Type 2 diabetes mellitus: A review of current trends. Oman Med. J. 27:269–273.

Olypher AV, Prinz AA (2010) Geometry and dynamics of activity-dependent homeostatic regulation in neurons. J Comput Neurosci 28:361–374.

Paolisso G, Scheen AJ, Giugliano D, Sgambato S, Albert A, Varricchio M, D'Onofrio F, Lefebvre, PJ (1991) Pulsatile insulin delivery has greater metabolic effects than continuous hormone administration in man: Importance of pulse frequency. J Clin Endocrinol Metab 72:607–615.

Peercy BE, Sherman AS, Bertram R (2015) Modeling of glucose-induced cAMP oscillations in pancreatic β-Cells: cAMP rocks when metabolism rolls. Biophys J 109:439–449.

Pinton P, Giorgi C, Siviero R, Zecchini E, Rizzuto R (2008) Calcium and apoptosis: ER-mitochondria Ca^{2+} transfer in the control of apoptosis. Oncogene 27:6407–6418.

Plant TD (1988) Na^{+} currents in cultured mouse pancreatic β-cells. Pflügers Arch 411:429–35.

Polonsky KS, Given BD, Hirsch LJ, Tillil H, Shapiro ET, Beebe C, Frank BH, Galloway JA, Van Cauter E (1988) Abnormal patterns of insulin secretion in non-insulin-dependent diabetes mellitus. N Engl J Med 318:1231–1239.

Pørksen N (2002) The in vivo regulation of pulsatile insulin secretion. Diabetologia 45:3–20.

Pyne NJ, Furman BL (2003) Cyclic nucleotide phosphodiesterases in pancreatic islets. Diabetologia 46:1179–1189.

Quesada I, Tudurí E, Ripoll C, Nadal Á (2008) Physiology of the pancreatic α-cell and glucagon secretion: Role in glucose homeostasis and diabetes. J. Endocrinol. 199:5–19.

Rao A, Luo C, Hogan PG (1997) Transcription factors of the NFAT family: Regulation and function. Annu Rev Immunol 15:707–747.

Ren J, Sherman A, Bertram R, Goforth PB, Nunemaker CS, Waters CD, Satin LS (2013) Slow oscillations of K_{ATP} conductance in mouse pancreatic islets provide support for electrical bursting driven by metabolic oscillations. Am J Physiol 305:E805-817.

Richard P (2003) The rhythm of yeast. FEMS Microbiol Rev 27:547–557.

Rinzel J, Ermentrout GB (1989) Analysis of neural excitability and oscillations. In: Koch C, Segev I (eds) Methods in Neuronal Modeling, 2nd edn. MIT Press, Cambridge, MA, pp 251–292

Rinzel J and Lee YS (1987) Dissection of a model for neuronal parabolic bursting. J Math Biol 25:653–675.

Riz M, Braun M, Wu X, Pedersen MG (2015) Inwardly rectifying Kir2.1 currents in human β-cells control electrical activity: Characterisation and mathematical modelling. Biochem Biophys Res Commun 459:284–287.

Robb-Gaspers LD, Burnett P, Rutter GA, Denton RM, Rizzuto R, Thomas AP (1998) Integrating cytosolic calcium signals into mitochondrial metabolic responses. EMBO J 17:4987–5000.

Rorsman P, Braun M (2013) Regulation of insulin secretion in human pancreatic islets. Annu Rev Physiol 75:155–79.

Rorsman P, Eliasson L, Kanno T, Zhang Q, Gopel S (2011) Electrophysiology of pancreatic β-cells in intact mouse islets of Langerhans. Prog Biophys Mol Biol 107:224–235.

Rosati B, McKinnon D (2004) Regulation of ion channel expression. Circ Res 94:874–883.

Rosen LB, Ginty DD, Greenberg ME (1995) Calcium regulation of gene expression. Adv Second Messenger Phosphoprot Res 30:225–253.

Rosenfeld L (2002) Insulin: discovery and controversy. Clin Chem 48:2270–2288.

Ruppersberg JP, Fakler B (1996) Complexity of the regulation of Kir2.1 K^+ channels. Neuropharmacology 35:887–893.

Salazar C, Politi AZ, Hofer T (2008) Decoding of calcium oscillations by phosphorylation cycles: Analytic results. Biophys J 94:1203–1215.

Satin LS, Cook DL (1985) Voltage-gated Ca^{2+} current in pancreatic β-cells. Pflügers Arch Eur J Physiol 404:385–387.

Schuster S, Knoke B, Marhl M (2005) Differential regulation of proteins by bursting calcium oscillations - A theoretical study. BioSystems 81:49–63.

Seghers V, Nakazaki M, DeMayo F, Aguilar-Bryan L, Bryan J (2000) Sur1 knockout mice. A model for K_{ATP} channel-independent regulation of insulin secretion. J Biol Chem 275:9270–9277.

Segil N, Roberts SB, Heintz N (1991) Mitotic phosphorylation of the Oct-1 homeodomain and regulation of Oct-1 DNA binding activity. Science 254:1814–1816.

Seino S (2012) Cell signalling in insulin secretion: The molecular targets of ATP, cAMP and sulfonylurea. Diabetologia 55:2096–2108.

Sheng M, Thompson MA, Greenberg ME (1991) CREB: A Ca^{2+}-regulated transcription factor phosphorylated by calmodulin-dependent kinases. Science 252:1427–1430.

Sjöholm Å (1995) Regulation of insulinoma cell proliferation and insulin accumulation by peptides and second messengers. Ups J Med Sci 100:201–216.

Smedler E, Uhlén P (2014) Frequency decoding of calcium oscillations. Biochim Biophys Acta - Gen Subj 1840:964–969.

Smith PA, Ashcroft FM, Rorsman P (1990) Simultaneous recordings of glucose dependent electrical activity and ATP-regulated K^+-currents in isolated mouse pancreatic β-cells. FEBS Lett 261:187–190.

Smolen P (1995) A model for glycolytic oscillations based on skeletal muscle phosphofructokinase kinetics. J Theor Biol 174:137–148.

Song SH, McIntyre SS, Shah H, D. Veldhuis J, Hayes PC, Butler PC (2007) Direct measurement of pulsatile insulin secretion form the portal vein in human subjects. Teh J Clin Endocrinol Metab 85:4491–4499.

Stemmer PM, Klee CB (1994) Dual calcium ion regulation of calcineurin by calmodulin and calcineurin B. Biochemistry 33:6859–6866.

Stendahl JC, Kaufman DB, Stupp SI (2009) Extracellular matrix in pancreatic islets: Relevance to scaffold design and transplantation. Cell Transplant 18:1–12.

Swulius MT, Waxham MN (2013) Ca^{2+}/Calmodulin-dependent protein kinases. Cell Mol Life Sci 65:2637–2657.

Szollosi A, Nenquin M, Aguilar-Bryan L, Bryan J, Henquin JC (2007) Glucose stimulates Ca^{2+} influx and insulin secretion in 2-week-old β-cells lacking ATP-sensitive K^{+} channels. J Biol Chem 282:1747–1756.

Taskinen M-R, Borén J (2015) New insights into the pathophysiology of dyslipidemia in type 2 diabetes. Atherosclerosis 239:483–95.

Temporal S, Lett KM, Schulz DJ (2014) Activity-dependent feedback regulates correlated ion channel mRNA levels in single identified motor neurons. Curr Biol 24:1899–1904.

Tomita T (2002) New markers for pancreatic islets and islet cell tumors. Pathol. Int. 52:425–432.

Tornheim K (1988) Fructose 2,6-bisphosphate and glycolytic oscillations in skeletal muscle extracts. J Biol Chem 263:2619–2624.

Tornheim K (1997) Are metabolic oscillations responsible for normal oscillatory insulin secretion? Diabetes 46:1375–1380.

Tsien RY, Li W, Llopis J, Whitney M, Zlokarnik G (1998) Cell-permeant caged InsP3 ester shows that Ca^{2+} spike frequency can optimize gene expression. Nature 392:936–941.

Turrigiano G, Abbott LF, Marder E (1994) Activity-dependent changes in the intrinsic properties of cultured neurons. Science 264:974–977.

Van Belle T, Coppieters K, Von Herrath M (2011) Type 1 Diabetes: Etiology, immunology, and therapeutic strategies. Physiol Rev 91:79–118.

Vigmond EJ, Trayanova NA, Malkin RA (2001) Excitation of a cardiac muscle fiber by extracellularly applied sinusoidal current. J Cardiovasc Electrophysiol 12:1145–1153.

Von Engelhardt D (1989) Diabetes. Its medical and cultural history. Springer, Berlin-Heidelberg.

Wang Z, Zhou Y, Luo Y, et al (2015) Gene expression profiles of main olfactory epithelium in adenylyl cyclase 3 knockout mice. Int J Mol Sci 16:28320–28333.

Watts M, Fendler B, Merrins M, Satin LS, Bertram R, Sherman A (2014) Calcium and metabolic oscillations in pancreatic islets: Who's driving the bus? SIAM J Appl Dyn Syst 13:683–703.

Weckbecker G, Lewis I, Albert R, Schmid HA, Hoyer D, Bruns C (2003) Opportunities in somatostatin research: biological, chemical and therapeutic aspects. Nat Rev Drug Discov 2:999–1017.

Weiss M, Steiner DF, Philipson LH (2000) Insulin Biosynthesis, Secretion, Structure, and Structure-Activity Relationships. [Updated 2014 Feb 1]. In: De Groot LJ, Chrousos G, Dungan K, et al., editors. Endotext [Internet]. South Dartmouth (MA): MDText.com, Inc.; 2000-. Available from: https://www.ncbi.nlm.nih.gov/books/NBK279029/

West AE, Chen WG, Dalva MB, Dolmetsch RE, Kornhauser JM, Shaywitz AJ, Takasu MA, Tao X, Greenberg ME (2001) Calcium regulation of neuronal gene expression. Proc Natl Acad Sci 98:11024–11031.

Whitmarsh AJ, Davis RJ (2000) Regulation of transcription factor function by phosphorylation. Cell Mol Life Sci 57:1172–1183.

Wu Z, Xing J (2012) Functional roles of slow enzyme conformational changes in network dynamics. Biophys J 103:1052–1059.

Xu M (2003) Enhanced expression of L-type $Ca_v1.3$ Calcium channels in murine embryonic hearts from $Ca_v1.2$-deficient mice. J Biol Chem 278:40837–40841.

Yildirim V and Bertram R (submitted) Ca^{2+} oscillation frequency sensitive gene regulation and homeostatic compensation in pancreatic β-cells. Bull Math Biol.

Yildirim V, Vadrevu S, Thompson B, Satin LS, Bertram R (submitted) Upregulation of an inward rectifying K^+ channel can rescue slow Ca^{2+} oscillations in K(ATP) channel deficient pancreatic islets. PLoS Comp Biol

Zhang L, Liu QH, Liu CF, Zhai XW, Feng QL, Xu RL, Cui XL, Zhao ZQ, Cao JM, Wu BW (2013) Zacopride selectively activates the Kir2.1 channel via a PKA signaling pathway in rat cardiomyocytes. Sci China Life Sci 56:788–796.

Zhang M, Goforth P, Sherman A, Bertram R, Satin LS (2003) The Ca^{2+} dynamics of isolated mouse β-cells and islets: Implications for mathematical models. Biophys J 84:2852–2870.

Zhang Q, Bhattacharya S, Andersen ME (2013) Ultrasensitive response motifs: Basic amplifiers in molecular signalling networks. Open Biol 3-re:130031.

Zhou J, Kodirov S, Murata M, Buckett PD, Nerbonne JM, Koren G (2003) Regional upregulation of $K_v2.1$-encoded current, $I_{K,slow2}$, in K_v1DN mice is abolished by crossbreeding with K_v2DN mice. Am J Physiol 284:H491-500.

Zhu L, Luo Y, Chen T, Chen F, Wang T, Hu Q (2008) Ca^{2+} oscillation frequency regulates agonist-stimulated gene expression in vascular endothelial cells. J Cell Sci 121:2511–2518.

BIOGRAPHICAL SKETCH

Education

PhD in Biomathematics (Spring, 2017)
Florida State University, Tallahassee, FL

Master of Science in Biomathematics (Spring, 2014)
Florida State University, Tallahassee, FL

Bachelor of Science in Mathematics (Spring, 2010)
Uludağ University, Bursa, Turkey

Erasmus Exchange Student Program (Fall, 2009)
Technical University of Liberec, Liberec, Czech Republic

Academic Work Experience

Research Assistant, Florida State University, Tallahassee, FL (Aug. 2016-April 2017)

Graduate Teaching Assistant, Florida State University, Tallahassee, FL (Dec. 2013-June 2016)

- Graduate Student Seminar, Organizer, Fall-2015, Spring-2016
- Pre-Calculus, Instructor, Spring 2016
- Bio-Calculus, Computer Lab Instructor, Fall-2015
- Trigonometry, Computer Lab Proctor, Spring-2015
- Math for Liberal Arts, Computer Lab Proctor, Grader Fall-2014

Research Assistant, Bingöl University, Bingöl, Turkey (Fall-2011, Spring-2012)

Volunteer,

- **Judge**, 2014 Capital Regional Science & Engineering Fair, Tallahassee, FL (Feb. 2014)
- Florida State University Department of Mathematics Outreach Program, Gilchrist Elementary School, Tallahassee, FL (Jan 2016)

Publications

Upregulation of an Inward Rectifying K^+ Channel can Rescue Slow Ca^{2+} Oscillations in K(ATP) Channel Deficient Pancreatic Islets. (submitted) Vehpi Yildirim, Suryakiran Vadrevu, Benjamin Thompson, Leslie S. Satin, Richard Bertram

A Ca^{2+} Frequency-Dependent Compensation Mechanism for K(ATP) Channel Deficient Mouse Pancreatic β-Cells. (submitted) Vehpi Yildirim and Richard Bertram

Projects and Presentations

A K(ATP) Channel Independent Bursting Mechanism for $SUR1^{-/-}$ Pancreatic Beta-Cells. European Conference for Mathematical and Theoretical Biology (ECMTB), University of Nottingham (July, 2016)

Calcium Oscillation Frequency Regulation of Ion Channel Gene Expression. Poster, European Conference for Mathematical and Theoretical Biology (ECMTB), University of Nottingham (July, 2016)

A Mathematical Model for Bursting Electrical Activity Recovery in Pancreatic Beta-Cells. Annual Meeting of The Society for Mathematical Biology (SMB), Georgia State University (June, 2015)

Transcriptional Control of Circadian Melatonin Synthesis: A Mathematical Study. Graduate Student Seminar, Florida State University (January, 2015)

A Mathematical Model for Activity Dependent Control of Ion Channel Expression in Excitable Cells. Poster, Institute of Molecular Biophysics, Florida State University (March, 2014)

Professional Skills

Python, MATLAB, XPP/XPPAUT, Linux, LaTeX,
Applications of Microsoft Office,

Systems Biology, Dynamical Systems, Bifurcation Theory,
Control Theory, Machine Learning Algorithms

Honors and Awards

- **Higher Education Grant for Graduate Studies**, Turkish Republic Department of Education (2011-2017)

- **Evelyn and John Baugh Scholarship, 'Outstanding PhD Student in the Field of Mathematics Award'**, Florida State University (April, 2015)

Professional Societies

American Mathematical Society (AMS)
Society for Industrial and Applied Mathematics (SIAM)
Society for Mathematical Biology (SMB)
American Association for the Advancement of Science (AAAS)